Dynamics of Laminar Premixed Flame under Equivalence Ratio Oscillations

Thesis by

Mohd Rosdzimin bin Abdul Rahman

In Partial Fulfillment of the Requirements for the Degree of

Doctor of Philosophy in Engineering

January 2014

Graduate School of Science and Technology
Keio University, JAPAN

Acknowledgements

In the name of Allah, who is Beneficent and Merciful

First, I would like to show my gratitude to my advisor, *Prof. Toshihisa Ueda*, for his guidance and patience in encouraging me during my study in Keio University. I also would like to thank the committee members *Prof. Norimasa Iida*, *Prof. Akiko Matsuo* and *Prof. Takeshi Yokomori*, for their efforts to examined and evaluated my Phd thesis.

I thank *Uemura-san* for developing the 'precious' oscillator system, and even a newer one. I feel indebted to *Tatsuya Hagita-san* for developing the stagnation flow burner and acetone ultra violet induced fluorescence. Million thank to *Tomita-san* and *Tomiura-san* for helping me with the calibrations and experimental works and *Kubo-san*, *Kizu-san* and *Kato-san* for helping me in numerical works. I thank my friends *Faizal-san*, *Sugimoto-san*, *Sasakura-san*, *Shi-san*, *Miyame-san* who always have been inspiring me.

I thank my lovely wife *Siti Noor Aliah Baharom*, my kids *Ahmad Aqil Iman* and *Ahmad Afif Iman* who always have been encouraging and inspiring me through hard times, who always stayed beside me in times of difficulties, I really appreciate your love and support.

Finally, I would like to show my deepest love and respect to my parents and parent in law for their dedication and sacrifice.

Again, I would like to thank everybody, including those who may not have been mentioned above for the limited space, for everything they did to help this thesis make its way out to the world.

Thank you very much!

Jazak Allah Khayr

Abstract

Dynamics of laminar-premixed flames of CH_4/air mixture under equivalence ratio oscillations were experimentally and numerically investigated for stagnation flame and conical flame by focusing on the oscillation wavelength is larger than the nominal flame thickness. In an experimental work, lean region is focused because flame moves monotonically in equivalence ratio variations. It was observed that the flame moves periodically following the variation of the equivalence ratio. This movement is primarily due to the equivalence ratio oscillations, since the velocity perturbation is significantly suppressed. Furthermore, it was observed that the flame dynamics is influenced by the characteristic of the piston type oscillator at the quasi-steady regime (St < 1.0) by an increase in amplitude of the flame motion with an increase in the frequency of the equivalence ratio variation. On the other hand, an increase in the oscillation frequency of the equivalence ratio variation decreases the flame motion amplitude as it was influenced by the oscillation frequency at the unsteady regime (St > 1.0). The numerical work for the stagnation flame was focused at St > 1.0 in the lean, rich and lean rich crossover cases and the results are agreed with the experimental works. Moreover, numerical work demonstrated that, the back support effect influences the dynamic response of the flame movement, in that, the direction of the cycles of the dynamic response in the lean and the rich conditions are different. In addition, hysteresis of the flame movement is seen in the numerical and experimental works. An explanation of this hysteresis was done by introduces concept of the non-uniform scalar value profile and was clarified by development of simplified qualitative mathematical model. For conical flame, the quasi-steady manner of the flame tip movement was

observed at $St < 1.0$. At $St > 1.0$, we found that the attenuation of the flame tip motion is affected by the wrinkling of the flame surface in addition to the attenuation of the equivalence ratio oscillation amplitude. Overall, a ratio between the characteristics time of the flow and the characteristics time of the oscillation called *Strouhal* number is an important parameter to categories the dynamics of the laminar premixed flame in quasi-steady ($St < 1.0$) or unsteady ($St > 1.0$) manner either the stagnation or conical flame configurations.

Nomenclature

a	crank length, m
A	pre-exponential factor
b	connecting rod length, m
BR	blowing ratio
Cp	specific heat of constant pressure, kJ/kgK
Dia	diameter, m
D_i	mass diffusivity of species *i*
f	frequency, 1/s
g	gravitational acceleration, m/s^2
h	specific enthalpy, J/kg
k	heat conductivity
L	length, m
m	mass flux
p	static pressure
q	heat release per unit mass of fuel reacted
R	universal gas constant
r	radial coordinate
T	period of oscillation, s
t	time, s
U	velocity, m/s
u	velocity in *x*-direction, m/s
y	longitudinal coordinate
A_i	pre-exponential factor of reaction *i*
A_{cross}	cross-sectional area
A_{piston}	piston area, m^2
E_a	activation energy, J/k mol
f^*	characteristic oscillation frequency
f_{cutoff}	cut-off frequency
F_r	external force in r-direction
F_y	external force in y-direction
l_f	flame length, mm
m_o	non-dimensional mass flux
Q_o	non-dimensional heat
Q_x	flow rate of *x*
Q	heat [kJ/m^{2}s]

S_d	flame displacement speed, m/s
S_m	source term
S_u	flame speed, m/s
S_u^o	flame speed at adiabatic condition, m/s
T_a	activation temperature, K
T_b	burned gas temperature, K
T_f	flame temperature, K
T_u	unburned gas temperature, K
U_o	incoming velocity, m/s
u_f	unburned gas velocity, m/s
v_r	velocity in *r*-direction, m/s
v, v_y	velocity in *y*-direction, m/s
y_f	flame location, mm
Y_i	mass fraction of species, *i*
Yk	reaction rate
$\sqrt{\overline{u'^2}}$	root mean square of the fluctuating velocity, m/s
$\bar{u}$	average velocity, m/s

Greek alphabet

$\emptyset_i$	equivalence ratio of *i*
$\emptyset_f$	equivalence ratio of unburned mixture
α, β	angle, degree (^{o})
δ_R	thickness of the reaction zone
δ_m	thickness of the pre-heat zone
λ	thermal conductivity
λ_i	wavelength of *i*
μ	viscosity
ρ	density, kgm^3
τ	convective transport time, s
ω	angular velocity, rads^{-1}

Sub-script alphabet

A	amplitude
ad	adiabatic
b	burned

b_i	backward reaction *i*
c	critical
ex	experimental work
eq	equivalence ratio
f	fuel
f_i	forward reaction *i*
$lean$	lean equivalence ratio case
m	mean
max	maximum value
min	minimum value
$prim$	primary
ref	reference
$rich$	rich equivalence ratio case
s	numerical work
sec	secondary
st	stoichiometric
$steady$	steady state case
u	unburned

Table of contents

List of Figures

List of Tables

Chapter 1

Introduction

1.0 Introduction

Since the industrial revolution, we have used combustion technology to obtain power and heat, while it induces some environmental issues, such as NOx formation, increase in CO_2, etc. Although new technologies, such as photovoltaic, wind, hydro, geothermal, etc have been developed to supply energy, it may be difficult to supply enough energy for the worldwide demand. Thus, the energy saving and low emission combustion technology need to be developed. Regulation about the NOx emission is very strict and every year the rules have been improved by reducing the percentage of the NOx releases by combustor to the atmosphere. Currently, combustor that would release low emission is supposed to be a lean premixed combustor. This combustor operates at lean condition where in this regime emission of not only NOx but also the CO_2 are low. Moreover, lean premixed combustion is economical because it uses less fuel. Recently, the lean premixed combustion is used in power plants and factories to reduce the NOx emission (Ishida, 2003 and Matsuyama *et al.*

2012).

Operating condition of the lean premixed combustor in the lean regime has brought up some technical problems that have not yet been solved, such as combustion instability. Combustion instability is one of the main subjects of current combustion science. Combustion instability as functions of combustor geometry, operating conditions and fuel have not yet been clarified (Alan, 2012). Moreover, Lieuwen *et al.* (1998) showed that reactant un-mixed also could drive strong instabilities in a lean premixed combustor. Combustion instability occurs when the pressure oscillation is in phase with the heat release oscillation, then induces poor performance of the combustor and to some extend it may break the combustor.

One approach to solve the combustion instability is by modulating the equivalence ratio injected into the combustion chamber. Richards *et al.* (1999) and Yu and Wilson (2002) have studied the modulating of the equivalence ratio and found that the instability can be suppressed by this approach.

Practically, the combustion instability can be controlled by equivalence ratio perturbation. This is because the heat release oscillation can stabilize by repeated the conditions at it or lower frequency than that heat release oscillation frequency (Richards *et al.*, 1999). Moreover, researches on the control system have been done (Richards *et al.* 1999 and Yu and Wilson, 2002). Unfortunately, they are no general rule to design the system because as mention by Alan (2012), the combustion instability depends on combustor geometry, operating conditions and fuel. Therefore, to develop the general rule of the control design system, understanding of fundamental mechanism of the flame response to the equivalence ratio perturbation is needed.

In the combustor, turbulent combustion is occurred. To understand the fundamental

structure and dynamic response of the turbulent combustion is very difficult. Therefore, the simplest and an easy way to understand the turbulent combustion is by analyzing the laminar flames. The laminar flames is significantly contributes to the better understanding of the turbulent combustion (Law, 1989). Furthermore, key parameter in turbulent combustion modeling is a scalar dissipation rate of the progress variable of reaction (Bray *et al.* 2005). Zhou and Hochgreb, (2013) conducted laminar flame study and showed that the scalar dissipation rate is linearly proportional to the heat release rate. Thus, it gives an easy way to measure the heat release rate as a scalar dissipation rate compared to the measurement of the reaction rate in the turbulent combustion (Zhou and Hochgreb, 2013).

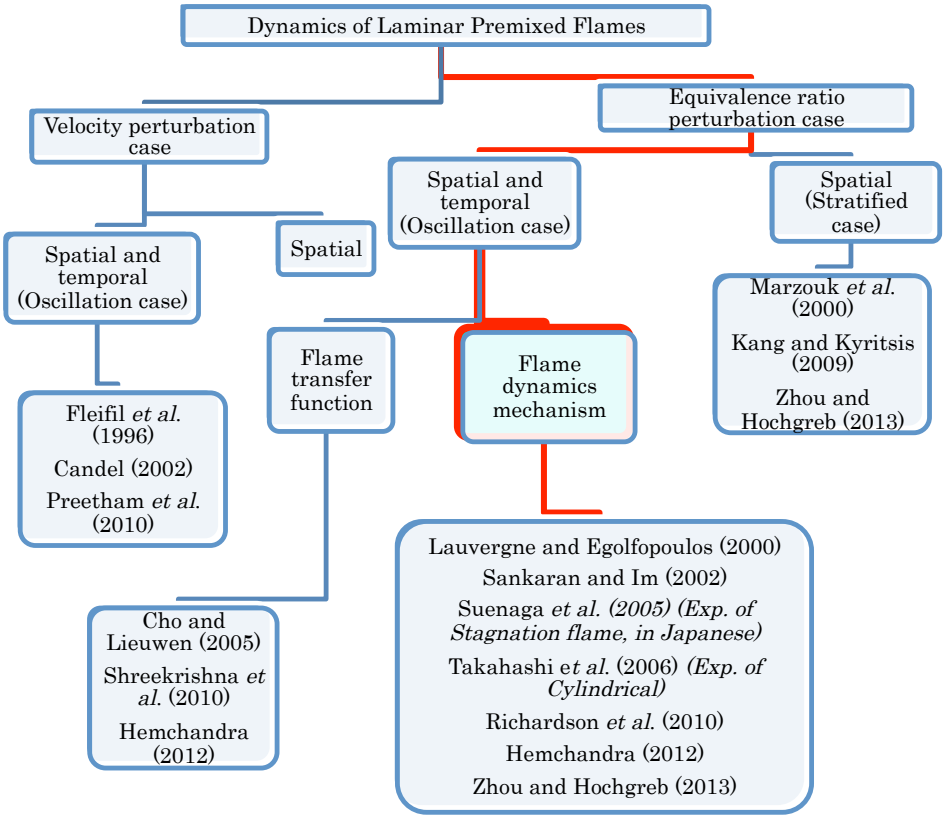

Figure 1-1 An overview of the dynamics of laminar premixed flames study.

1.1 Dynamics of laminar premixed flames

Figure 1-1 shows an overview of the dynamics of laminar-premixed flames studies that have been done. This chapter and the following will discuss in details about the previous studies of the dynamics of laminar premixed flame and direction of this thesis.

Premixed flame is formed when ignition takes place in fuel and air mixture. The flame propagates into the unburned fuel/air mixture and relaxes at the point where the incoming velocity is equal to the flame speed. The premixed flame is a wave phenomenon. Wave propagation can be in subsonic and supersonic condition. Subsonic wave propagation is known as deflagration wave and detonation wave is supersonic wave propagation. This dissertation focuses on the propagation of deflagration wave commonly called laminar premixed flames. General structure of the laminar-premixed flame is shown in Fig. 1-2. Premixed flame consists of pre-heat and reaction zones. In the pre-heat zone, the reactant is diffusing and the temperature starts to rise due to heat conduction from the reaction zone. Reaction taking places in the reaction zone by consuming the reactant while temperature reach at the peak downstream of the reaction zone. Moreover, the laminar-premixed flame is a propagation of the deflagration wave therefore; laminar flame speed is an important parameter to describe the physic-chemical information of the mixture. The laminar flame speed is a reference parameter to describe the extinction, flash back, blow off and turbulent flame propagation for many premixed flame phenomena (Law, 2006).

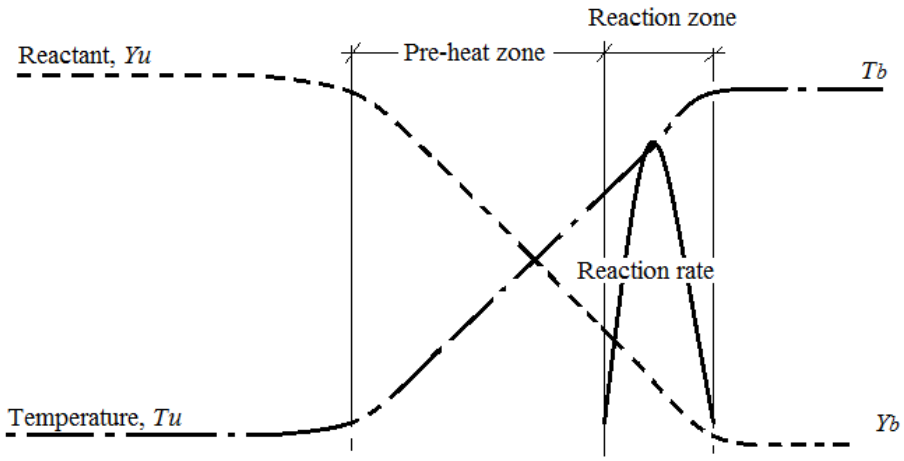

Figure 1-2 General structure of the premixed flame.

The dynamics of laminar-premixed flames is to study the flame response such as the flame response to the velocity and/or that to the fuel concentration (equivalence ratio) perturbations. The response of the flame towards the perturbation can be categories into quasi-steady and unsteady cases. Quasi-steady case exists if the characteristic time of the perturbation is longer than the flame time scale. On the other hand, small characteristic time of the perturbation compared to the flame time scale evolve the unsteady case (Fig. 1-3) (Law, 2006).

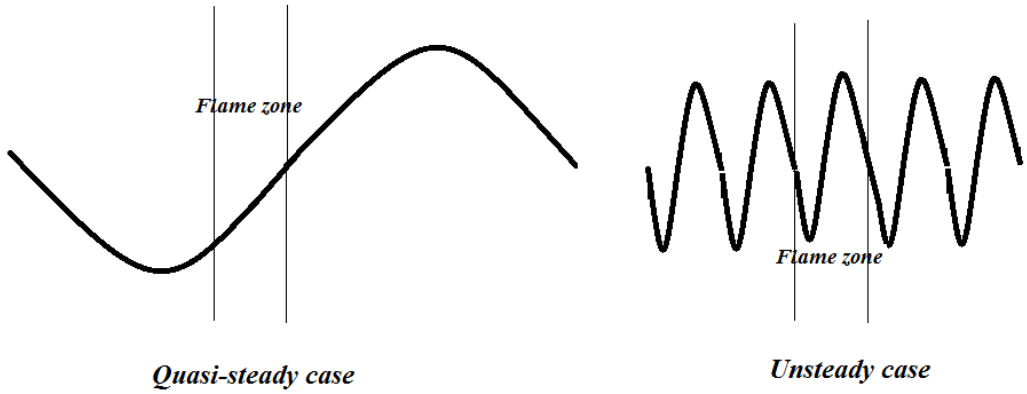

Figure 1-3 Perturbation wavelength.

Studies on the dynamics of laminar-premixed flames are too wide and can be flame-flow interaction, flame-vortex interaction, flame-reactant interaction, flame-burner interaction and etc (Candel, 2002). Mallard and Le Chatellier started this study and later Zeldovich and Frank-Kamenetski was setup the basis for modern combustion theory (Goey *et al.* 2011). Most of the dynamic laminar premixed flame study was focused on the flame-flow interaction (Egolfopoulos and Campbell, 1996, Im et al., 1996, Fleifil et al., 1996, Sung and Law, 2000, Im and Chen, 2000, Candel, 2002, Kornilov, 2006, Nader et al. 2009, Preetham et al., 2010, Riazi and Farshchi, 2011). Lauvergne and Egolfopoulus (2000) conducted flame-flow studies and found that the strain rate oscillation causes equivalence ratio perturbation in front of the reaction zone. Therefore, the dynamic of laminar-premixed flame in flame-flow interaction consists of equivalence ratio perturbation effect. Based on this observation it is compulsory to separate these two perturbations because each perturbation would bring different mechanism that affected the flame dynamics.

1.2 Velocity perturbation

Researches on velocity perturbations induced by acoustic wave have been carried out and the data have been used to develop the model describing interactions between the flame and the system, to analyze the instability regime of the system, to investigate the active and passive control system and numerical work also been carried out and clarified experimentally (Fleifil *et al.* 1996, Candel, 2002 and Preetham *et al.* 2010). In a nutshell, interaction between the velocity perturbation and flame is well understood.

1.3 Equivalence ratio perturbation

Introducing the equivalence ratio perturbation in combustion is challenging since its characteristic timescale can couple with that of convection, diffusion and reaction (Egofolpoulos and Campbell, 1996). Equivalence ratio perturbation in combustion is a flame-reactant interaction. This interaction is a one kind of the combustion instability. When the equivalence ratio perturbation approaching edge of the preheat zone it convects into the flame zone as a results the heat release is perturbed. Moreover, perturbation in heat release couples with the acoustic mode of combustor sustaining the combustion instability (Hemchandra, 2012). Studies on the equivalence ratio perturbation can be divided into spatial or spatial and temporal perturbation cases.

1.3.1 Spatial equivalence ratio perturbation

Spatial perturbation is related with stratified case. The stratified case occurs when a flame propagates into fuel/air mixture with varies in equivalence ratio. The equivalence ratio variations could be varied toward the lean or rich conditions. This case has been studied rigorously in numerical and experimental. Most of the research in spatial

perturbation case such as the compositionally stratified suggested that heat from the product side influences the flame dynamics in lean case (Marzouk et al. 2000, Pires et al. 2000, Kang and Kyritsis, 2007, Kang and Kyritsis, 2007, Kang and Kyritsis, 2009, Richardson et al. 2010, Zhou and Hochgreb, 2013). Moreover, in rich side addition of the H_2 mass flux into the flame zone from the product side affected the flame dynamics (Pires et al. 2000, Zhou and Hochgreb, 2013). Zhou and Hochgreb (2013) suggested that at near lean or rich flammability limit, both heat and mass flux significantly affects the flame dynamics by helping to stabilize the flame beyond this limits. The flame behavior underlying mechanisms has been published and some researchers suggested that it could be used to explain the flame behavior in spatial and temporal equivalence ratio perturbation case (Pires et al. 2000, Zhou and Hochgreb, 2013).

1.3.2 Spatial and temporal equivalence ratio perturbation

Spatial and temporal perturbations are related with the oscillation case. This oscillation could be in lean, rich or crossover lean rich cases. Fundamentally, in the spatial and temporal perturbations, flame zone thickness could be smaller, equal or larger than that wavelength of the equivalence ratio oscillation. Therefore, effect of the oscillation frequency is significant. These cases have been studied widely in numerical and less effort in an experimental work. Numerical work is possible to implement without the velocity perturbation. On the other hand, velocity perturbation is hard to vanish in experimental work and up to this date there is no experimental work on the equivalence ratio oscillation has been successfully done.

Researchers have conducted fundamental studies by numerical method to understand the mechanism of the dynamic flame response to equivalence ratio oscillations for

stagnation flame configuration under lean condition (Lauvergne and Egolfopoulos, 2000, Sankaran and Im, 2002, Richardson et al. 2010). Egolfopoulos and Campbell (1996) studied response of the one-dimensional counter flowing strained diffusion CH_4/air flames by introducing the equivalence ratio oscillation at the exit of nozzle using numerical analysis. In the study, C_2 reaction mechanism was used. Egolfopoulos and Campbell (1996) proposed that the analogy of the Stokes second problem could explain the oscillation of the equivalence ratio at nozzle exit leads to oscillation at the beginning of the main transport zone.

One-dimensional strained laminar premixed C_3H_8/air flame established in a stagnation flow field was done by Lauvergne and Egolfopoulos (2000). The C3 sub-mechanism was used as a reaction mechanism. Lauvergne and Egolfopoulos (2000) claimed that the time required for a perturbation to propagate through convection and diffusion process inside the flame layer influences the flame response. These perturbations attenuated as they propagating inside the flame, with amplitude

$$A(x) = A_O e^{-x(\omega/2D)^{0.5}} \qquad (1-1)$$

where *D* is an average diffusivity of the fuel within the transport zone. Moreover, they also suggested that the flame response could be predicted from the history of incoming flows (Lauvergne and Egolfopoulos, 2000). The cutoff frequency, which the flame response is un-responsive to perturbation above this value mentioned in Eq. (1-2) was introduced (Lauvergne and Egolfopoulos, 2000).

$$f_{cutoff} = \frac{\ln (0.1)^2 {S_u}^2}{\pi D} \qquad (1-2)$$

where, *Su* is the laminar burning velocity and *D* the average mass diffusivity of fuel within the diffusion zone.

Sankaran and Im (2002), investigated the dynamic flammability limit of the CH_4/air flame with equivalence ratio oscillation using one-dimensional counter flow filed configuration. The reaction mechanism of GRI-Mech 3.0 has been used in the study. Sankaran and Im (2002) investigated the strong and weak strain rates and observed that the dynamic flammability limit was dependent upon the mean equivalence ratio and frequency of the fluctuation. Moreover, the flammability limit is further extended to a leaner condition with increasing frequency or mean equivalence ratio fluctuation (Sankaran and Im, 2002).

Zhou and Hochgreb (2013) conducted one-dimensional numerical analysis of the counter flow premixed CH_4/air flames with the GRI 3.0 natural gas mechanism. They suggested that the flame response in spatial equivalence ratio perturbation case represent the flame response in spatial and temporal equivalence ratio perturbations case as long as local equivalence ratio and it gradient at the point of peak heat release rate are equal in both cases.

Conical-shaped and V-shaped flames have been used as well as the stagnation configuration (Cho and Lieuwen, 2005, Birbaud et al. 2008, Ax et al. 2009, Shreekrishna et al. 2010, Riazi and Farshchi, 2011, Hemchandra, 2012). These configurations were used in studying the flame transfer function by reduced order modeling approach under a lean condition (Cho and Lieuwen, 2005, Shreekrishna et al. 2010, Riazi and Farshchi, 2011, Hemchandra, 2012). Researchers found that the variations in the heat of reaction and flame speed are directly generated by equivalence ratio perturbations and indirectly cause the flame pattern to vary (Cho and Lieuwen, 2005, Shreekrishna et al. 2010, Riazi and

Farshchi, 2011).

Cho and Lieuwen (2005) found that three processes control the heat release oscillation response to equivalence ratio oscillations namely: flame speed, heat of reaction and flame surface area oscillation. They also found that, a decrease in the mean equivalence ratio oscillation towards a leaner equivalence ratio increases the flame response. Later, Riazi and Farshchi (2011) observed that responses of the V-shape flame are stronger than those of the conical flame in equivalence ratio oscillation by analyzing the flame transfer function. They concluded that V-shaped flames are more susceptible to combustion instabilities than conical flames.

Unfortunately, these studies (Cho and Lieuwen, 2005, Shreekrishna et al. 2010, Riazi and Farshchi, 2011) were based on simple assumptions and no theoretical explanations were given for a possible breaking of the flame front or for the interaction of the flame with fresh stream dynamics (Birbaud et al. 2008), which are also important for characterizing practical flames and would lead to disparity. This agrees with the experimental results obtained for the lean premixed conical flame with velocity perturbation when it shows discrepancy with the published results using reduced order-modeling approaches (Karimi et al. 2009).

Garrido-Lopez and Sarkar, (2005), has studied two-dimensional direct numerical simulation of C_3H_8/air flames with the one-step reaction mechanism in lean condition. They imposed composition and velocity fluctuations of various intensities and found that a significant enhancement of the flame length exists when the inhomogeneity level of the composition fluctuations is larger than the velocity fluctuations. Two-dimensional numerical analysis of the premixed CH_4/air inverted V flames was done by Birbaud *et al.* (2008). The one-step reaction mechanism of CH_4/air was used and focused on the linear

variation in the flame speed at lean condition. They found that high level of equivalence ratio modulation induces axial velocity perturbation that interacts with the flame surface and modify the flame response. Moreover, non-linear heat release response due to rupture of the V flame tip in the equivalence ratio oscillation at high oscillation frequency was observed (Birbaud *et al.* 2008). The rupture of the V flame tip was found because of the extension of the flame waveform beyond the fresh stream mixture (Birbaud *et al.* 2008).

Hemchandra (2012) conducted a two-dimensional slot stabilized premixed laminar ch4/air flame using one-step reaction mechanism and the result was compared with the Reduced Order Modeling approach. He found that reduced order modeling approaches failed to predict the magnitude and phase of the flame response compared to multidimensional flames when the Darrieus-Landau instability has maximum influenced because of the exception effect of the gas expansion across the flame surface.

Realization of the numerical study could not be achieved without the verification through an experimental work. Other researchers have done on the equivalence ratio oscillation experimentally. Takahashi *et al*., (2006), Suenaga *et al*., 2010 investigated the cylindrical-shaped of the premixed flame experimentally and observed an increases in the oscillation amplitude of the burning velocity, burnt gas temperature, burnt gas composition and flame luminosity with equivalence ratio oscillations exceeded those of the steady state case. Moreover, near the lean flammability limit recovery of the flame intensity was observed in their experiment and effect of the Lewis number towards the recovery mechanism was examined. Methane was strengthening by the Lewis number compared to the propane flame by that effect. In 2009 (Ax et al. 2009) an experiment was conducted under a low-pressure environment to investigate the premixed CH_4/air flames with forced periodic mixture fraction oscillation. They have observed the flame tip response to the

equivalence ratio variation in the lean case experimentally. The OH chemiluminescence was measured to qualitatively analyze the flame response and they found that the flame position and flame shape changed in equivalence ratio oscillation. Unfortunately, there is no detail discussion on the flame response while they focused on presenting the experimental realization and measurement techniques. The latest paper regarding the experimental work on equivalence ratio oscillation was written by Schwarz *et al*. 2010. Unfortunately, the experiment could not diminish the velocity oscillation and concluded that the velocity perturbations imparted to the mainstream induced by the modulation mainly determined response of the weakly turbulent flame subject to equivalence ratio oscillation.

It is interesting to see in the numerical analysis, there are disagreements between reduced order modeling and multidimensional flame studies (Karimi *et al*. 2009 and Shreekrishna *et al*. 2010). A detailed study of the multidimensional flame to understand the flame response would be beneficial for both fundamental understanding and practical interest. In spite of the numerical analysis, there is no experimental work have been done and produces reliable data for the validation of the numerical work.

1.3.3 Oscillation frequency regime

Researches of the laminar premixed flame response to the equivalence ratio oscillation were conducted at intermediate oscillation frequency between 50 to 1000 Hz by numerical analysis (Lauvergne and Egolfopoulos, 2000, Sankaran and Im, 2002, Richardson *et al.* 2010, Hemchandra, 2012 and Zhou and Hochgreb, 2013). Lauvergne and Egolfopoulos (2000) and Sankaran and Im (2002) investigated the laminar premixed flame response to the equivalence ratio oscillation at frequency range 100 – 2000 Hz. Moreover, Richardson

et al. (2010), Hemchandra, (2012) and Zhou and Hochgreb (2013) in the range of 50 – 200 Hz. Numerical analysis at 10 Hz oscillation frequency was done by Sankaran and Im (2002) and Richardson *et al.* (2010) unfortunately there was no detail discussion has been made. On the other hand, an experimental work was done at low frequency regime using cylindrical flame configuration (Suenaga *et al*. 2010).

The combustion instability is divided into three regimes, low (<50Hz), intermediate (50 -1000Hz) and high (> 1000Hz) oscillation frequency (Krebs *et al.* 2005). High frequency regime involve three dimension acoustic mode and equivalence ratio variation is supposed to be a minor significant effect due to the attenuation. Other researchers (Lauvergne and Egolfopoulos, 2000, Sankaran and Im, 2002, Richardson *et al.* 2010, Hemchandra, 2012 and Zhou and Hochgreb, 2013) did intermediate frequency regime and flame dynamics mechanism is discussed. Moreover, there is no detail discussion have been made at low frequency regime. Low frequency regime is important since, it produces noise (rumble) and also blowout and reignite is observed in the combustor (Mongia *et al*. 2005). In addition, at low frequency regime, the equivalence ratio oscillation wavelength are larger than that the nominal flame thickness. At this conditions there is some question that not yet been answered;

- will the flames respond in quasi-steady manner.
- will the lean flammability extend.
- will the presence of gradient in stratified case can be used to explain behavior in low oscillation frequency case.

Following the above reasons, to provide the fundamental knowledge for the explanations of the flame dynamics mechanism seen in the combustor and answering the questions, an investigation of the flame dynamics under equivalence ratio oscillation at low oscillation

frequency is needed.

1.4 Objectives and methods

In this dissertation, the objectives are to elucidate dynamics and mechanism effects, of the equivalence ratio oscillation on a laminar-premixed flame response at the low oscillation frequency (oscillation wavelength is larger than that nominal flame thickness). Dynamics of the flames is important to characterize the combustion instability. Moreover, combustion instability includes the flame extinction and flame fluctuation (movements). Mechanisms that drive the flame dynamics in unsteady case are less understand and some questions have arisen: “What is the dominant mechanism for the flame dynamics?” and “Could the mechanism in the steady state with equivalence ratio gradient explaines the flame dynamics behavior in the equivalence ratio oscillation case?”. On the other hand, there are disagreements between reduced order modeling and multidimensional flame studies (Karimi *et al*. 2009 and Shreekrishna *et al*. 2010). Thus, a detail study of the multidimensional flame to understand the flame response would be beneficial for both fundamental understanding and practical interest. In addition, the flame response to the equivalence ratio oscillation would be in various flame configurations and it is important to generalize the control parameter of the flame dynamics. Therefore, to accomplish our objectives, we experimentally and numerically investigated the response of the laminar premixed CH_4/air flame to the equivalence ratio oscillation.

The experimental work was conducted based on stagnation configuration. Oscillations of different frequencies and amplitude were used to determine the flame response as a function of oscillation frequency and oscillation amplitudes. The flame response in lean conditions was focused, because in the lean region the flame varies monotonically with

equivalence ratio variations.

In the numerical analysis, an ideal flame response to equivalence ratio oscillation without any other perturbation such as incoming velocity fluctuation was investigated. An ideal flame response was analyzed and the results were compared with previous study and revealed the mechanism of the flame dynamics. Numerical approached was based on the stagnation and conical flame configuration. These configurations are widely used previously in combustion instability study thus it opened large space for comparison with the present study.

The results of this investigation will improve the current state of combustion knowledge in several ways;

First, intermediate frequency of the equivalence ratio oscillation case has been reported (Lauvergne and Egolfopoulos, 2000, Sankaran and Im, 2002) and there is no detail discussion of the low frequency response fundamentally. Therefore, the present analysis will fill the data gap at low oscillation frequency case. Furthermore, low frequency case allows direct comparison with stratified case because the perturbation length was considered larger than that flame zone thickness. Thus, the present result can answer the questions arose previously. In addition, multidimensional numerical analysis was conducted in the present work. Therefore, the data can be compared directly with practical flame of the interest.

Secondly, there is no experimental work produced reliable data and allow direct comparison with the numerical study for the laminar premixed flames. Moreover, the present experimental work using novel design of burner with equivalence ratio oscillation system and turbulent reduction method produces laminar premixed flames with lower flow velocity fluctuation disturbance at ambient conditions that never been reported previously.

Thus, the experimental data can be used to verify the numerical work of the present study and the flame response to the equivalence ratio oscillation can be clearly seen.

1.5 Outline of the dissertation

This dissertation is organized as follows;

Part I (Chapter 2 and 3) refers to the stagnation laminar premixed flames configuration.

Part II (Chapter 4) regards to the conical laminar premixed flames configuration.

In Chapter 2, CH_4/air flame is form in stagnation condition using convergence nozzle burner. Injecting secondary lean and rich mixture of the CH_4/air mixture using novel design oscillator forms equivalence ratio oscillation at nozzle burner exit. Flame dynamics was investigated by examined the flame position and flame luminosity. Formation of the equivalence ratio variations was measured using ultra-violet induced fluorescent system.

Chapter 3 is related to numerical analysis. Laminar premixed CH_4/air flame was simulated using an axis-symmetric flow field. CH_4/air mixture used as a fuel and an oscillation was introduced at the inlet nozzle burner using sinusoidal function. The one-step reaction mechanism with Arrhenius rate of reaction was used as a chemical reaction mechanism. This simplified reaction model was used to discuss fundamental mechanism of flame dynamics. Flame dynamics was determined by investigating scalar properties as a function of equivalence ratio oscillation.

In Chapter 4, concept of mechanisms that have affected the flame dynamics influenced by the equivalence ratio oscillation seen in experimental and numerical work is introduced. The concept is developed based on non-uniform scalar value profile in the upstream and downstream of the flame zone. Furthermore, clarification of this concept is carry out by developing a simplified qualitative mathematical model using an approximation method.

Chapter 5 is discussing about the numerical analysis of the conical flame configuration. CH_4/air mixture was used as a fuel and an oscillation was introduced at the inlet nozzle burner using sinusoidal function. The one-step and two-step reaction mechanism with Arrhenius rate of reaction was used as a chemical reaction mechanism. One-step and two-step were selected because rich condition of the equivalence ratio is discussed. Flame dynamics was determined by investigating scalar properties as a function of the equivalence ratio oscillation. Moreover, convective transport time was examined to categorize the flame dynamics.

Chapter 6 summarizes of the conclusion the current work with a discussion of directions for the future research.

Chapter 2

Dynamics of the stagnation laminar premixed flames – An experimental study

2.1 Introduction

Experimental work of the flame response to the equivalence ratio oscillation was done in several configurations. Ax *et al.* (2009), Schwarz *et al*. (2010) conducted the experimental work using conical flame configuration and Takahashi *et al*., (2006), Suenaga *et al*., (2010) using cylindrical flame configuration. On the other hand, numerical work was focused on stagnation flame configuration (Lauvergne and Egolfopoulous, 2000, Sankaran and Im, 2000, Rahman *et al*., 2012). Thus, there is no experimental work to verify the numerical work to this date. Therefore, this work conducted the experimental study of the flame response to the equivalence ratio oscillation as to verify the numerical result.

In this study, the experiment work was performed using a stagnation flow field test rig with novel oscillator to induce equivalence ratio oscillations to the nozzle exit flow. The

stagnation flow field was considered because the flame response to the equivalence ratio oscillation in stagnation flow field is easy to measure in term of flame position and flame speed. Therefore, it can be used to compare with the numerical result of the flame dynamics.

Experimental work of the flame response to the equivalence ratio oscillation is very complicated due to an incorporated of the velocity perturbation. Velocity perturbation is a major problem to be solved in the equivalence ratio oscillation case. Low-pressure environment was used by Ax *et al.* (2009) to reduce the velocity perturbation. Takahashi *et al*., (2006) and Suenaga *et al*., (2010) using porous structured. In this study, we implemented the combination of honeycomb and wire mesh screen to reduce the velocity fluctuation. Combination of the honeycomb and wire mesh screen is use in the wind tunnel system to reduce the turbulence in the flow (Loehrke and Nagib, 1972). Basically, wire mesh screen reduces axial fluctuation (Derbunovich *et al.*, 1993) and honeycomb reduces lateral fluctuation (Mikhailova *et al.*, 1994). Therefore, combination of these two leads to reduction of turbulence in the flow (Kulkarni *et al.*, 2011).

Acetone Laser Induces Fluorescent was used to measure the concentration variations of the fuel (Hirota *et al*. 2009), flame position (Nakamura *et al.*, 2011) and flame temperature (Thurber, 1999) quantitatively. In the present study, Acetone Ultraviolet Light Induces Fluorescent was employed to measure the concentration oscillation qualitatively.

The hot wire anemometer was used to measure velocity profiles in the isothermal stagnation flow exposed to the secondary injection oscillations. These velocity profiles were used to examine effects of oscillations and how the flow field was modified.

2.2 Experimental setup

2.2.1 Flow system

Figure 2-1 shows the schematic diagrams of the flow system. A primary flow of CH_4/air mixture of the system was in lean condition. The CH_4 and air were supplied from the pressurize cylinder and the air compressor respectively. Moreover, mass flow controller measured flow rate of both CH_4 and air. The primary flows mass flow controller of Azbil (Yamatake Corp.) was used with measurement ranges of 0.04 - 5.0 lpm for CH_4 and 0.4 - 50.0 litres per minute (lpm) for air. Flow mixture of the CH_4/air at the nozzle exit burner was a combination of flow from the primary and secondary flow. The secondary flow consists of lean and rich of the CH_4/air mixture. The mass-flow rates of lean and rich secondary air and also the lean and rich secondary CH_4 were measured and controlled using Azbil digital mass-flow controller (Yamatake Corp.) with measurement ranges of 0.2 - 20.0 lpm, 0.04 - 5.0 lpm, 0.02 - 2.0 lpm and 0.04 - 5.0 lpm respectively. The lean and rich CH_4/air mixture was supplied to the burner from an oscillator. The oscillator supplied the lean and rich CH_4/air mixture with 180^o phase difference respectively. Therefore, the combination of the primary and the secondary flows were mixed at the mixing zone of the burner and produces equivalence ratio variation at the exit of the nozzle burner.

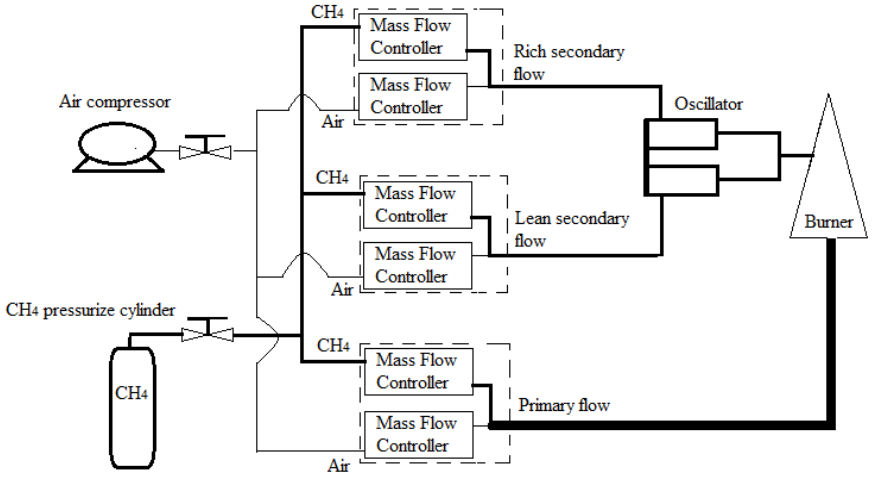

Figure 2-1 Schematic diagrams of the flow system.

2.2.2 Burner system

An overview of the burner system is shown in Fig. 2-2. Moreover, nozzle section with coordinate system and detailed are shown in Figs. 2-3 and 2-4. Primary flow of the CH_4 and air was mixed in mixing chamber of the burner. Moreover, damping wire mesh screen and honeycomb were used to reduce the turbulent of the flow in mixing chamber before it reach to the nozzle burner. Furthermore, flat velocity profile at exit of the nozzle was produced using convergent nozzle. Stagnation flow field condition was established by installing the stagnation plate at the top of the nozzle burner exit with ratio between the length of the stagnation plate from burner nozzle exit, L to the burner diameter, Dia, is L/Dia = 1.0. The stagnation plate is made of a ceramic disk with 76 mm diameter. Flat laminar premixed CH_4/air flame was formed in the stagnation region when CH_4/air mixture issued form the nozzle with 20 mm diameter ignited. Co-flow of the N_2 was issued surrounding the main nozzle burner to minimize the interaction of the flame edge with the ambient air, to make the flame flat and increase the flatness of the flame shape. The

coordinate y and r were defined as the upstream direction from the stagnation plate along the center axis and in radial direction of the burner nozzle respectively.

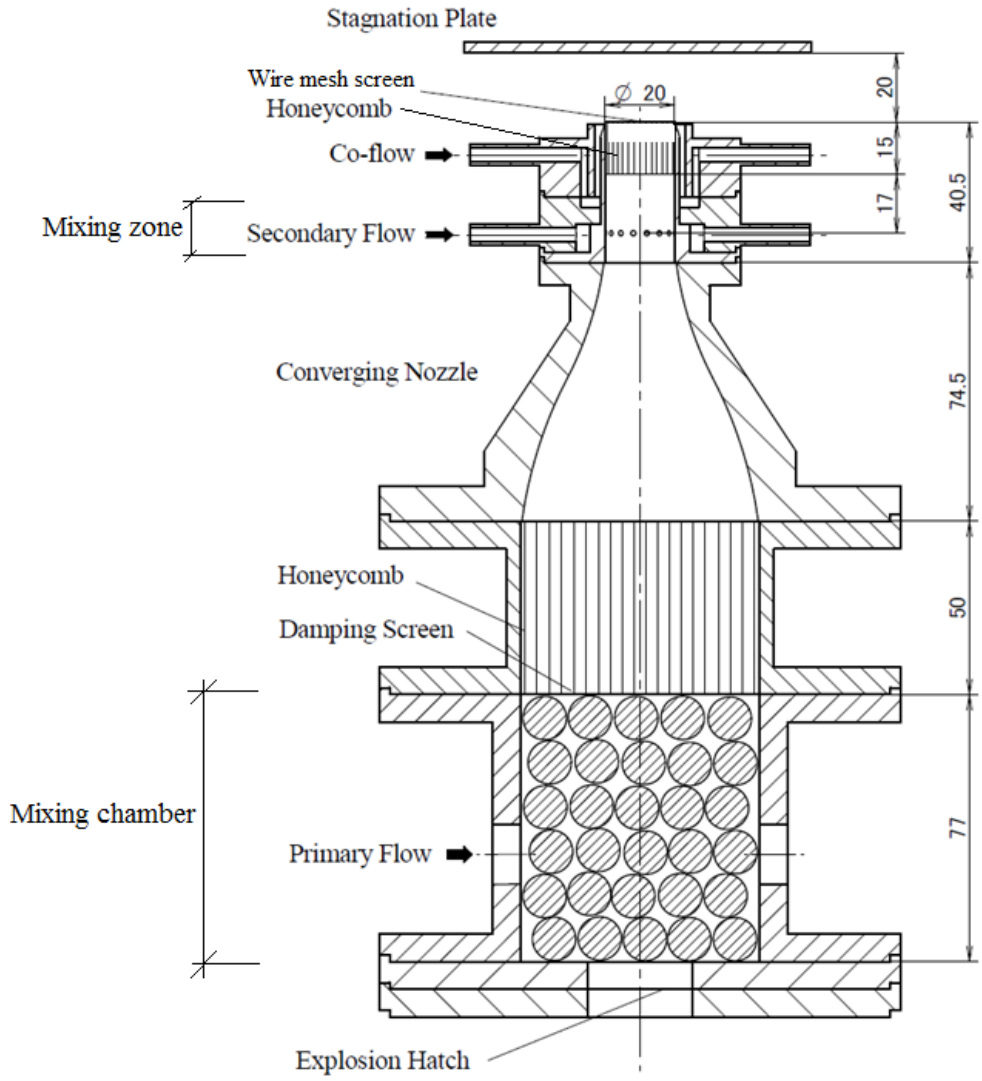

Figure 2-2 Overview of the burner system.

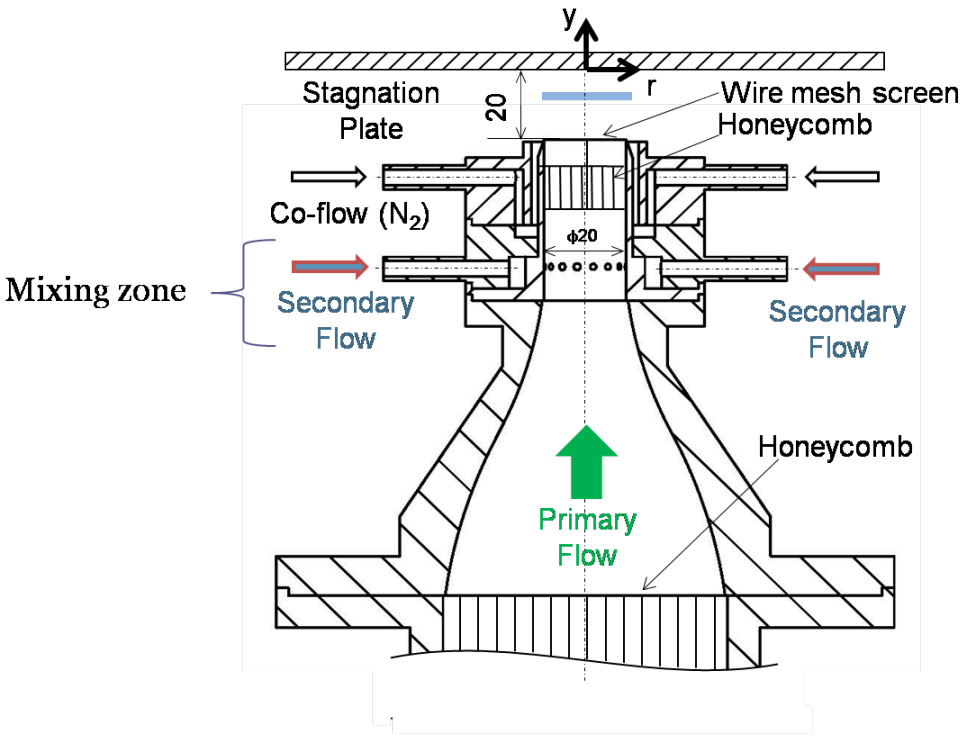

Figure 2-3 Nozzle section with coordinate system.

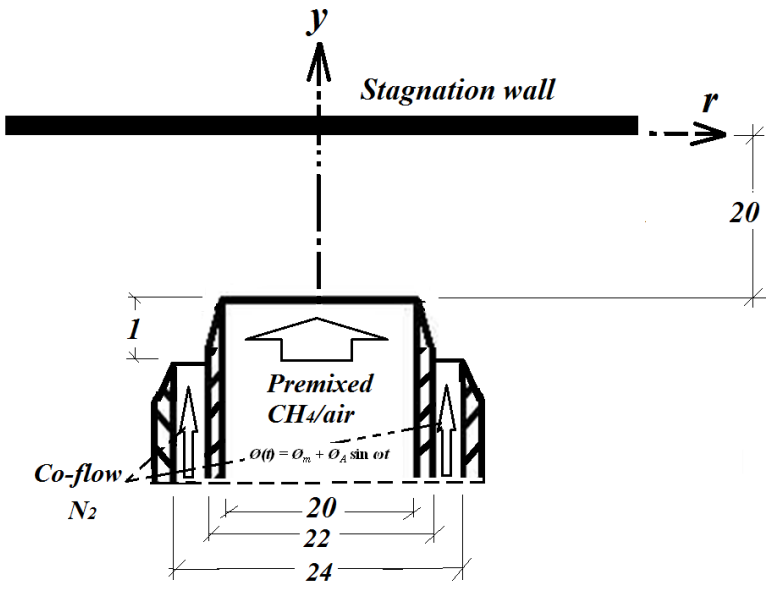

Figure 2-4 Schematic of the nozzle section with coordinate system.

2.2.3 Equivalence ratio oscillation system

The equivalence ratio oscillation was produced by injected lean and rich equivalence ratio into the primary flow from a secondary flow pipes at the mixing zone of the burner (Figs. 2-2 and 2-3). A detail of the mixing zone is shown in Fig. 2-5. Injection port consists of 16 holes with 1.5 mm in diameter at 32 mm upstream of the burner nozzle exit to inject CH_4/air mixture into the primary flow. The CH_4/air mixture was supplied into the injection port from 8 holes with 4.0 mm in diameter. Each incoming port was connected with two tubes, one for lean mixture and the other rich mixture. The CH_4/air mixtures with lean and rich equivalence ratios were supplied from the oscillator system simultaneously.

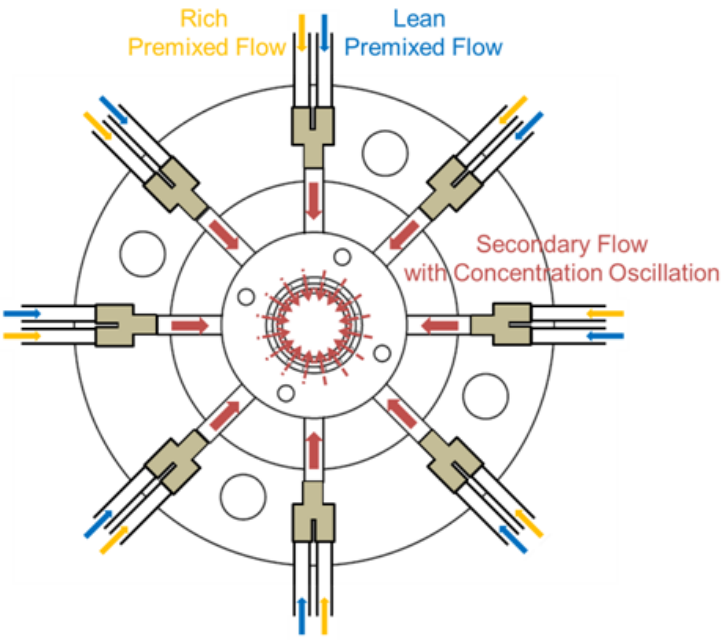

Figure 2-5 Mixing zone.

2.2.4 Oscillator system

Novel oscillator consists of two chambers with volume of 785 mm^3 each (bore × stroke = 10 mm × 10 mm) was developed. The oscillator body is made from an aluminum alloy. Moreover, the chambers lining and the pistons of the oscillator are made from high tempered glass. Cross-section of the oscillator is shown in Fig. 2-6. The oscillator piston moves by crank mechanism that connects to the DC motor (Oriental Motor Co., Ltd., brushless DC motor BLF46A-A-3) by pulley-belt system. This motor can produce 80 ~ 4000 rpm of the rotational speed with the accuracy ± 0.2 %. The piston moves up and down sinusoidal with a 180-phase lag for each. Sinusoidal movement of the piston causes the alternate supply of the CH_4/air mixture to the injection chamber.

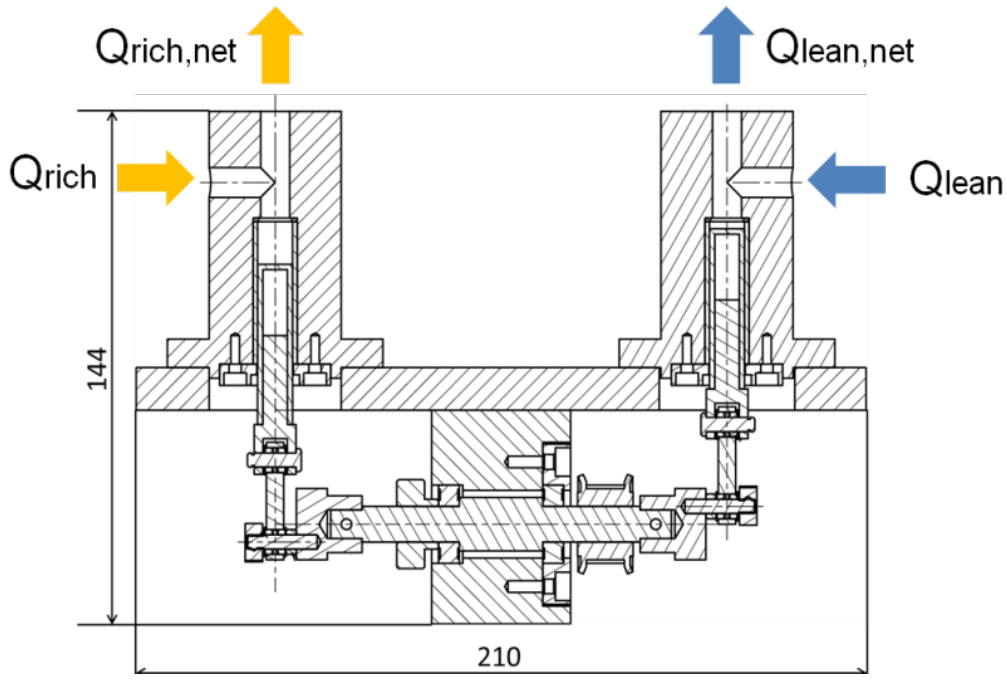

Figure 2-6 Cross-section of the oscillator.

2.3 Flow Dynamics analysis of the oscillator

2.3.1 Theoretical analysis

Flow dynamics analysis was carried out to examine the flow produces by the oscillator. Position of the each piston in the left and right, is represented by the following equation.

$$x_{rich,piston} = L\sin(2\pi ft) \tag{2-1}$$

$$x_{lean,piston} = L\sin(2\pi ft - \pi) \tag{2-2}$$

where, L is the half-stroke of the piston and $x_{rich,piston}$ and $x_{lean,piston}$ are the movement of the piston in a half cycle of the rich and lean chamber as shown in Figure 2-7. Flow rate variation of each chamber ($Q_{rich,chamber}$ and $Q_{lean,chamber}$) that contains the premixed gas is given by the product of piston velocity and piston cross-sectional area A_{cross} and dx_{piston}/dt.

$$Q_{rich,chamber} = A_{piston}\frac{dx_{rich,piston}}{dt} = 2\pi A_{piston} fL\cos(2\pi ft) \tag{2-3}$$

$$Q_{lean,chamber} = A_{piston}\frac{dx_{lean,piston}}{dt} = 2\pi A_{piston} fL\cos(2\pi ft - \pi) \tag{2-4}$$

Assuming that small amount volume of the mixture is leaked at rich Q_{rich} and lean Q_{lean} into the chambers. Therefore, net flow rate from the piston outlet for both rich and lean, is expressed in the following equations,

$$Q_{rich,net} = Q_{rich} + Q_{rich,chamber} = Q_{rich} + 2\pi A_{piston} fL\cos(2\pi ft) \quad (2\text{-}5)$$

$$Q_{lean,net} = Q_{lean} + Q_{lean,chamber} = Q_{lean} + 2\pi A_{piston} fL\cos(2\pi ft - \pi) \quad (2\text{-}6)$$

where the 180 phase lag phase is considered in Eq. (2-6).

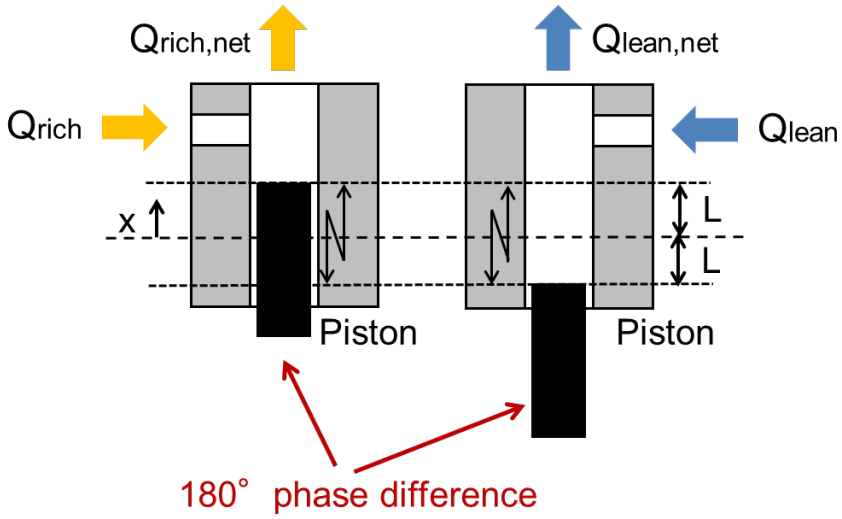

Figure 2-7 Piston movements.

Furthermore, the total flow rate Q_{total} at the exit burner nozzle is defined as,

$$Q_{total} = Q_{primary} + \left[Q_{rich} + 2\pi A_{piston} fL\cos(2\pi ft)\right] + \left[Q_{lean} + 2\pi A_{piston} fL\cos(2\pi ft - \pi)\right] \quad (2\text{-}7)$$

Thus, the total flow rate of the fuel and air at a given time, can be determined by the following equations,

$$Q_{fuel} = Q_{primary}Y_{primary,fuel} + \left[Q_{rich} + 2\pi A_{piston} fL\cos(2\pi ft)\right]Y_{rich,fuel}$$
$$+[Q_{lean} + 2\pi A_{piston} fL\cos(2\pi ft - \pi)]Y_{lean,fuel} \quad (2\text{-}8)$$

$$Q_{air} = Q_{primary}Y_{primary,air} + \left[Q_{rich} + 2\pi A_{piston} fL\cos(2\pi ft)\right]Y_{rich,air}$$
$$+[Q_{lean} + 2\pi A_{piston} fL\cos(2\pi ft - \pi)]Y_{lean,air} \quad (2\text{-}9)$$

In addition, the equivalent ratio is,

$$\emptyset(t) = \frac{(Q_{fuel}/Q_{air})}{(Q_{fuel}/Q_{air})_{st}} \quad (2\text{-}10)$$

where $(Q_{fuel}/Q_{air})_{st}$ is a stoichiometric equivalent ratio. It is found that, by substitutes Eqs. (2-8) and (2-9) into Eq. (2-10), gives sinusoidal variations in equivalence ratio at a given time (Fig. 2-8). Moreover, it is also found that the equivalence ratio oscillation amplitude produces by an oscillator increase monotonically following increases in injected equivalence ratio oscillation amplitude and oscillation frequency of the oscillator (Fig. 2-9).

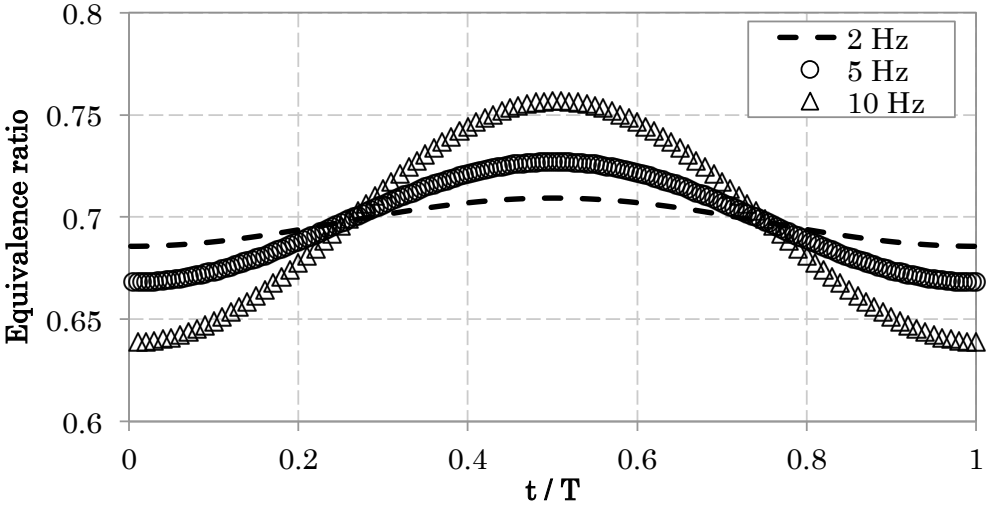

Figure 2-8 Equivalences ratio variations produces by oscillator in theoretical analysis at various oscillation frequency.

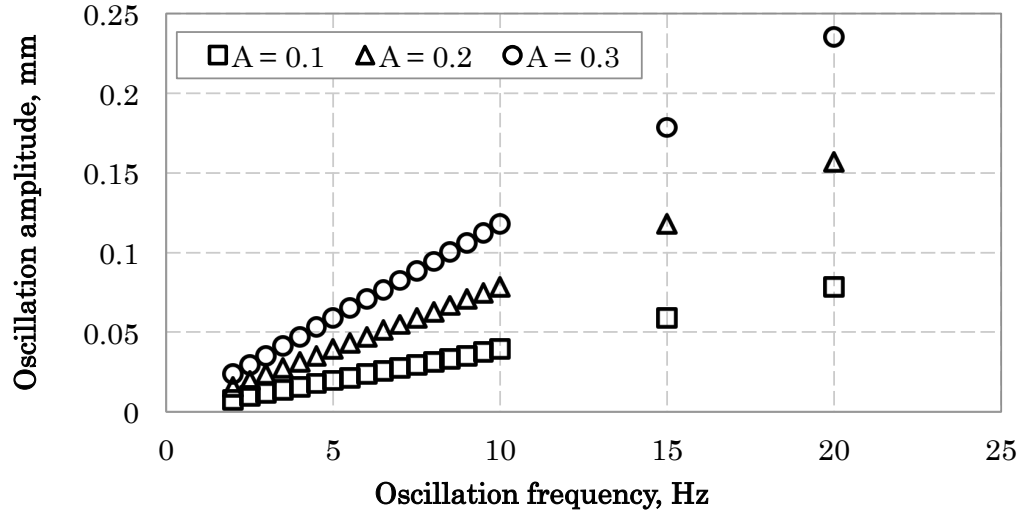

Figure 2-9 Oscillator behaviors as a function of the oscillation frequency.

2.3.2 Piston crank system

As previously mentioned, when the piston of the oscillator moves and rich mixture of the secondary flow flows into the injection chamber. On the other hand, lean mixture flow is stopped flowing into the injection chamber. An opposite working conditions of the rich and the lean secondary flow system produces constant mixtures flow without velocity perturbation. Following previous hypothesis, it is important to analyze the behavior of the oscillator as to examine the velocity perturbation.

Using a model of the piston crank mechanism shown in Figure 2-10, variations in flow rate produces by both chamber was analyzed. In Fig. 2-10, *a*, is a crank length, *b* is a length of the connecting and ω is an angular velocity.

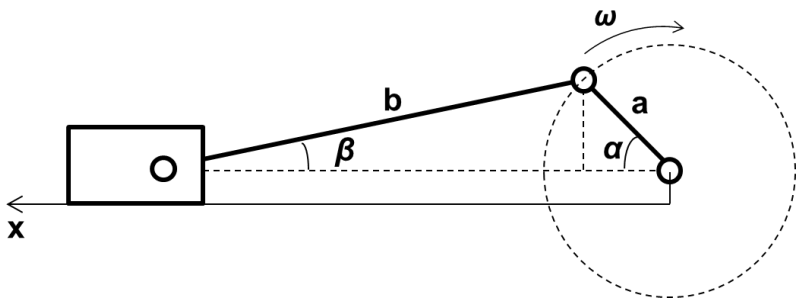

Figure 2-10 Piston crank model.

From Figure 2-10, the geometric relationship of the following holds,

$$\begin{cases} x = a\cos\alpha + b\cos\beta \\ a\sin\alpha = b\sin\beta \end{cases} \tag{2-11}$$

where, *x* is the position of the piston. Re-arranging for *x* in Eq. (2-11) gives,

$$x = a\cos\alpha + b\sqrt{1 - \left(\frac{a}{b}\sin\alpha\right)^2} \tag{2-12}$$

By differentiating the Eq. (2-12) with respect to time, piston velocity could be obtained as,

$$v = \frac{dx}{dt} = -a\omega\left\{\sin\alpha + \frac{a/b\sin 2\alpha}{2\sqrt{1-(a/b\sin\alpha)^2}}\right\} \tag{2-13}$$

Therefore, flow rate of each sides in lean and rich secondary flow are as follows,

$$Q_{rich,piston} = -A_{piston}a\omega\left\{\sin\alpha + \frac{a/b\sin 2\alpha}{2\sqrt{1-(a/b\sin\alpha)^2}}\right\} \tag{2-14}$$

$$Q_{lean,piston} = -A_{piston}a\omega\left\{\sin(\alpha-\pi) + \frac{a/b\sin 2(\alpha-\pi)}{2\sqrt{1-\{a/b\sin(\alpha-\pi)\}^2}}\right\} \tag{2-15}$$

Based on the Eqs. (2-14) and (2-15), with the following physical data of the oscillator (Table 2-1), the flow rate produced by both pistons are plotted (Fig. 2-11). It can be seen that there is a slight offset of the flow rate fluctuation between both pistons from the hypothesis. Therefore, imperfect 180-phase lag between both pistons would produce fluctuation in velocity that disturbed the flow practically.

Table 2-1 Physical data

Oscillation frequency, f	[Hz]	5.0
Angular velocity, ω	[rad/s]	31.4
Crank length, a	[mm]	5.0
Connecting rod length, b	[mm]	23.0
Piston area, A_{piston}	[mm^2]	78.5

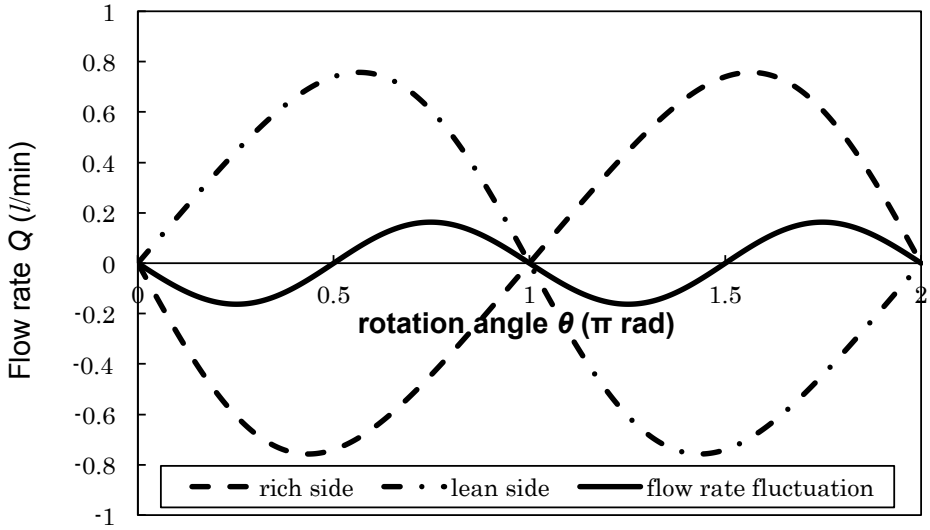

Figure 2-11 Flow rate fluctuations.

2.4 Measurement method

Flame position was measured by direct photograph using binaries image. Measurement was conducted by taken the flame movement images using high-speed video

camera (KEYENCE VW-6000) with Nikkor lens (Nikkor 58 mm F1.2). Still image was extracted from the video images using open source video playback software called GOM Player. Image analysis tools in Mathematica 8 were used to convert the image into binaries and measured the flame position. Figure 2-12 shows the definition of the flame positions. Flame position was determined as the lowest point of the binaries still image from the nozzle exit along the central axis of the burner exit nozzle.

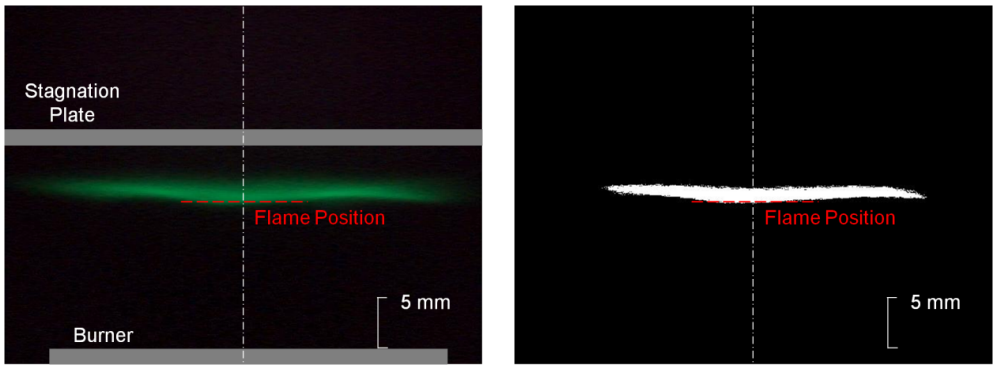

(a) Direct flame image (b)Binaries image

Figure 2-12 Definition of flame position.

2.4.1 Hot wire anemometer

Flow velocity variations were measured using hot wire anemometer. The Panasonic Corp. PC Let's Note and data acquisition system NR-350 KEYENCE PC card-type were used to record the output voltage. Sampling time is 1 ms and total time of minimum recorded data was 2.5 s. Figure 2-13, shows the measurement position and the measured interval is 1 mm.

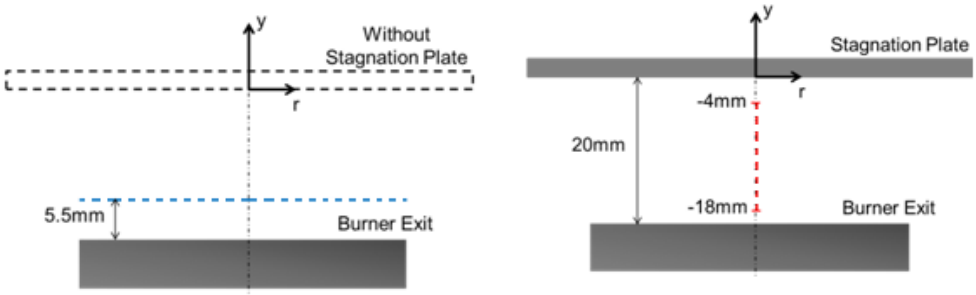

(a) Velocity profile (b) Velocity fluctuation

Figure 2-13 Measuring points.

2.4.2 Acetone Ultraviolet Light Induced Fluorescents

Schematic of the Ultra Violet Induces Fluorescent apparatus used in the present study is shown in Figure 2-14. In this study, the Hamamatsu Photonics LC8 ultra-violet light was used as a light source. A uniform intensity of the ultraviolet light was created by fixed the uniform illumination lens (E5147-06 manufactured by Hamamatsu Photonics) at the ultra-violet light source head. Light sheet with 2.0 mm thickness and 20.0 mm height was developed at the area above the burner nozzle exit using three spherical lenses and a slit. An optical arrangement is shows in Fig. 2-14.

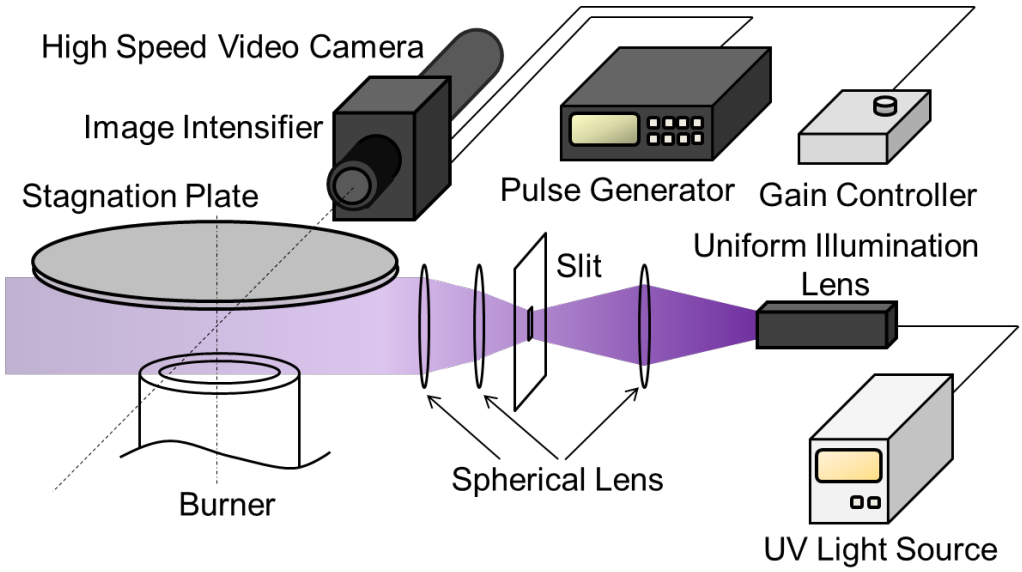

Figure 2-14 Schematic of the ultra violet acetone fluorescence with optical system.

Acetone vapor was added to the rich secondary flow by flows the rich secondary air through the acetone container as shown in Figure 2-15. Vaporization of the acetone was maintained by placing the acetone container in a water bath (AS ONE Co. HWA-50D) to keep the temperature at 20 ^{o}C. Needle valve was used to control the acetone volume fraction to confirm the sufficient fluorescence intensity to be observed by ICCD camera. The acetone fluorescence was recorded by a high-speed CCD camera (KEYENCE, VW-6000) with image intensifier (II, Delft Hi-Tech Co., Ltd. 1450 system) and Nikkor lens 58 mm F1.2 with auto extension ring (Nikon Inc. PK-11). Pulse generator and gain controller controlled opening time and light intensity of the image intensifier respectively.

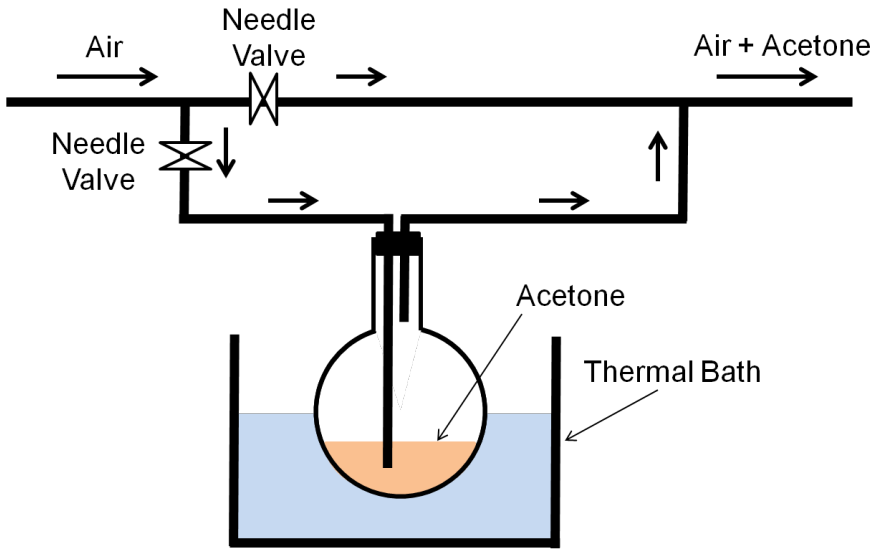

Figure 2-15 Acetone water bath system.

2.4.3 Synchronization

Local equivalence ratio concentration at the flame was calculated relative to the intensity of the acetone fluorescence at the flame position. An image analysis tool in the Mathematica 8 was used to extract the acetone luminescence based on the green luminosity. In this experiment, the acetone significantly affected the flame when it was flowing with CH_4/air mixture. Thus, it is impossible to measure the equivalence ratio concentration variation with the flame and then the synchronize system is needed.

Synchronize system was developed to lock the phase between acetone fluorescence and flame response. The synchronize system is shown in Fig. 2-16. Light from LED was transmitted to pulley of the oscillator. Reflections of the light by pulley were transmitting to high-speed camera by four mirrors. An image of the LED light was captured by high-speed camera for both experiments in thermal and isothermal condition. Later, image of the flame movement with LED light was superimposed in the image of the acetone

fluorescence to lock the phase.

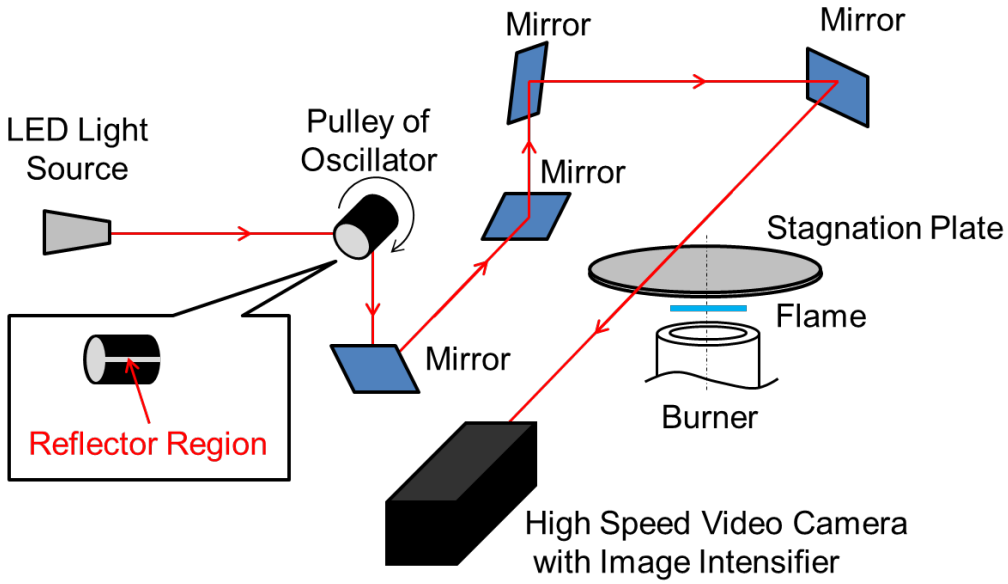

Figure 2-16 Phase synchronization method.

2.5 Results and discussion

2.5.1 Blowing ratio

Blowing ratio is an important parameter that characterizes the mixing in the cross flow mixing process. The blowing ratio is the ratio between momentum of the secondary flow and momentum of the primary flow,

$$BR = \left(\frac{\rho_{sec} v_{sec}^2}{\rho_{prim} v_{prim}^2}\right)^{1/2} \quad (2\text{-}16)$$

Shcwarz, 2010, conducted an experimental work of the conical flame and showed that higher number of the blowing ratio is needed to get the uniform distribution of the equivalence ratio. Unfortunately, increase in the blowing ratio produces velocity perturbation in primary flow because of the cross flow of the secondary flow disturbing the primary flows. In the present experiment, we found that by increasing the blowing ratio, it significantly disturbed the primary flow. Disturbance in the primary flow produced turbulent flow and the turbulent reduction method was used to suppress it. Thus, with the turbulent reduction method the blowing ratio BR = 4.5 was used in the present work.

2.5.2 Flow velocity variations

Figure 2-17 shows the flow velocity in the downstream side of the burner towards the stagnation plate at various oscillation frequencies. The measurement detail was explained in the Section 2.4.1. It is clearly seen that close to the burner exit (y = -16 mm) the variation in flow velocity is significant as increases in oscillation frequency. On the other hand, near the stagnation plate (y = -4 mm) the velocity variation is suppressed.

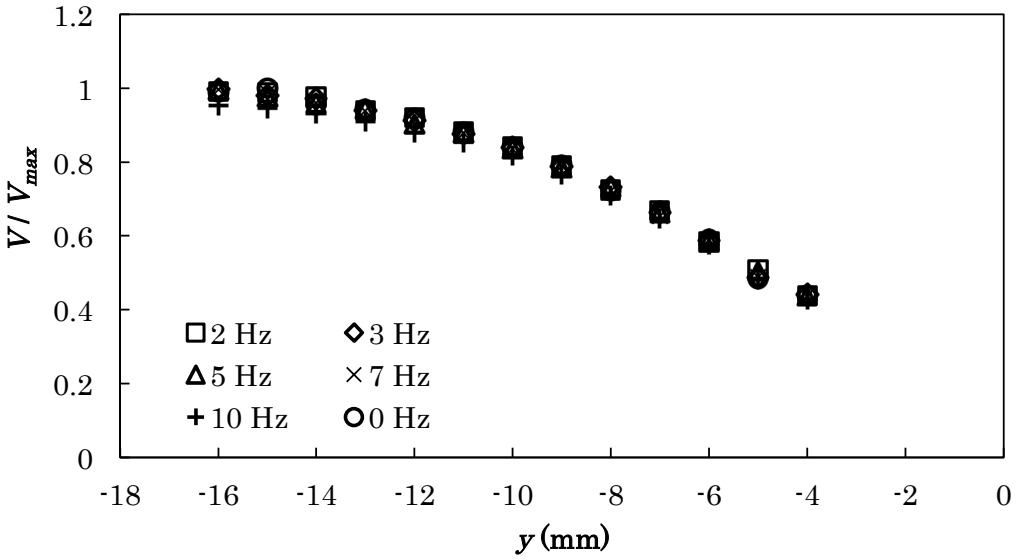

Figure 2-17 Flow velocity variations using hot-wire anemometer.

2.5.3 Effect of the equivalence ratio oscillation amplitude on flame dynamics

Stagnation laminar CH_4/air premixed flame was formed by issuing inlet velocity 0.8 m/s. Mean equivalence ratio is, $\phi_m = 0.7$ with the equivalence ratio oscillation amplitude of $\phi_A = 0.0$, 0.1, 0.2 and 0.3 at the oscillation frequency of f = 2, 5, 10 and 15 Hz were investigated. The equivalence ratio oscillation amplitude was focused in the lean region because the flame position is proportional to the equivalence ratio as shown in Fig. 2-18. In this experiment, an extinction limit is found at $\phi = 0.66$. The equivalence ratio oscillation amplitude is defined as the value of an equivalence ratio injected from the secondary flow and not a local value at a flame front in the present study.

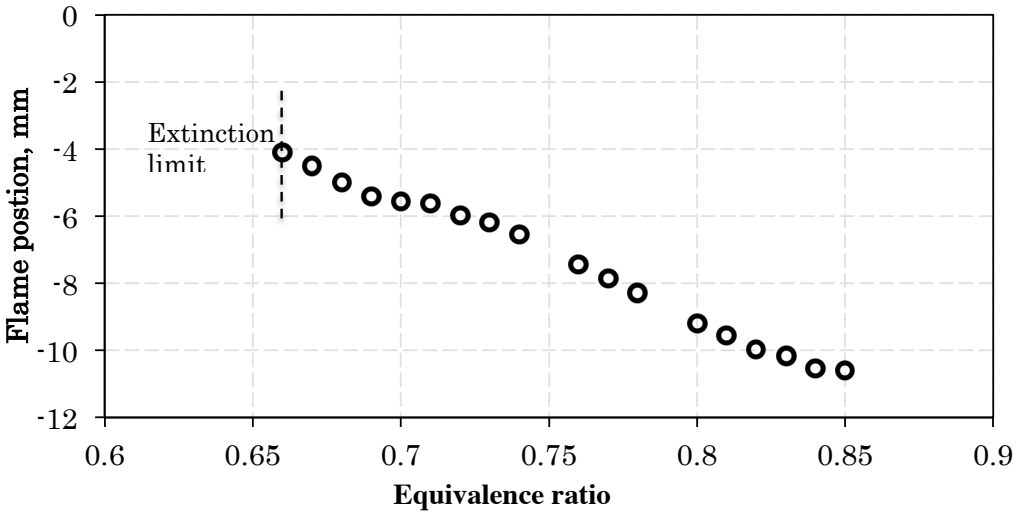

Figure 2-18 Flame position in a steady state case at various equivalence ratios.

Initially, it is important to verify an effect of the velocity perturbation on the flame dynamics. Velocity perturbation was examined by injecting the secondary flow that had an equal equivalence ratio as in primary flow. Injected equal equivalence ratio from secondary into primary flows suppressed the equivalence ratio variation. Thus, a movement of the flame at this condition is strongly due to velocity perturbation in the primary flow. Figure 2-19 shows the response of the flame position at various oscillation frequencies with $\phi_A = 0.0$ equivalence ratio oscillation amplitude. In Fig. 2-19, it is clearly seen that at 2, 5, 10, 15 and 20 Hz oscillation frequencies, the flame position variations is significantly small. Thus, it can be concluded that the velocity perturbation is significantly suppressed in the examination range.

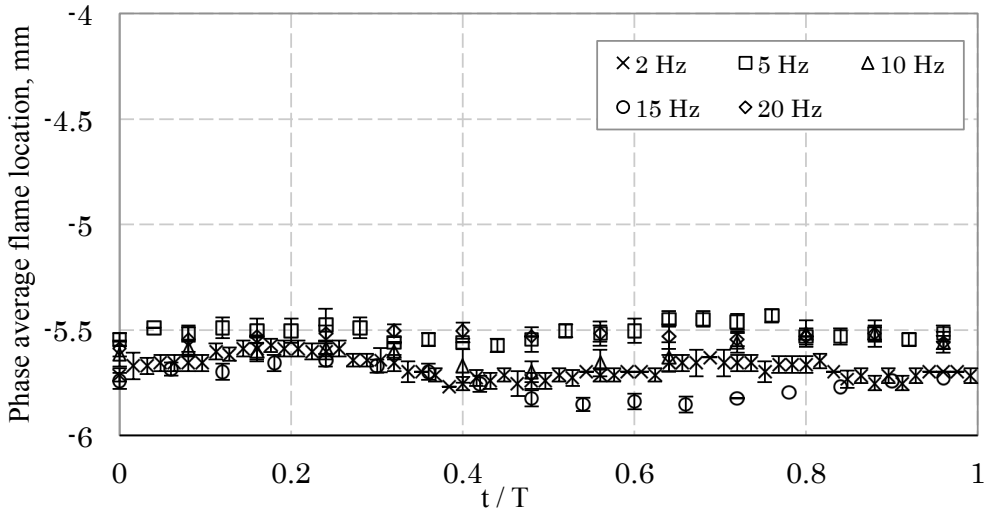

Figure 2-19 Cyclical variation of the flame position at 0.0 oscillation amplitude for various equivalence ratio oscillation frequencies.

Figures 2-20, 2-21, 2-22 and 2-23 show periodical variations of the flame position response to the equivalence ratio oscillation at f = 2, 5, 10 and 15 Hz of the oscillation frequency with the oscillation amplitude, $\phi_A =$ 0.0, 0.1, 0.2 and 0.3. It is important to determine the initial position of the flame movement because it will show the phase lag. Therefore, synchronizing system was used to evaluate the starting point of each oscillation case. In synchronizing system, each starting point is at the same location by referring to rotations of the oscillator pulley. Thus, every equivalence ratio oscillation cases are in a same phase. In Figs. 2-20, 2-21, 2-22 and 2-23 flame moves in sinusoidal shape and it is clearly seen that the flame movements is proportional to the amplitudes of the equivalence ratio variations. Since the velocity perturbation is significantly suppressed as shown in Fig. 2-19, the flame movement in Figs. 2-20, 2-21, 2-22 and 2-23 is primarily due to the equivalence ratio oscillations. At $\phi_A =$ 0.1, amplitude of the flame movements is low but it variations is larger than $\phi_A =$ 0.0 case. Significantly increase in the flame movement

amplitude is seen at $\phi_A = 0.3$ compared to $\phi_A = 0.1$ and 0.2 oscillation amplitudes.

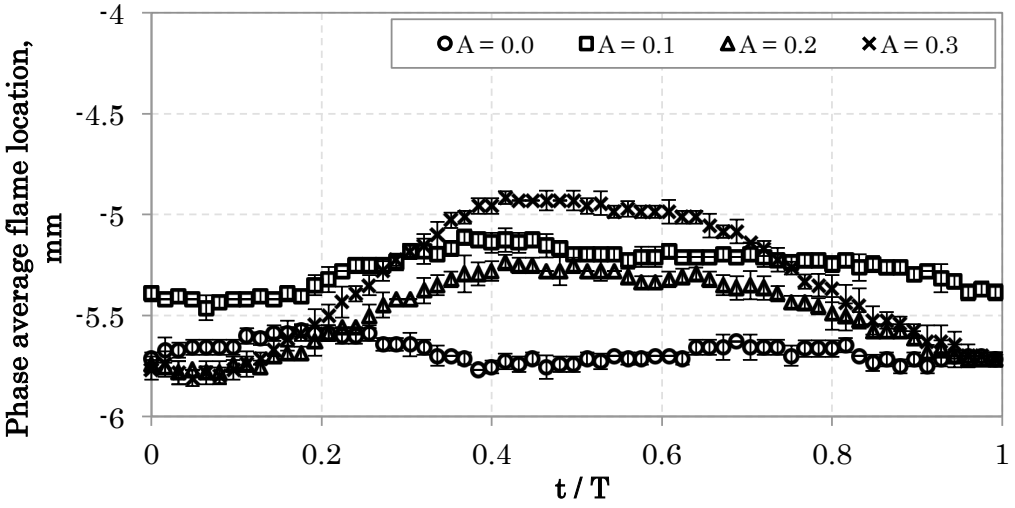

Figure 2-20 Cyclical variation of the flame position for 2 Hz case at various equivalence ratio oscillation amplitudes.

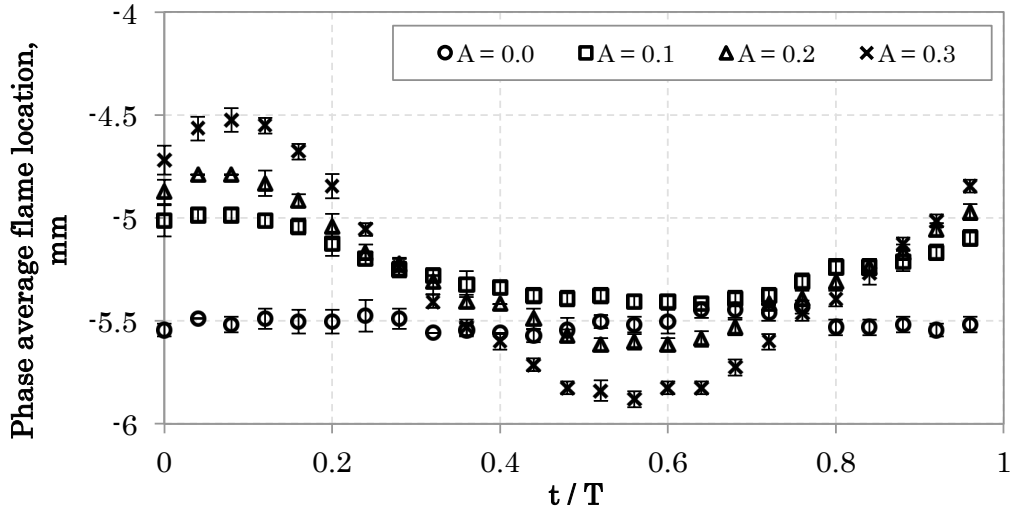

Figure 2-21 Cyclical variation of the flame position for 5 Hz case at various equivalence ratio oscillation amplitudes.

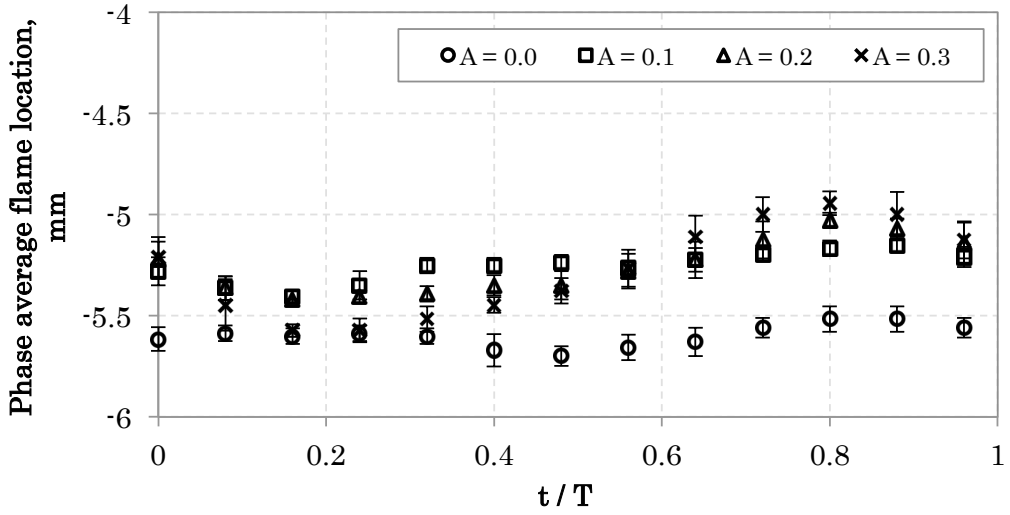

Figure 2-22 Cyclical variation of the flame position for 10 Hz case at various equivalence ratio oscillation amplitudes.

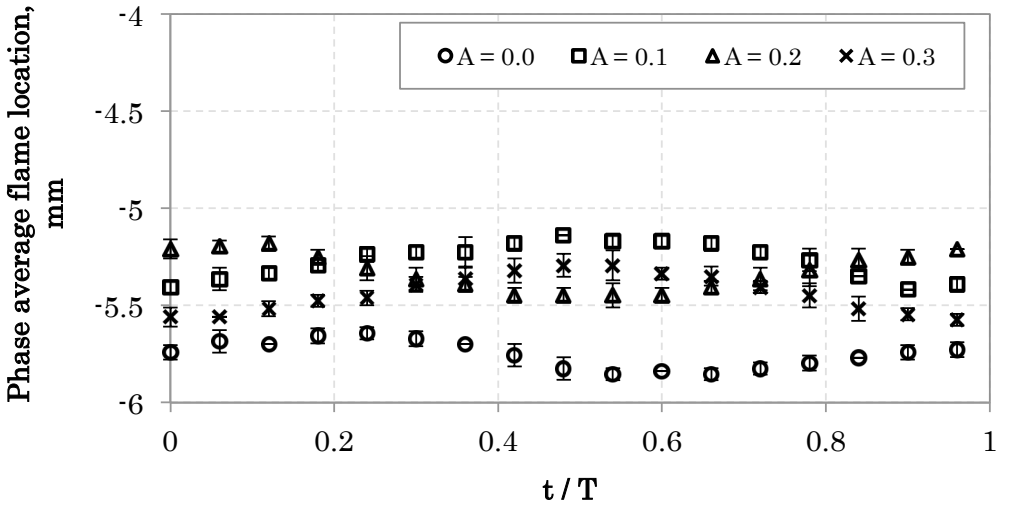

Figure 2-23 Cyclical variation of the flame position for 15 Hz case at various equivalence ratio oscillation amplitudes.

2.5.4 Effect of the equivalence ratio oscillation frequency on flame dynamics

Responses of the stagnation laminar premixed CH_4/air mixture flame to the equivalence ratio oscillation with mean equivalence ratio oscillation at, $\phi_m = 0.7$ and equivalence ratio oscillation frequency of f = 2 to 20 Hz with oscillation amplitude of $\phi_A = 0.1$, 0.2 and 0.3 were investigated. It is clearly shown that the flame movement amplitude is inversely proportional to the equivalence ratio oscillation frequency in Fig. 2-24. These behavior occur because, an attenuation of the equivalence ratio oscillation amplitude is significant towards the downstream direction as increase in oscillation frequency. Furthermore, it seen that the mean flame position is shifted towards the stagnation plate as increase in oscillation frequency at same equivalence ratio oscillation amplitudes.

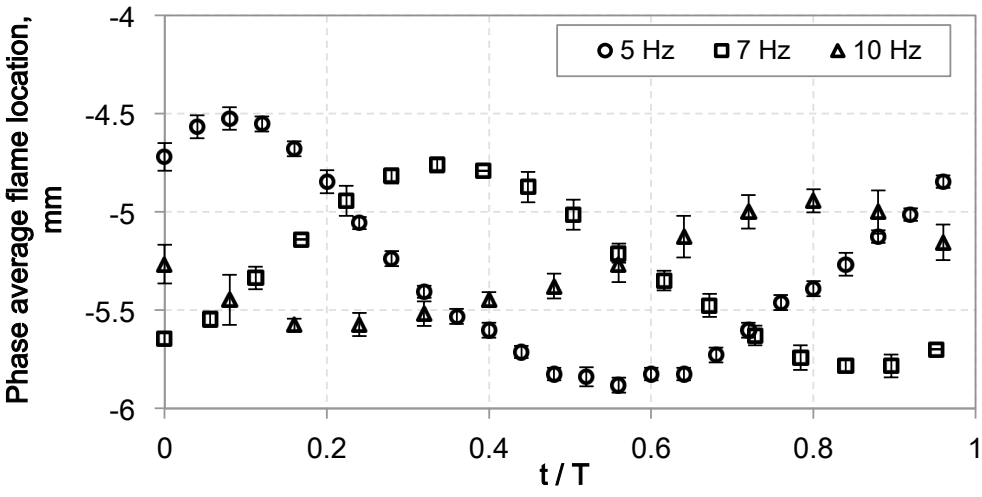

Figure 2-24 Cyclical variations of the flame location in experimental study with ϕ_m = 0.7, $\phi_A = 0.3$ at various oscillation frequency.

Previously, Figs. 2-20, 2-21, 2-22 and 2-23 for 2, 5, 10 and 15 Hz cases respectively

have showed an interesting behavior. The flame amplitude movement at 2 Hz is smaller than that 5 Hz case. On the other hand, the 5 Hz case is larger than that 10 and 15 Hz cases. These observations are ambiguity since the attenuation of the oscillation amplitude should be increased following the increases in the oscillation frequency. In order to examine these behaviors, Figs. 2-25 and 2-26 were plotted. Fig. 2-25 and 2-26 show variations of the flame oscillation amplitude and the mean flame position at various oscillation equivalence ratio frequencies and amplitude respectively. In both figures, the flame responses increase monotonically as a function of the oscillation frequency at 2 to 5 Hz cases. On the other hand, the flame responses decrease when the oscillation frequency increasing beyond the 5 Hz. Moreover, in Fig. 2-26, it is seen that small/significant variations of the mean flame position at 2 to 5 Hz/ beyond 5 Hz cases exist as a function of the oscillation amplitude. Based on these observations, the flame dynamics could be divided into two categories namely quasi-steady and unsteady regimes. In the unsteady regime (> 5 Hz) it is clearly seen that an attenuation of the flame movement amplitude increases significantly and mean flame position also varies significantly following an increases in oscillation frequency. While, in the quasi-steady regime small variations of the mean flame position and monotonically variation of the flame movement oscillation amplitude, as a function of the oscillation frequency exists. Monotonically variation in the quasi-steady regime is supposed to be influenced by the oscillator. A clarification of this observation was done by examining the theoretical analysis of the flow dynamics produces by the oscillator in Sec. 2.2.1. Previously, Figure 2-9 shows that amplitude of the equivalence ratio variation produces by the oscillator increases as increase in oscillation frequency. This analysis was verified by measurement of the acetone luminescence and it give the similar trend at 2 and 5 Hz oscillation frequency (Fig. 2-27). Thus, in the present study, the flame dynamics in

quasi-steady regime influenced by the characteristic of the oscillator and monotonically variation exists.

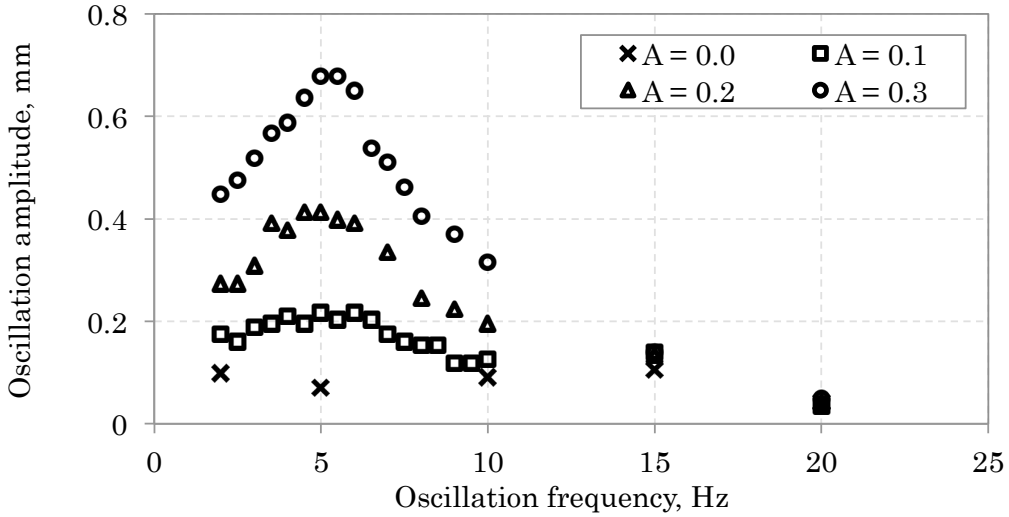

Figure 2-25 Oscillation amplitude variations of the flame location in experimental study with $\phi_m = 0.7$ at various equivalence ratio oscillation frequency and amplitudes.

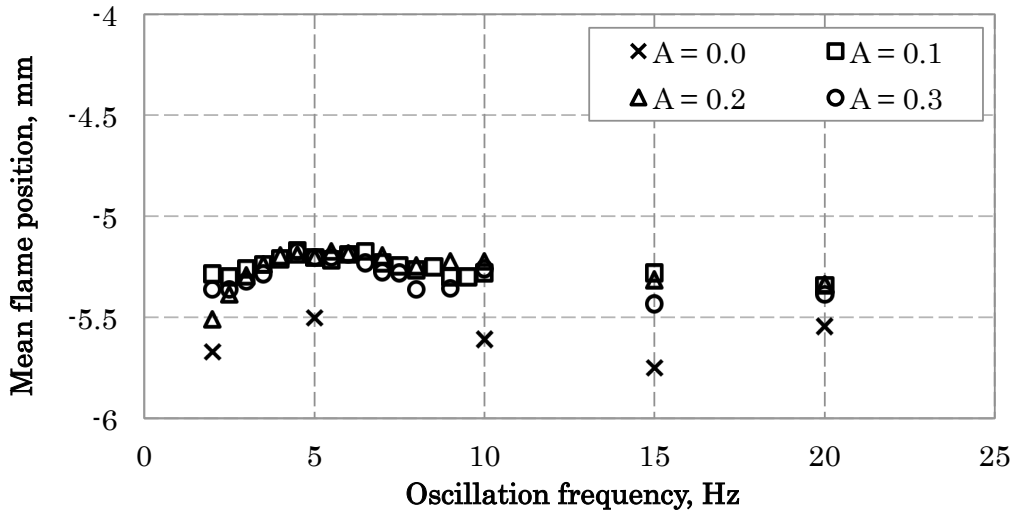

Figure 2-26 Mean flame position variations at various oscillation frequency and amplitudes.

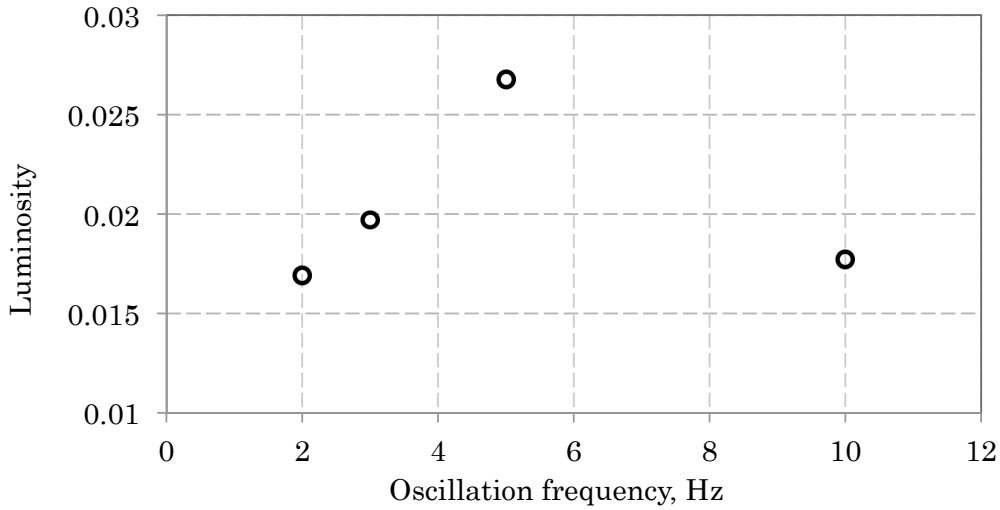

Figure 2-27 Variations in acetone luminescence (luminosity) at various oscillation frequency.

Figure 2-28 shows the oscillation amplitude variations of the flame location as a function of *Strouhal* number. In this study, the *Strouhal* number is defined as a ratio between the characteristic time of flow (L / U_o) and the characteristic time of oscillation ($1/2\pi f$). L and U_o, are defined as a length from the nozzle exit burner to the stagnation plate and a velocity inlet respectively. It is clearly seen in Fig. 2-28, the oscillation amplitude variation decreases significantly beyond the St = 1.0. In the previous discussion, the oscillation amplitudes of the flame location are divided into two regimes, quasi-steady and unsteady regimes. In the unsteady regime, the amplitude variation decreases significantly. Thus, a ratio between the characteristics time of the flow and the characteristics time of the oscillation called *Strouhal* number is an important parameter that divide the dynamics of the laminar premixed flame in quasi-steady (St < 1.0) or unsteady (St > 1.0) manner.

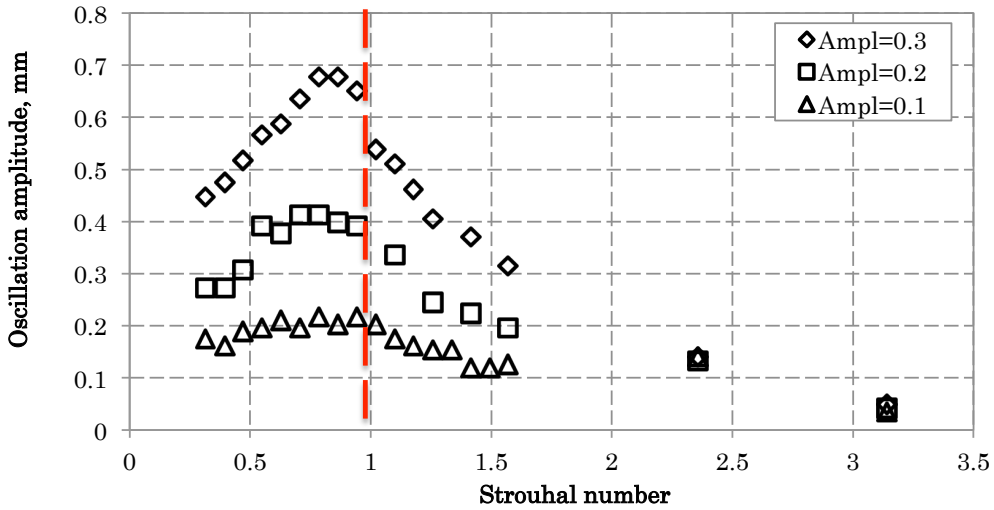

Figure 2-28 Oscillation amplitude variations of the flame location in experimental study with $\phi_m = 0.7$ as a function of *Strouhal* number and equivalence ratio oscillation amplitudes.

2.6 Concluding remarks

The effect of the equivalence ratio oscillation on a premixed laminar CH_4/air flame motion was studied experimentally using stagnation flow field burner. The flame response to the oscillation frequencies of the equivalence ratio of 2 to 20 Hz at lean oscillation case was investigated. Novel oscillator does the oscillation conditions and significant suppression of the velocity perturbation was achieved by turbulence reduction method.

The flame movement amplitude increases as increase in oscillation frequency at 2 to 5 Hz oscillation frequency. Increase in the flame movement amplitude is found because of the characteristics of the oscillator influences flame dynamics in the quasi-steady regime. On the other hand, beyond the 5 Hz increase in the oscillation frequency significantly decreases the flame movement amplitude. Decrease in the flame movement amplitudes as increase in oscillation frequency is in agreement with numerical result. It is because the

attenuation of the equivalence ratio oscillation amplitude is significant as increase in oscillation frequency. As a result flame movement amplitude decreases. Moreover, phase shift of the flame movement at different oscillation frequency is seen as increase in oscillation frequency. In a nutshell, a ratio between the characteristics time of the flow and the characteristics time of the oscillation called *Strouhal* number is an important parameter that categories the dynamics of the laminar premixed flame in quasi-steady ($St < 1.0$) or unsteady ($St > 1.0$) manner.

Chapter 3

Dynamics of the stagnation laminar premixed flames – A numerical study

3.1 Introduction

Laminar strained flames under equivalence ratio oscillation produced by counter flow configuration was simulated by Lauvergne and Egolfopoulos (2000). Their results showed that the flame response was due to the time required for a perturbation to propagate through a flame layer and was predictable from the history of the incoming flow. Moreover, the equivalence ratio oscillation also extended the extinction limits as a result of the amplitude attenuation caused by the diffusion (Egolfopoulos and Campbell, 1996). Sankaran and Im (2002) investigated the strong and weak strain rate and observed that the dynamic flammability limit was dependent upon the mean equivalence ratio and frequency of the oscillation and established concept of the flame dynamic flammability limit. They also observed that the flammability limit is extended to a leaner condition with increasing frequency or mean equivalence ratio oscillation (Sankaran and Im, 2002). Multidimensional flame responded to the equivalence ratio oscillation was conducted by Birbaud *et al.* (2008) using inverted "V" flame shaped. They found that a high level

modulation induces axial velocity perturbations, which in turn, interacts with the flame and modifies its responses.

Analysis performed by Cho and Lieuwen (2005) and Hemchandra (2010) also provides valuable information regarding equivalence ratio oscillation. They found that disturbance in reaction heat and flame speed was directly generated by equivalence ratio oscillations and indirectly caused the flame pattern to vary. In a nutshell, all researches to date have represented the flame speed based on the consumption speed and few have discussed the flame displacement speed. Unfortunately, the consumption speed does not correctly represent the response of the flame speed as reported by Hawkes and Chen (2006). They found that in general, consumption speeds showed poorer correlation to laminar models than displacement speeds. Furthermore, the flame location movements which is important to estimate the displacement speed due to the equivalence ratio oscillation has not been discussed in details in previous research, although Suenaga *et al.* (2005) pointed out the attenuation of the flame location movement with increasing oscillation frequency.

It is interesting to see the influence of the spatial and temporal perturbations of the equivalence ratio on the premixed flames motion, which has been less well explored than diffusion flames. Moreover, results of the experiment have shown that the flame response is significantly effected by the equivalence ratio oscillation frequency at $St > 1.0$. Therefore, our goal is to investigate and elucidate the dynamical flame responses to the equivalence ratio oscillation of the stagnating planar laminar premixed flame at $St > 1.0$.

3.2 Numerical analysis

3.2.1 Computational domain

The computational domain along with the boundary conditions and coordinate system are shown in Fig. 3-1.The analysis was performed in an axi-symmetric stagnation flow field. CH_4/air mixture is issued from inlet (1) with equivalence ratio fluctuation. Methane was used as a fuel because CH_4/air flames are well characterized in experiments and numerical calculations. In the present study, air is assumed to be a mixture of 21 mol% oxygen and 79 mol% nitrogen. Details of the boundary conditions are explained in Sec.

3.2.4.

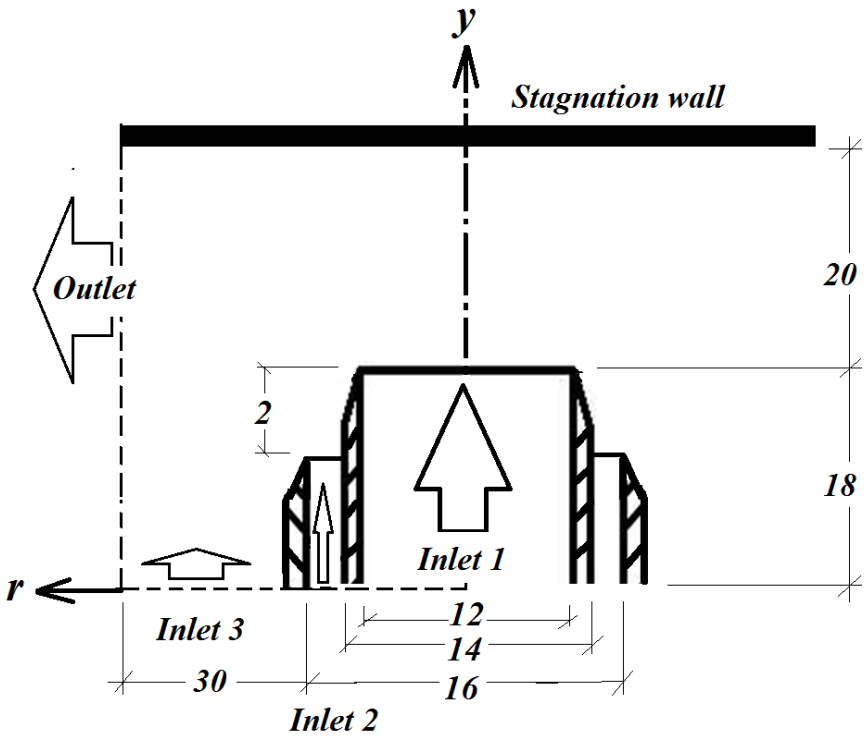

Figure 3-1 Computational domains with boundary conditions.

3.2.2 Governing equations

Chemically reacting flow are governed by the conservation laws of mass, momentum, energy and species. The conservation equations of mass and the momentum are given as following in the axi-symmetric coordinate (r, y),

$$\frac{\partial \rho}{\partial t} + \frac{\partial}{\partial y}(\rho v_y) + \frac{\partial}{\partial r}(\rho v_r) + \frac{\rho v_r}{r} = S_m \qquad (3-1)$$

$$\frac{\partial}{\partial t}(\rho v_y) + \frac{1}{r}\frac{\partial}{\partial y}(r\rho v_y v_y) + \frac{1}{r}\frac{\partial}{\partial r}(r v_r v_y) = -\frac{\partial p}{\partial y} + \frac{1}{r}\frac{\partial}{\partial y}\left[r\mu\left(2\frac{\partial v_y}{\partial y} - \frac{2}{3}(\nabla \cdot \vec{v})\right)\right] + \frac{1}{r}\frac{\partial}{\partial r}\left[r\mu\left(\frac{\partial v_y}{\partial r} - \frac{\partial v_r}{\partial y}\right)\right] + F_x \qquad (3-2)$$

$$\frac{\partial}{\partial t}(\rho v_r) + \frac{1}{r}\frac{\partial}{\partial y}\left(r\rho v_y v_r\right) + \frac{1}{r}\frac{\partial}{\partial r}\left(r v_r v_y\right)$$
$$= -\frac{\partial p}{\partial r} + \frac{1}{r}\frac{\partial}{\partial r}\left[r\mu\left(2\frac{\partial v_r}{\partial r} - \frac{2}{3}(\nabla\cdot\vec{v})\right)\right] + \frac{1}{r}\frac{\partial}{\partial y}\left[r\mu\left(\frac{\partial v_y}{\partial r} + \frac{\partial v_r}{\partial y}\right)\right] - 2\mu\frac{v_r}{r^2}$$
$$+ \frac{2}{3}\frac{\mu}{r}(\nabla\cdot\vec{v}) + F_r \qquad (3-3)$$

where y is the axial coordinate, r the radial coordinate, v_y and v_r the axial and radial velocities, S_m the source term, p the static pressure, F_x and F_r the external forces, μ the viscosity.

The energy and species conservation equations are,

$$\frac{\partial}{\partial t}(\rho E) + \nabla\cdot\left(\vec{v}(\rho E + p)\right) = \nabla\cdot\left(k\nabla T - \sum_{\mathrm{j}} h_i\vec{J_\iota} + (\bar{\bar{\tau}}\cdot\vec{v})\right) + S_h \qquad (3-4)$$

$$E = h - \frac{p}{\rho} + \frac{v^2}{2} \qquad (3-5)$$

$$\frac{\partial}{\partial t}(\rho Y_i) + \nabla\cdot(\rho\vec{v}Y_i) = -\nabla\cdot\vec{J_\iota} + R_i + S_i \qquad (3-6)$$

with the Fick's law for molecular diffusion,

$$\vec{J_\iota} = -D_{i,m}\nabla Y_i - D_{T,i}\frac{\nabla T}{T} \qquad (3-7)$$

where, $\bar{\bar{\tau}}$ is the stress tensor, k the thermal conductivity, S_h the heat formation of chemical reaction, h the specific enthalpy, $\vec{J_\iota}$ the diffusion flux of the species i, T the temperature, R_i the net rate of production of species i by chemical reaction, S_i the source term, Y_i the mass fraction of species i, $D_{i,m}$ the mass diffusivity for the species i in the mixture, and $D_{T,i}$ the thermal diffusion coefficient.

An ideal gas assumption was used and transport properties such as the viscosity and

heat conductivity of the individual species were estimated based on the kinetic theory. The specific heat was calculated using piece-wise-polynomial approximation, while the value of the transport properties of the mixture was calculated by the ideal gas mixing law. The thermal diffusivity and mass diffusivity of the mixture were estimated based on the kinetic theory. Moreover, Soret and Dufour effects and heat transfer by radiation are not considered in this study.

3.2.3 Chemical reaction model

Reaction rate is significantly depends on reactant concentration and temperature. A single forward chemical reaction is represent by

$$\sum_{i=1}^{N} v_i' M_i \overset{k_f}{\rightarrow} \sum_{i=1}^{N} v_i'' M_i \qquad (3-8)$$

Rate of change in the molar concentration c_i of species *i* is given as

$$\widehat{\omega}_i = \frac{dc_i}{dt} \qquad (3-9)$$

and related to $\widehat{\omega}_j$ of species *j* by

$$\omega = \frac{\widehat{\omega}_i}{v_i' - v_i''} = \frac{\widehat{\omega}_j}{v_j' - v_j''} \qquad (3-10)$$

Since ω is a species independent. Thus, it can be defined as reaction rate of Eq. (3-8) given by

$$\omega = k_f(T) \prod_{i=1}^{N} c_i^{v_i'} \qquad (3-11)$$

$k_f(T)$ is a specific reaction rate constant gives the reaction rate function on temperature.

The Arrhenius law states that

$$\frac{d \ln k(T)}{dT} = \frac{E_a}{R_o T^2} \qquad (3-12)$$

If E_a is a constant with respect to temperature, integrating Eq. (2-12) yields

$$k(T) = Ae^{-E_a/R_o T} \qquad (3-13)$$

where A is a pre-exponential factor (or frequency factor).

Global reaction is a lumped, one-step overall reaction involving starting reactants.

$$Fuel + Oxidizer \xrightarrow{k} Product$$

with the reaction rate given by

$$\omega = k \prod_{i=1}^{N} c_i^{n_i} \qquad (3-14)$$

where n_i is a reaction rate order with respect to the i th species.

CH_4/air mixture was used in this study. The CH_4/air combustion mechanism is very complex, consisting of hundreds of elementary reactions between dozens of intermediate gas species (Smith *et al.*), which uses lot of computation time. In the present study, detailed chemical information is not necessary and than the, the simplified mechanism that is able to predict variables of the flame dynamics experimentally is sufficient. Therefore, in this study we use an overall one-step reaction model and calibrate the flame speed to produce the data that agrees with the published data. The overall one-step reaction model as follows,

$$CH_4 + 2O_2 \longrightarrow CO_2 + 2H_2O \qquad (3-15)$$

The Arrhenius type reaction rate model (Westbrook and Dryer, 1981) as mentioned in Eq. (3-16) was used.

$$r_{CH4} = 7.24\times10^{11} \exp\left(-\frac{2.027\times10^{8}\left(\frac{\text{J}}{\text{kmol}}\right)}{RT}\right)\times[CH_4]^{0.2}[O_2]^{1.3} \qquad (3-16)$$

Following the suggestion by Westbrook and Dryer (1981), only pre-exponential factor is important in modifying the flame speed while the modification in an activation energy will change the flame thickness. Thus, the pre-exponential factors for the one-step was adjusted and comparing the flame speed with published data (Westbrook and Dryer, 1981, Pires *et al.* 2000 and Hemchandra, 2012) at around $\emptyset$=1.0 where the flame speed is at the maximum value. Initially, an original value of the pre-exponential by Westbrook and Dryer (1981) ($A = 6.7 \times 10^{12}$) was used. Unfortunately, the flame speed is higher and large deviation of the flame speed is obtained compare with the published data. Then, value of the pre-exponential factor is modified until the flame speed is comparable with the published data.

3.2.4 Boundary and initial conditions

1) Inlet (1): CH_4/air mixture is issued. The uniform velocity profile is assumed. The velocity and temperature are set as, v = 1.0 m/s and T = 300 K. The methane and air mass fractions were varied sinusoidal to make the equivalence ratio variation, keeping the volume flow rate constant. The equivalence ratio variation is expressed by; $\emptyset(t) = \emptyset_m + \emptyset_A \sin \omega t$. For example, the methane mass fraction is expressed by; $Y_{CH4}(t) = Y_{CH4m} + Y_{CH4A} \sin \omega t$.

2) Inlet (2): N_2 flows in with uniform inlet velocity, v = 1.0 m/s and T = 300 K.

3) Inlet (3): Air flows in with uniform inlet velocity, v = 0.01 m/s and T = 300 K. This is to prevent recirculation between the burner and the external boundary.

4) Axis of symmetry: The centerline of the burner corresponds to the axis of symmetry, hence the boundary conditions are $v_r = 0$ and $\frac{\partial}{\partial r} = 0$.

5) Stagnation surface (Wall): The stagnation surface was treated as an impermeable wall, i.e. a no-slip boundary condition was assumed for velocity and $\frac{\partial Y_i}{\partial r} = 0$ was assumed for all species. An adiabatic condition is assumed.

6) Outlet boundary (Outlet): The boundary from where the fluid flows out is assumed to be $\frac{\partial}{\partial r} = 0$.

3.2.5 Computational method

The Ansys. FLUENT 12.1 was employed to solve a set of conservation equations numerically. All conservation equations were solved using a segregated solver with an under relaxation method. Variable size grid with a minimum grid size of 1×10^{-5} m × 1×10^{-5} m was used. The fine grid is set in the region where the flame moves to deal with higher temperature and concentration gradients around the flame zone.

The isothermal flow field was first calculated. The mixture artificially ignited by setting the temperature at the ignition zone shown in Fig. 3-1 at 2500 K. When the reaction started and the flame was formed, the artificial ignition temperature was off and the flame was freely moved to a stable position at which the incoming unburned velocity to the flame was equal to the laminar burning velocity. Subsequently, the equivalence ratio at the inlet (1) was varied sinusoidal with the time step 1×10^{-5} s. The frequency of the equivalence ratio variation varies 10, 20 and 50 Hz. The simulations were performed on a quad-cores 3.33 GHz Intel Xeon processor with 12.0 GB RAM.

3.3. Results and discussion

3.3.1 Validation of the reaction model

Investigating the flame thickness and laminar flame speed has made to validate the one-step reaction model. The flame thickness at stoichiometric equivalence ratio is about 1

mm (Fig. 3-2) and the flame speed (Fig. 3-3) is agreed with the previous work done by Westbrook and Dryer (1981) and Hemchandra (2012) using one-step reaction model and Pires *et al.* (2000) using GRI 2.11 mechanism with 177 reactions and 32 species. Moreover, Fig. 3-4 shows streamlines and reaction rate contours in the lean and rich sides for the lean rich crossover case of the equivalence ratio oscillations at 10 Hz. The difference of the streamline pattern and reaction region shape is predicted as a function of equivalence ratio (Ø), indicating that the flow field and the flame vary with time. It can also be seen that the flame location moves, because the flame freely adjusts its position in response to the equivalence ratio variation in order to balance the laminar burning velocity of each equivalence ratio with the approaching unburned mixture velocity.

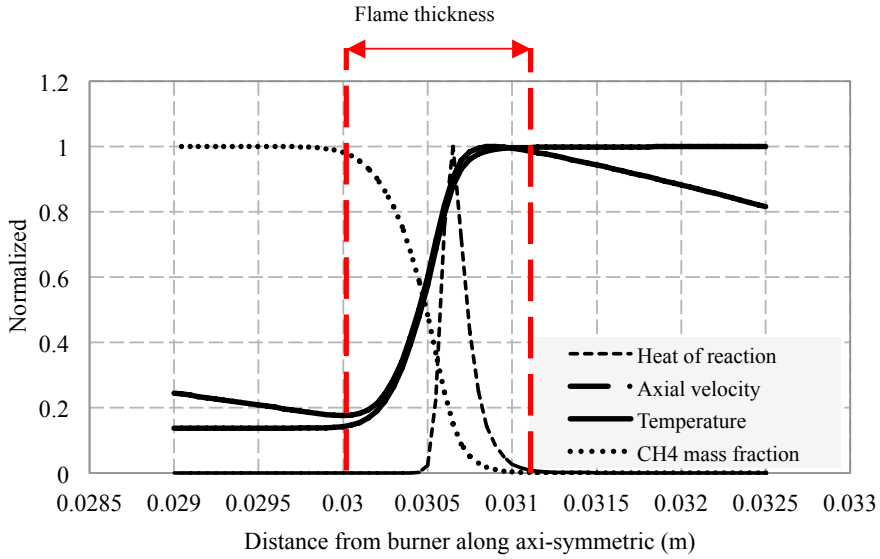

Figure 3-2, Flame structure at stoichiometric equivalence ratio.

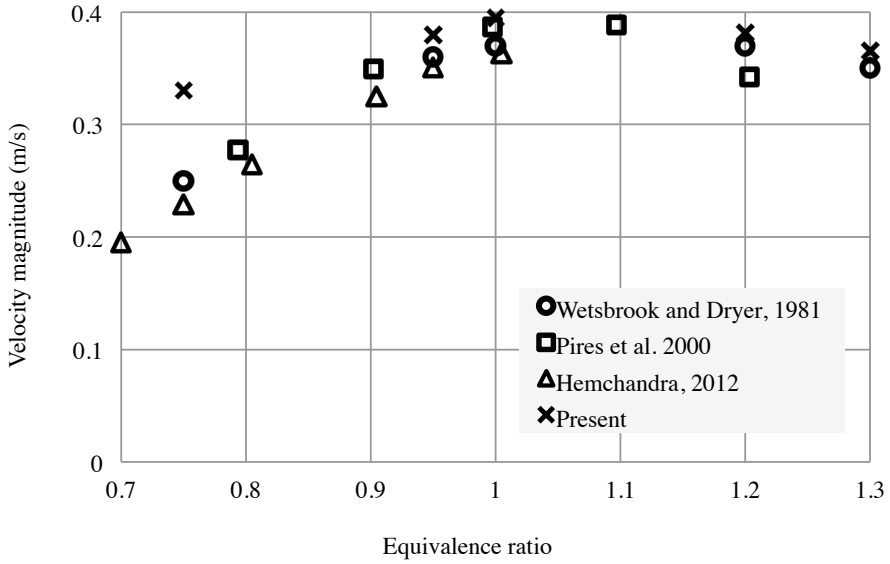

Figure 3-3, Laminar flame speed at various equivalence ratio.

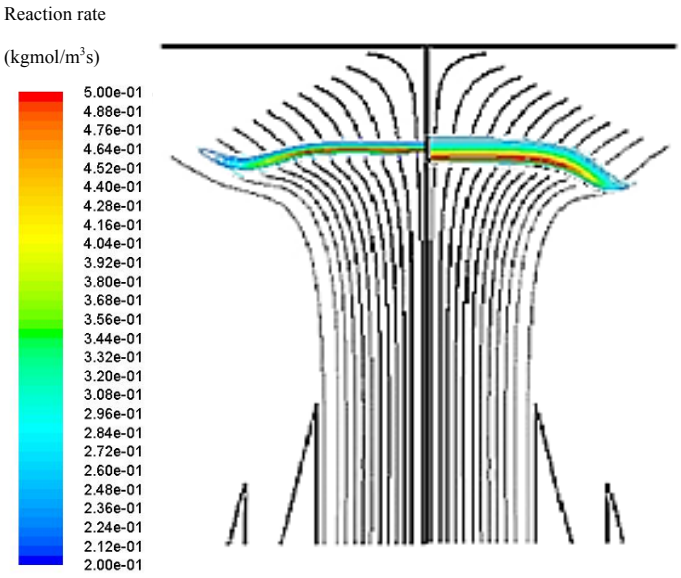

(a) (b)

Figure 3-4 Streamline and reaction rate contour at 10 Hz (a) $\emptyset(t)$=1.2, $\emptyset_m$=1.0, $\emptyset_A$=0.3 (b) $\emptyset(t)$=0.8, $\emptyset_m$=1.0, $\emptyset_A$=0.3.

3.3.2 Attenuation of the equivalence ratio oscillation

Figure 3-5 plots the attenuation of the equivalence ratio oscillation amplitude along the centerline from the inlet nozzle to the flame front. It is noticeable that the fuel

concentration oscillation amplitude imposed at the nozzle inlet is not the actual amplitude that affects the flame, which corresponds to results of Egolfopoulos and Campbell (1996) and Lauvergne and Egolfopoulos (2000). Figure 3-5 also shows that the amplitude attenuation is much significant for higher frequency of equivalence ratio oscillation.

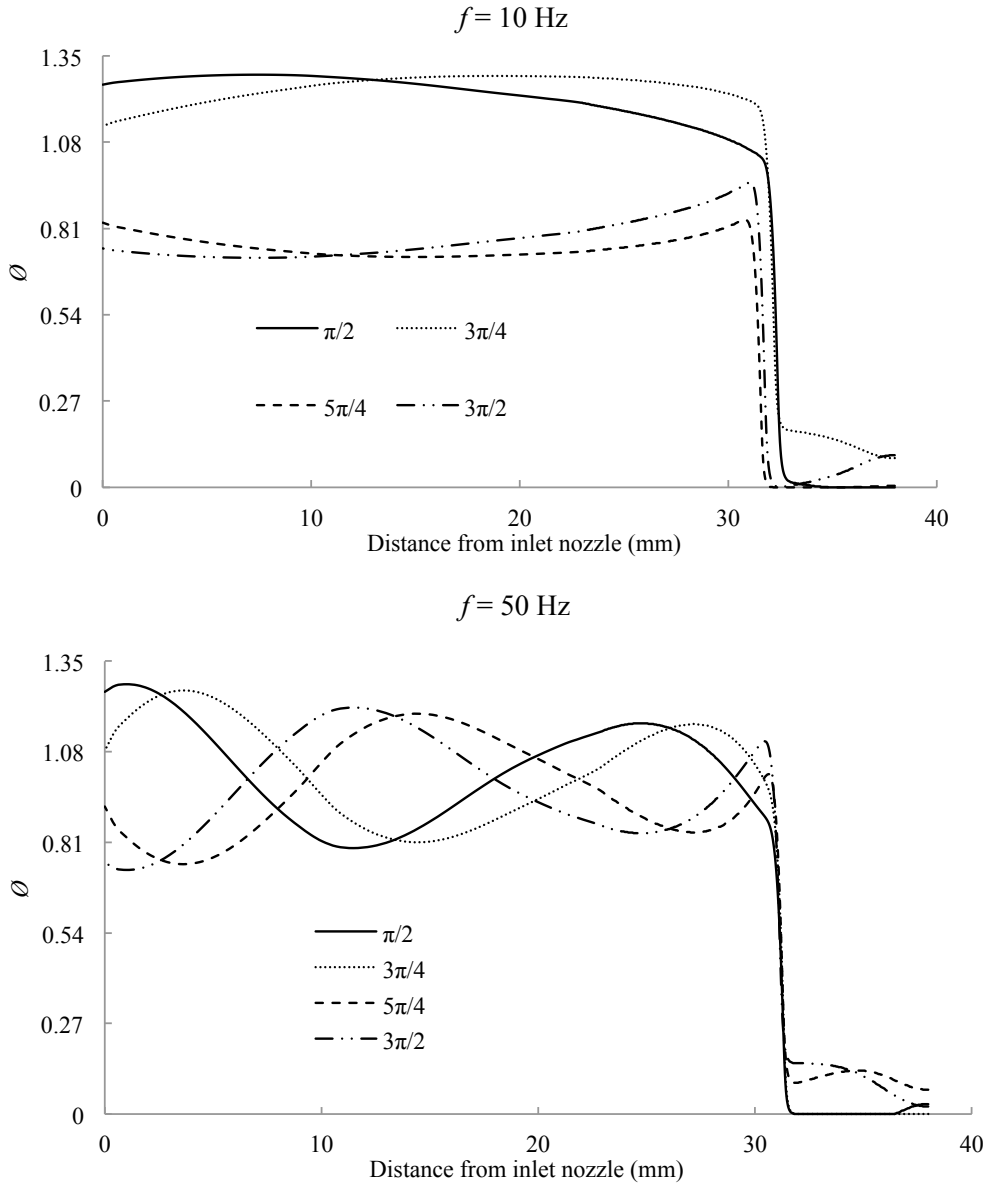

Figure 3-5 Attenuation of the equivalence ratio variation along the central axis (r =0) as a function of the oscillation frequency at $Ø_m$ = 1.0 and $Ø_A$ = 0.3

3.3.3 Flame response

In order to discuss the flame response by using numerical result, we defined variables that represent the flame characteristics as shown in Fig. 3-6. Figure 3-6 shows location of the variables in the present study. The flame location (y_f) is defined as the location where the heat release rate reaches maximum. The flame temperature (T_f) is measured at the location where the velocity profile becomes maximums. The unburned flow conditions, that is the unburned gas velocity (u_f) and the equivalence ratio ($\emptyset_f$) of the unburned mixture, are estimated at the location where the approaching flow velocity becomes minimum, where correspond to the upstream edge of the preheat zone.

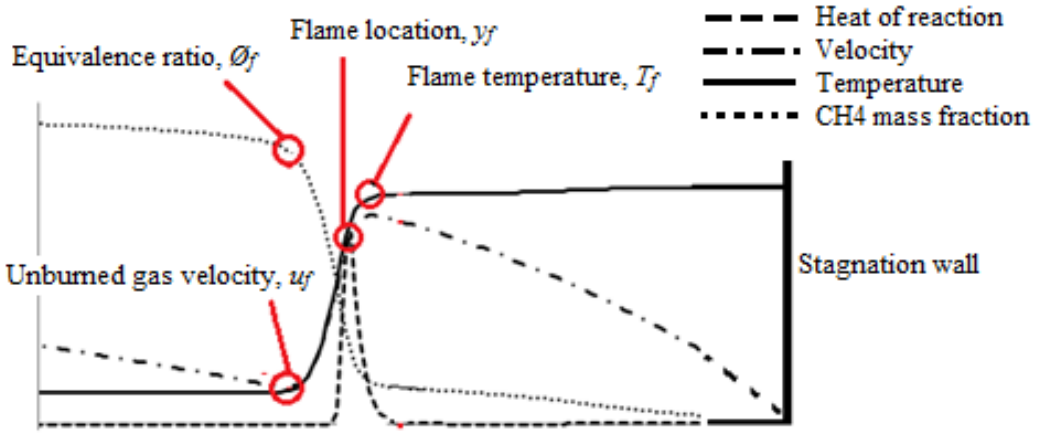

Figure 3-6 Measurement points of the respective variables along the central axis ($r = 0$)

The flame response for oscillation frequency of 10, 20 and 50 Hz in lean, rich and lean rich crossover cases was calculated. Figures 3-7 to 3-10, show the periodical variations of the equivalence ratio in upstream edge of the preheat zone ($\emptyset_f$) and the response of the flame temperature (T_f) in one period. In these figures, the simulation time was normalized with a period of each oscillation frequency (T). Figures 3-7 and 3-8 shows the results of the lean case with $\emptyset_m$=0.75 and $\emptyset_A$=0.1.

It can be seen that the amplitude of the equivalence ratio oscillation decreases with increasing frequency as mentioned in Sec. 3.2, which corresponds to the results of previous studies (Egolfopoulos and Campbell, 1996) and Lauvergne and Egolfopoulos, 2000). Furthermore, increase in the oscillation frequency decreases the flame movement

amplitude and the mean flame position is shifted towards downstream region (Fig. 3-7). These observations are also seen in the experimental work as shown in Fig. 3-8. Thus, the attenuation of the flame movement as increase in oscillation frequency is due to the attenuation of the equivalence ratio oscillation frequency at high oscillation frequency.

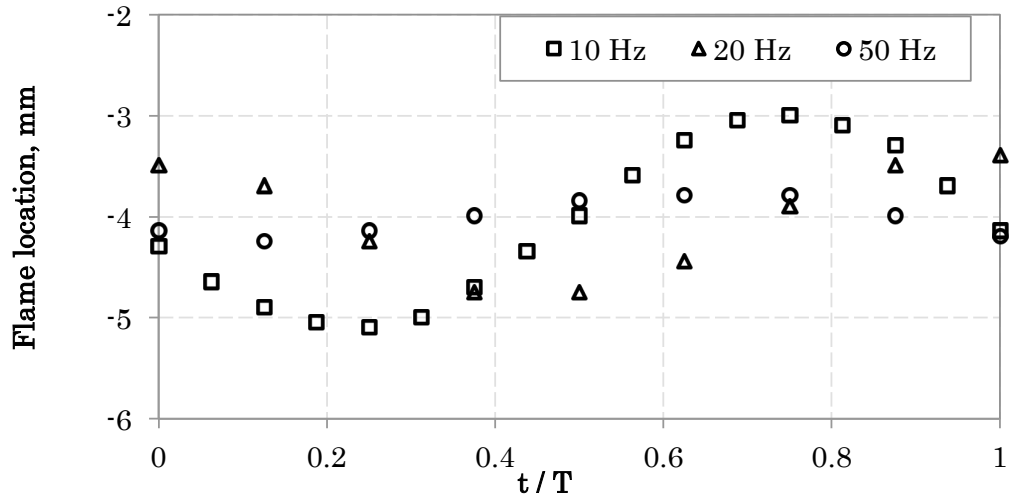

Figure 3-7 Cyclical variations of the flame location in numerical study with $\emptyset_m = 0.75$ and $\emptyset_A = 0.1$ at various oscillation frequency.

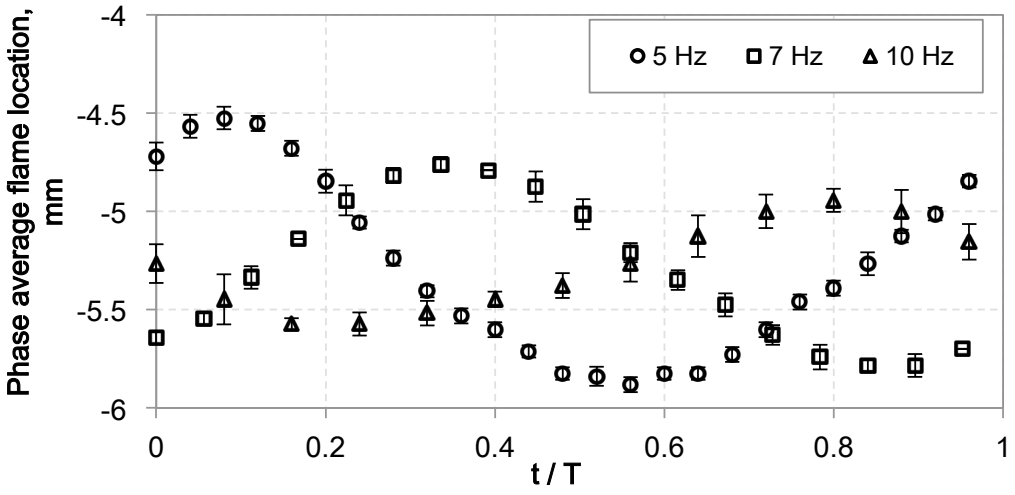

Figure 3-8 Cyclical variations of the flame location in experimental study with $\emptyset_m$ = 0.7 and $\emptyset_A$ = 0.3 at various oscillation frequency.

In the lean case, the temperature increases following increase in the equivalence ratio

because it approaches to the stoichiometric condition. As a result, the flame temperature (T_f) increases.

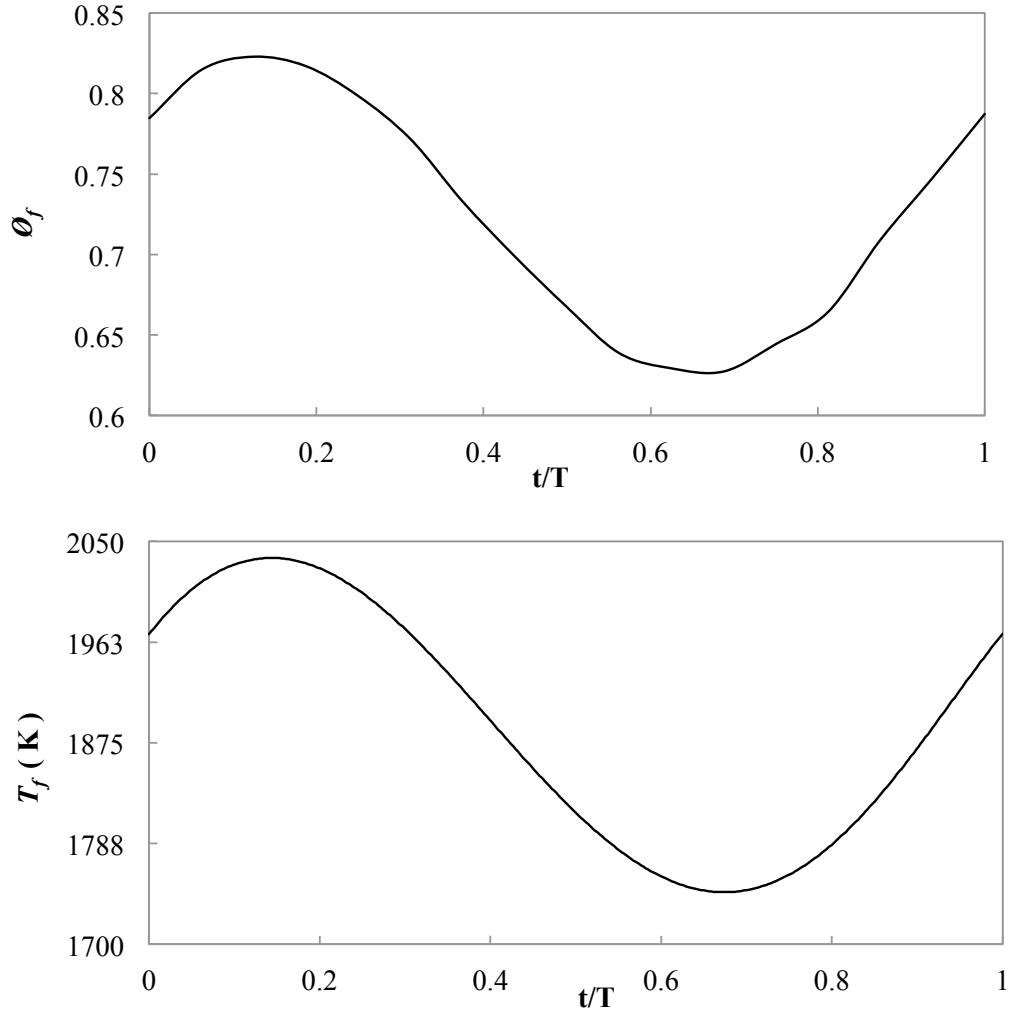

Figure 3-9 Variationsin the equivalence ratio in upstream edge of the preheat zone and the flame temperature in the lean case ($\emptyset_m$ = 0.75 and $\emptyset_A$ = 0.1) with f = 10 Hz.

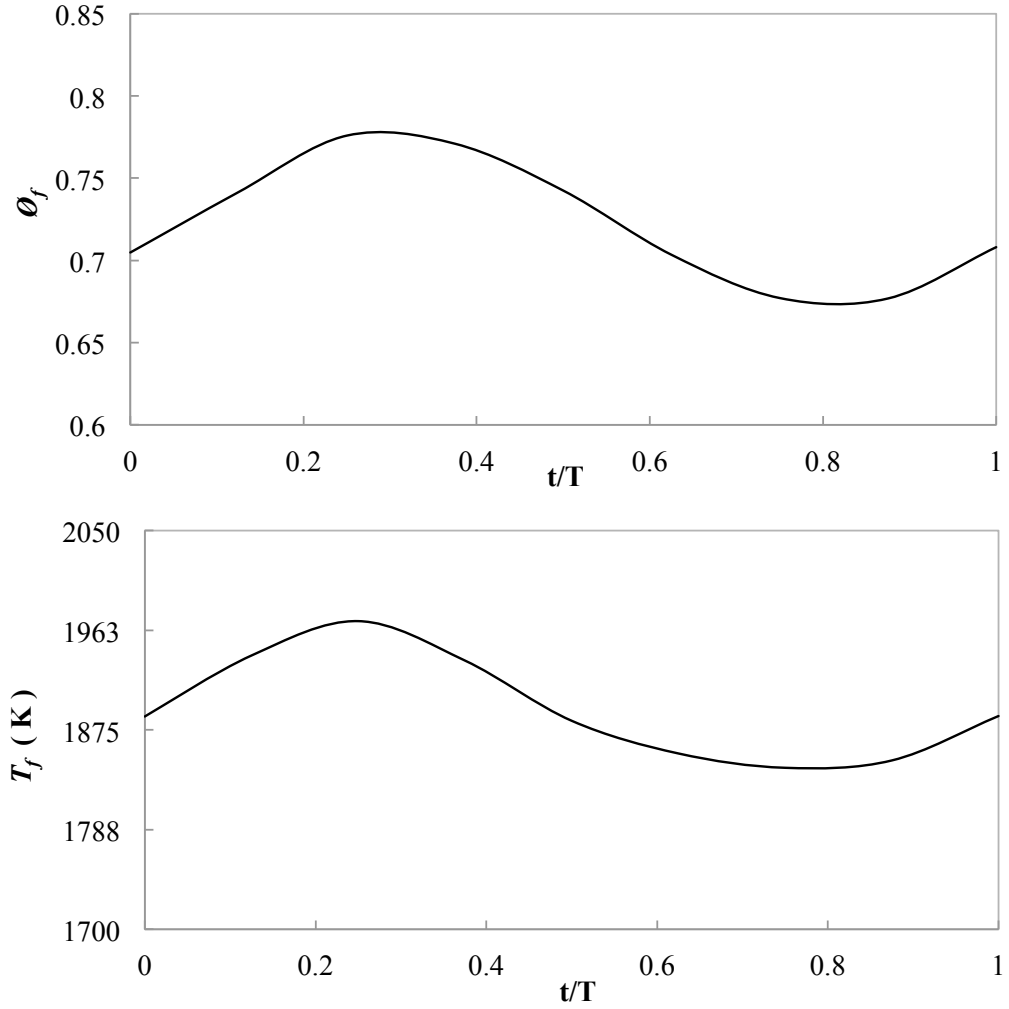

Figure 3-10 Variationsin the equivalence ratio in upstream edge of the preheat zone and the flame temperature in the lean case ($Ø_m$ = 0.75 and $Ø_A$ = 0.1) with f = 50 Hz.

On the other hand, an inverse relationship is observed between the flame temperature and the equivalence ratio as shown in Figs. 3-11 and 3-12 for the rich case ($Ø_m$= 1.15 and $Ø_A$=0.15). In the rich case, when the equivalence ratio is increased, it departs from the stoichiometric condition. As a result, the flame temperature decreases.

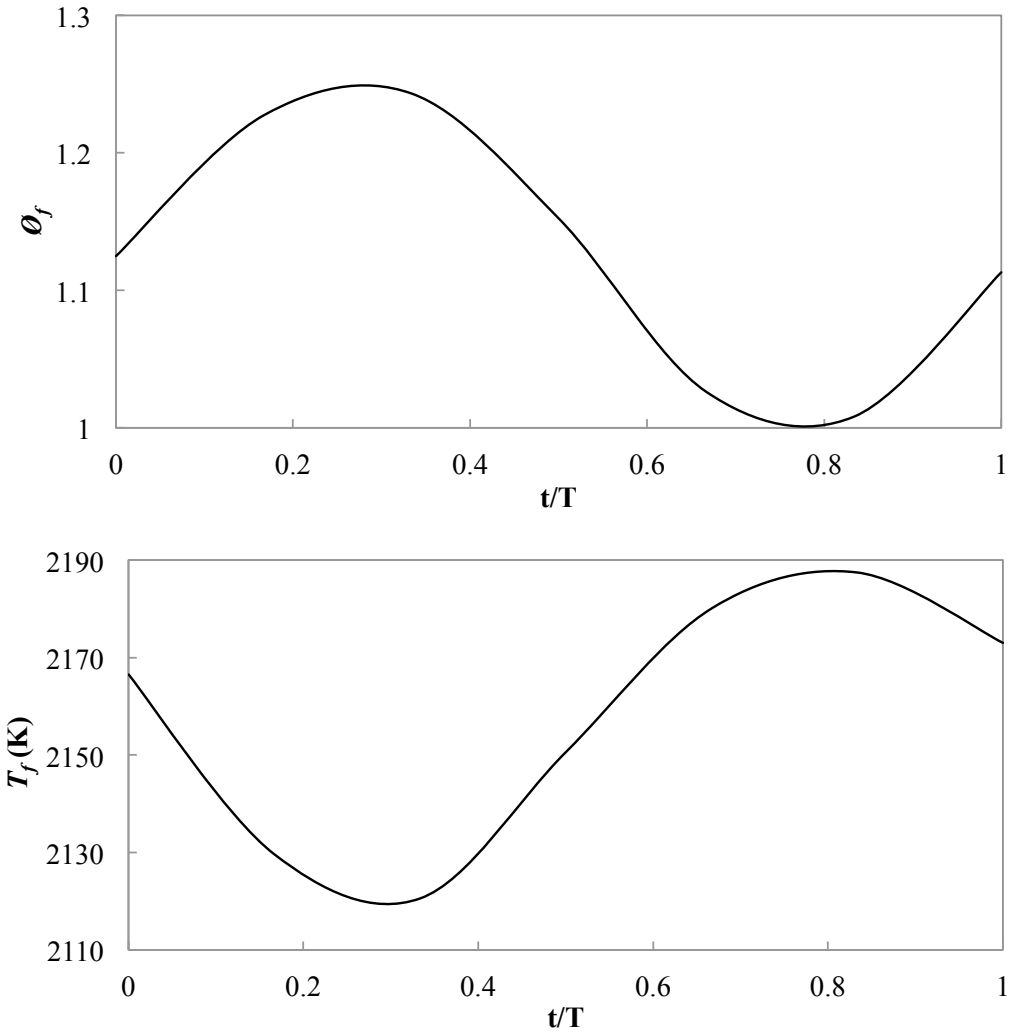

Figure 3-11 Variationsin the equivalence ratio in upstream edge of the preheat zone and the flame temperature in the rich case ($Ø_m$ = 1.15 and $Ø_A$ = 0.15) with f = 10 Hz.

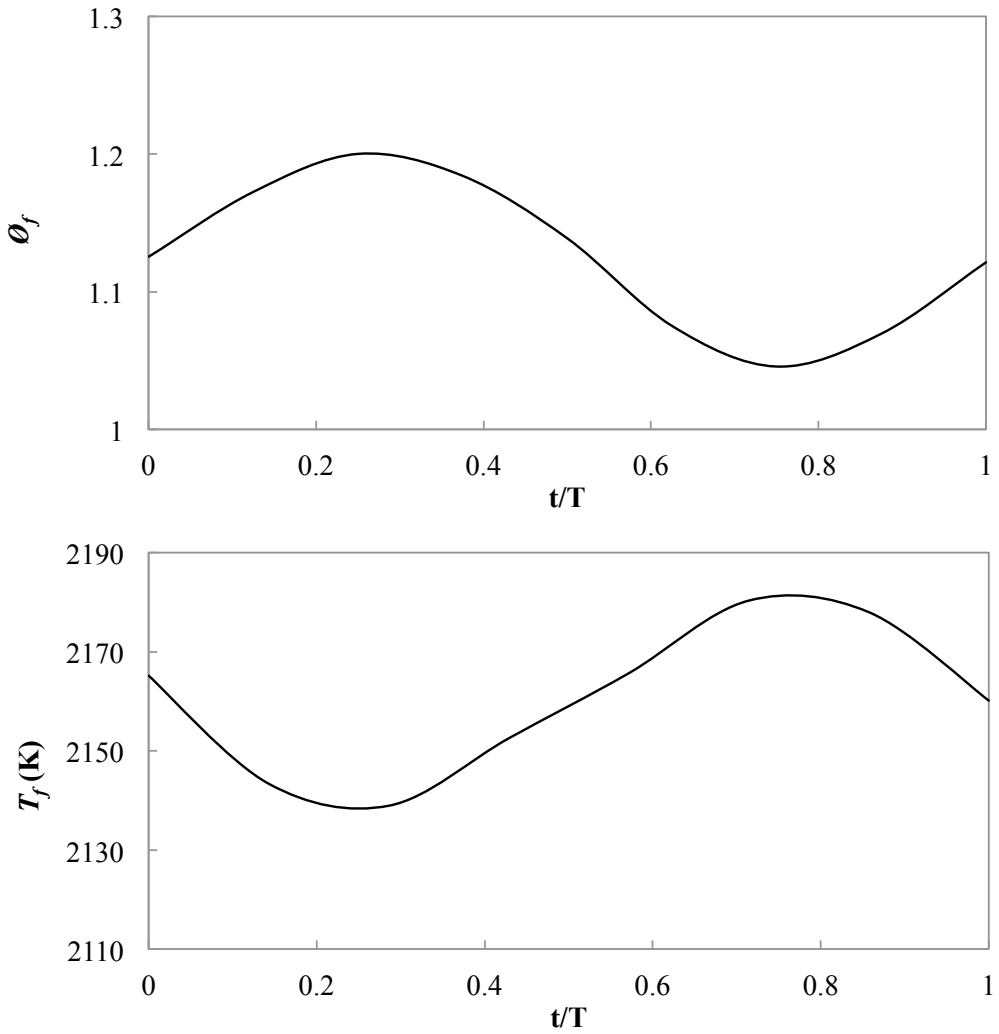

Figure 3-12 Variationsin the equivalence ratio in upstream edge of the preheat zone and the flame temperature in the rich case ($\emptyset_m$ = 1.15 and $\emptyset_A$ = 0.15) with f = 50 Hz.

For the lean rich crossover case ($\emptyset_m$=1.0 and $\emptyset_A$=0.3), it is interesting to note that the double cycles of the flame temperature variation is observed for one period of the equivalence ratio variation as shown in Figs. 3-13 and 3-14. This double cycle is due to the reactant variation from lean to rich and vice versa. These double cycles were observed in the experiment by Suenaga *et al.* (2005), while the single cycle is seen instead of the double cycles even in the case of the lean rich crossover case in analysis done by Lauvergne and Egolfopoulos (2000) at higher oscillation frequency.

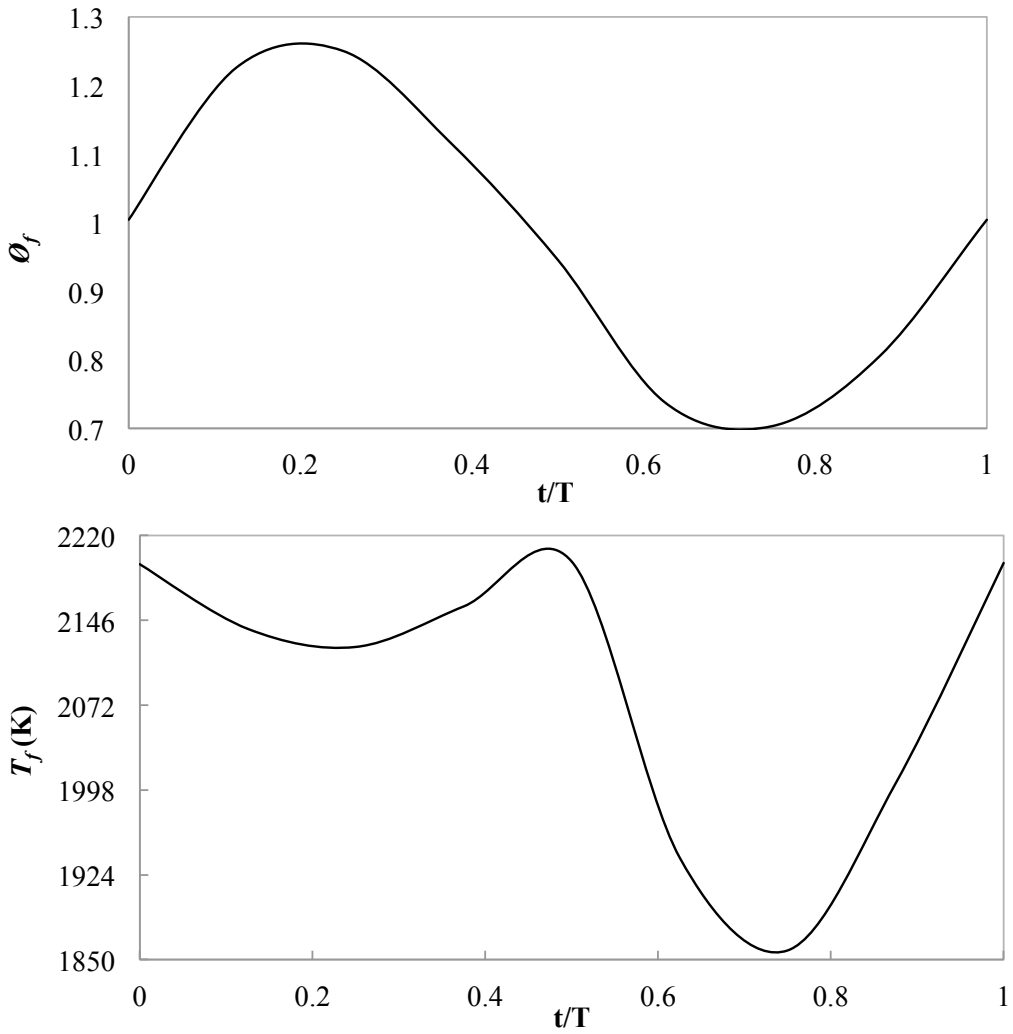

Figure 3-13 Variationsin the equivalence ratio in upstream edge of the preheat zone and the flame temperature in the lean rich crossover case ($\emptyset_m$ = 1.0 and $\emptyset_A$ = 0.3) with f = 10 Hz.

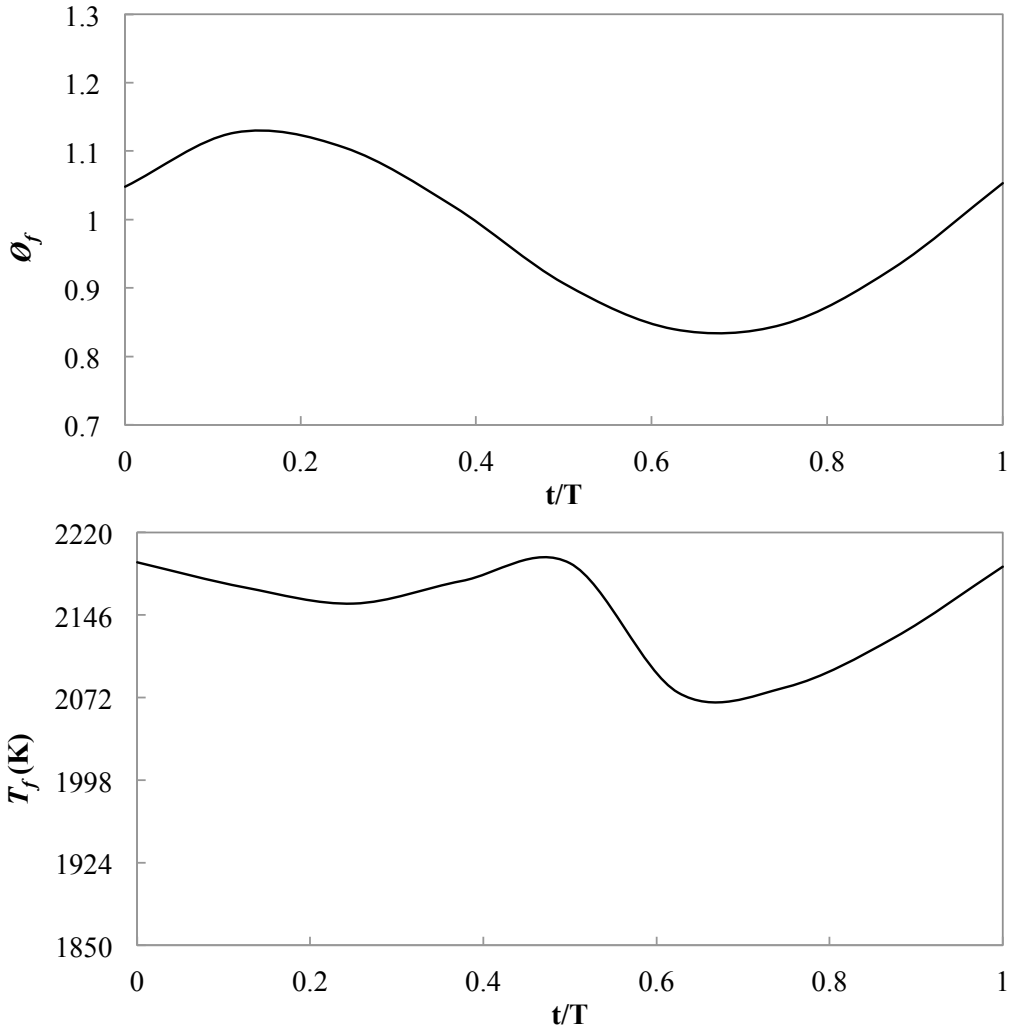

Figure 3-14 Variationsin the equivalence ratio in upstream edge of the preheat zone and the flame temperature in the lean rich crossover case ($Ø_m = 1.0$ and $Ø_A = 0.3$) with $f = 50$ Hz.

Marzouk *et al.*, (2000), mentioned that the flame response is controlled by the time gradient of the equivalence ratio at low oscillation frequency (Marzouk *et al.*, 2000) while Lauvergne and Egolfopoulos (2000) mentioned that at high oscillation frequency, the flame response is due to the time required for a perturbation to propagate through the flame layer. They have introduced a cutoff frequency mentioned in Eq. (3-17), above which the flame response is unresponsive.

$$f_{cutoff} = \frac{\ln (0.1)^2 U^2}{\pi D} \qquad (3-17)$$

Despite the frequency limit beyond which the flame no longer responds to the perturbation by Eq. (3-17), it is also interesting to examine the frequency at which the flame response mechanism change from the time gradient of the equivalence ratio (Marzouk *et al.*, 2000) to the time required for the perturbation to propagate through the flame layer (Lauvergne and Egolfopoulos, 2000). With reference to the cutoff frequency, it is noted that if no attenuation occurs in the diffusion zone, the term $\ln(0.1) \approx 1$. If the term is unity, the frequency will be similar to Egolfopoulos (1994). He proposed that $f = {U^2}/{\pi D}$ is a starting frequency at which substantial amplitude attenuation that is the attenuation of the time gradient commences. Therefore, it is found that the mechanism controlling the flame response changes at the characteristic oscillation frequency $f^* = {U^2}/{\pi D}$, where the amplitude attenuation in the flame diffusion zone commences. In the present study, the oscillation frequency is below the characteristic oscillation frequency f^*, and then the flame response is expected. As mentioned above, the analysis done by Lauvergne and Egolfopoulos (2000) could not show the double cycles. This is supposed to the frequency was between the f^* and the f_{cutoff}, in that the flame response attenuated but did not disappear.

The variation in the flame location in response to the equivalence ratio oscillation is discussed for three cases namely: (1) a lean case ($\emptyset_m = 0.75,\ \emptyset_A = 0.15$), (2) a rich case ($\emptyset_m = 1.15, \emptyset_A = 0.15$), (3) lean rich crossover cases ($\emptyset_m = 1.0, \emptyset_A = 0.3$). In addition, the effect of the amplitude of the equivalence ratio $\emptyset_A$, on the flame location for lean rich crossover cases at 10 Hz oscillation frequency is discussed.

The flame displacement speed was estimated because, it is not attributable to any chemical mechanism but due to the diffusive and hydrodynamic effects mentioned by Hirasawa *et al.* (2000). Moreover, the flame displacement speed can be estimated in experiments that enable the direct comparison between numerical results and experimental results. The flame displacement speed is defined as the normal flame front velocity with respect to unburned gas (Hirasawa *et al.* 2000). In the present study, the flame displacement speed is calculated by an unburned gas velocity at the upstream edge of the flame preheat zone and the time variation of the flame location as mentioned in Eq. (3-18).

This definition is the same as used in experimental studied (Hirasawa *et al.* 2000).

$$S_d = u_f - dy_f/dt \qquad (3-18)$$

where u_f is the unburned gas velocity at the upstream edge of the preheat zone, and y_f is the location of the flame.

3.3.3.1 Lean case

The dynamic response of the flame location in the lean case at various oscillation frequencies is shown in Fig. 3-15. The flame location moves making a closed cycle around flame location of the steady state case. It is seen the flame location profile is tilted from the steady state case profile and becomes almost flat at f = 50 Hz. This is because an attenuation of the amplitude of the equivalence ratio occurs at high oscillation frequency at the upstream edge flame preheat zone as shown in Fig. 3-5. In other words, the flame location response becomes weak with increasing frequency. This result corresponds to the experimental result done by Suenaga *et al.* (2003). Moreover, the overall results, namely the attenuation and phase delay response evolved with increasing oscillation frequency, as shown by the tilted dynamical response of the flame location from the steady state case correspond to those of previous research (Sankaran and Im, 2002). In Fig. 3-15, the dynamic response is turning in clockwise direction shown by two arrows for all oscillation frequencies. This behavior can be explained by the back support temperature phenomenon as discussed by Marzouk *et al.* (2000). In previous chapter, we have discussed the variation of the flame temperature in the lean case and found that the flame temperature increases when the equivalence ratio is increased. Therefore, the flame was intensified (weakened) in the lean case compared to the steady state case when the equivalence ratio decreases (increases) because the back support temperature is higher (lower) as shown in Fig. 3-16.

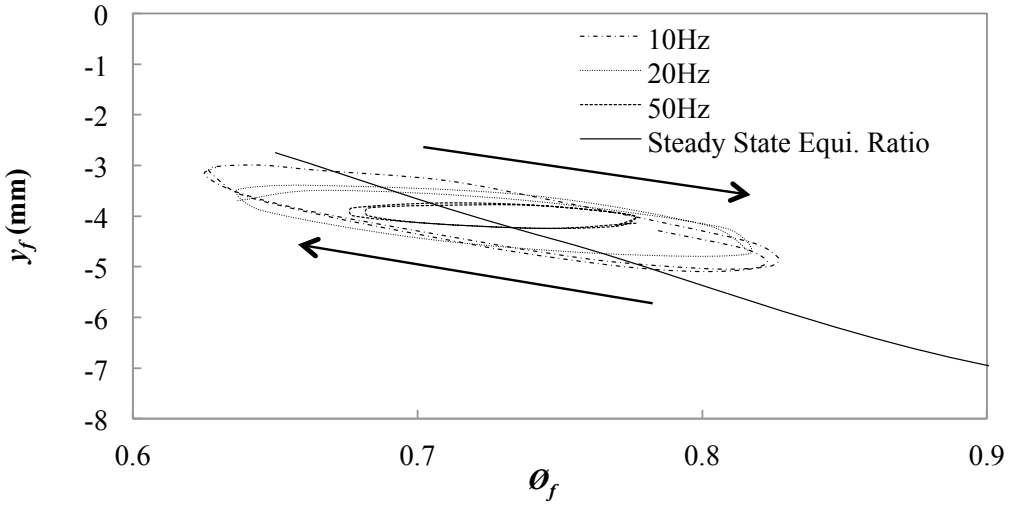

Figure 3-15 Dynamic response of the flame location in the lean case ($\emptyset_m$ = 0.75 and $\emptyset_A$ = 0.1) at various oscillation frequencies compared with the steady state equivalence ratio along the central axis (r = 0).

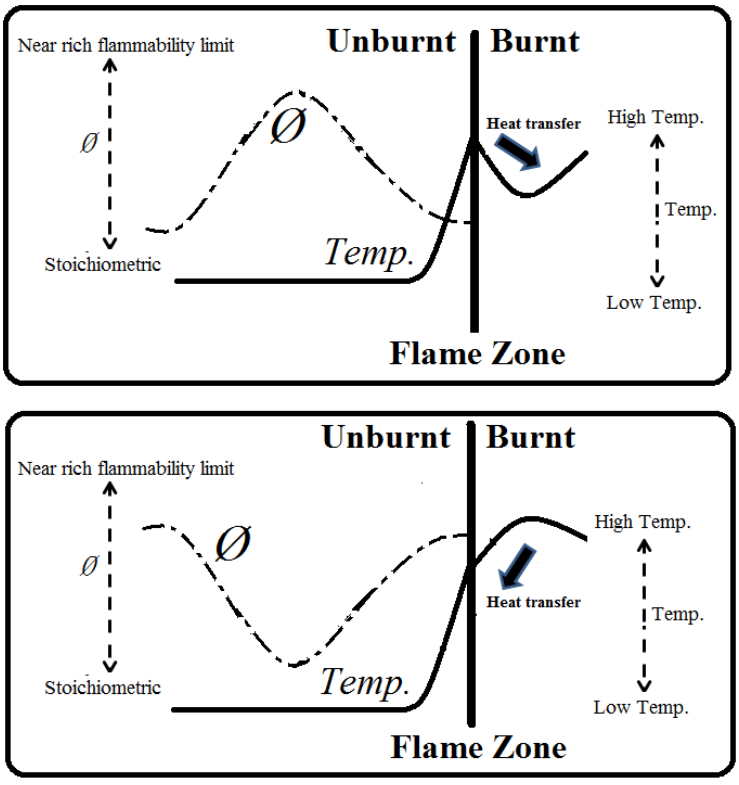

Figure 3-16 Back support mechanism.

Dynamic response of the flame displacement speed is shown in Fig. 3-17. In Fig. 3-17, the flame displacement speed varies around the steady state case. It is seen the flame moves upstream side compared to steady state location when the equivalence ratio moves to leaner where the unburned gas velocity u_f, is higher compared to the steady state case. Here, dy_f/dt is positive. As a result, S_d becomes lower than u_f, which closer to the steady state case.

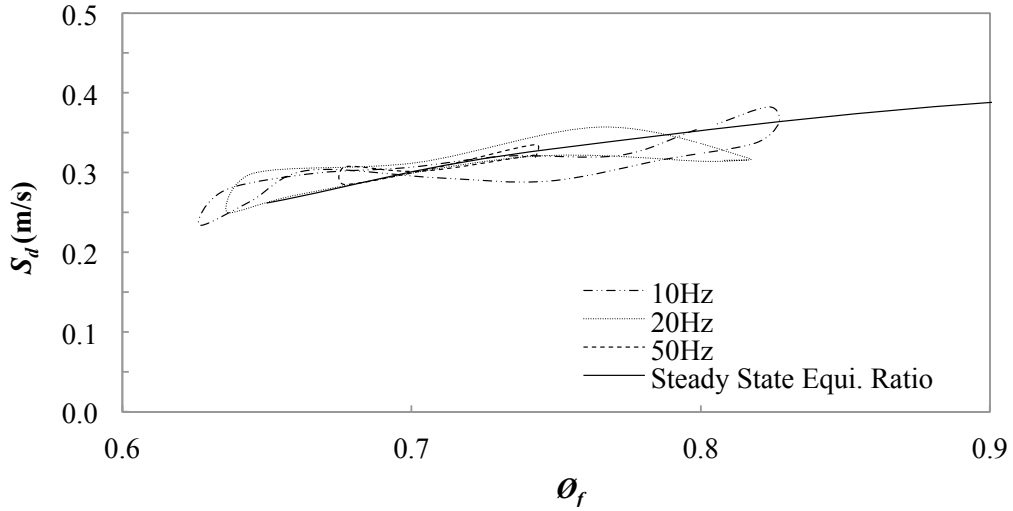

Figure 3-17 Dynamic response of the flame displacement speed in the lean case ($Ø_m$ = 0.75 and $Ø_A$ = 0.1) at various oscillation frequencies compared with the steady state equivalence ratio along the central axis (r = 0).

3.3.3.2 Rich case

Figure 3-18 shows the dynamic responses of the flame location in the rich case. The flame location movement is different from the lean case by making a closed cycle offset from the steady state case. Moreover, it is seen the dynamic response of the flame location almost flat for all oscillation frequency. Furthermore, in Fig. 3-18, the dynamic response is turning anti-clockwise shown by two arrows for all oscillation frequencies. This behavior as well as the lean case is explained by the back support temperature phenomenon as discussed by Marzouk *et al.* (2000). The variations of the flame temperature in the rich case have been discussed and found that the flame temperature increases when the equivalence ratio is decreased. Therefore, the flame was intensified (weaken) in the rich case when the equivalence ratio increases (decreases) because of the back support

temperature is higher (lower)(Fig. 3-16).

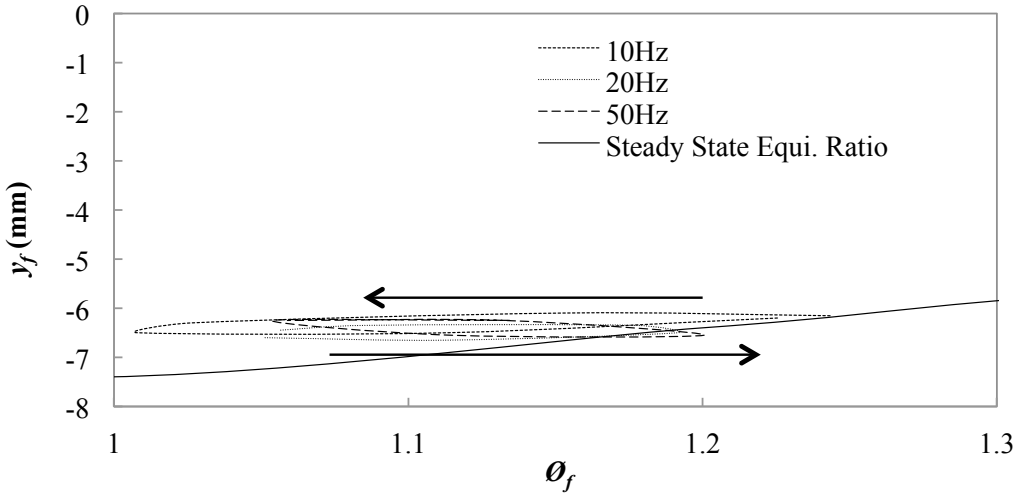

Figure 3-18 Dynamic response of the flame location in the rich case ($Ø_m$ = 1.15 and $Ø_A$ = 0.15) at various oscillation frequencies compared with the steady state equivalence ratio along the central axis (r = 0).

Figure 3-19 shows the flame displacement speed for the rich case. It is clearly seen the dynamic response of the flame displacement speed for the 50 Hz oscillation frequency showed significant variations. In discussing the lean case, we found that the derivative term of the flame location (dy_f/dt) contributes a major effect to the flame displacement speed in oscillation case compared to steady state case. These behaviors are similar to the rich case. Whereby, the flame location is failed to move significantly but the derivative of the flame location change significantly. As a result, the flame displacement speed in the rich case for 50 Hz oscillation frequencies varies significantly.

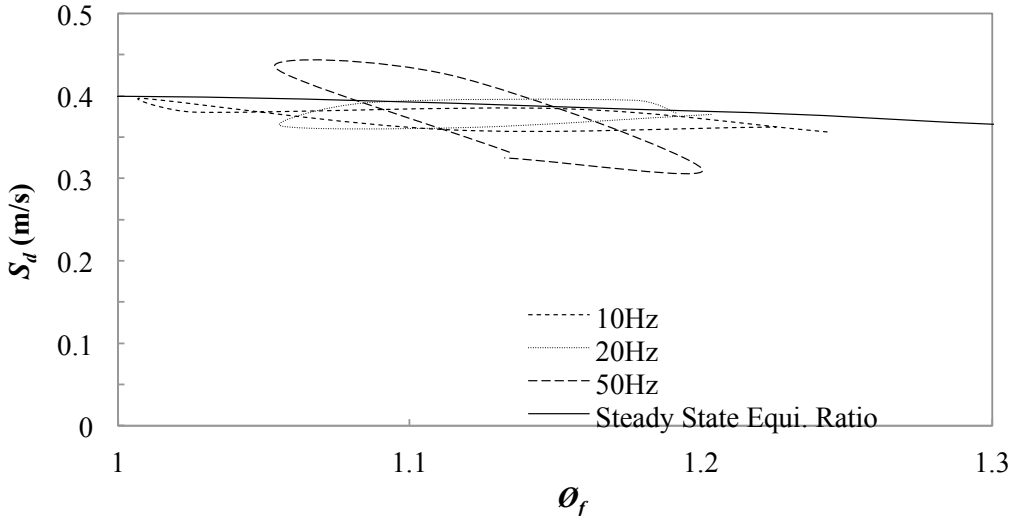

Figure 3-19 Dynamic response of the flame displacement speed in the rich case ($Ø_m$ = 1.15 and $Ø_A$ = 0.15) at various oscillation frequencies compared with the steady state equivalence ratio along the central axis (r=0).

3.3.3.3 Lean rich crossover case

The lean rich crossover case of the equivalence ratio oscillation is shown in Fig. 3-20. The dynamic response of the flame location and the flame displacement speed differ from the monotonic equivalence ratio oscillation in lean and the rich cases respectively. Overall, this was expected due to the non-monotonic equivalence ratio variation when the equivalence ratio crosses the stoichiometric value. As shown in Fig. 3-20, the flame location moves to makes two closed cycles and intersect near stoichiometric equivalence ratio. These two closed cycles are turning in different direction. At the equivalence ratio less than stoichiometric, the closed cycle is turning in the clockwise. On the other hand, the closed cycle in the equivalence ratio greater than stoichiometric ratio is turning anti-clockwise. These behaviors are similar to the lean and rich cases that are mainly due to the back support temperature.

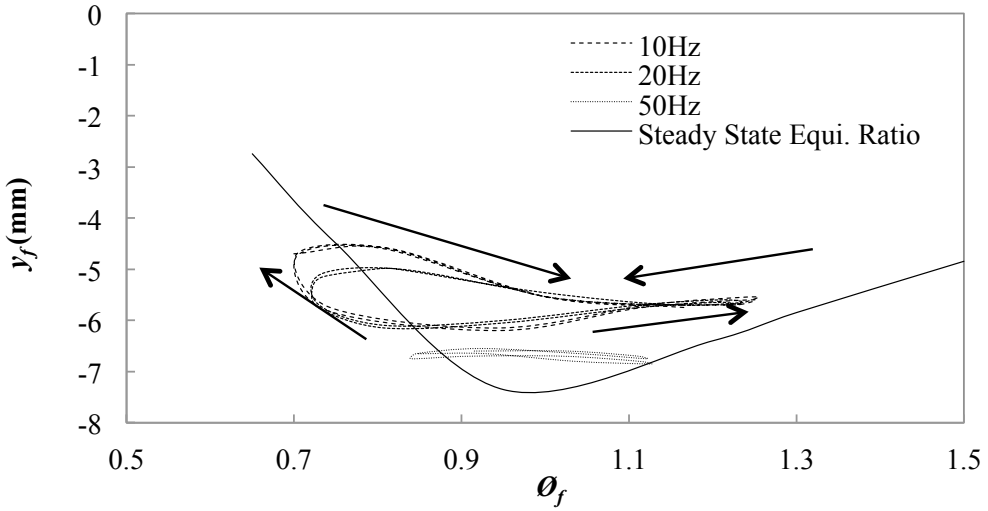

Figure 3-20 Dynamic response of the flame location in the lean rich crossover ($Ø_m$ = 1.0 and $Ø_A$ = 0.3) case at various oscillation frequencies compared with the steady state equivalence ratio along the central axis (r = 0).

Figure 3-21 shows the flame displacement speed for the lean rich crossover case. It is clearly seen that the dynamic response of the flame displacement speed for the 10, 20 and 50 Hz oscillation frequencies showed significant variations at off and near stoichiometric ratio. Once again, the derivative term of the flame location (dy_f/dt) was found to contribute a major effect to the significant variations in the flame displacement speed in lean rich crossover case. This finding reflects to the dynamic response of the flame location in Fig. 3-21. The derivative term of the flame location in the flame displacement speed equation is represented by the gradient of the closed cycles. As a result, the larger gradients of the closed cycles, the greater variations of the flame displacement speed.

Moreover, the flame displacement speed is relatively lower than the steady state case around $Ø$~1. The flame location around $Ø$~1 is closer to the stagnation wall compared to the steady state case. It means u_f, of oscillation case is lower than that of steady case. As a result, S_d becomes slightly lower than that of the steady state case eventhough the term dy_f/dt exist.

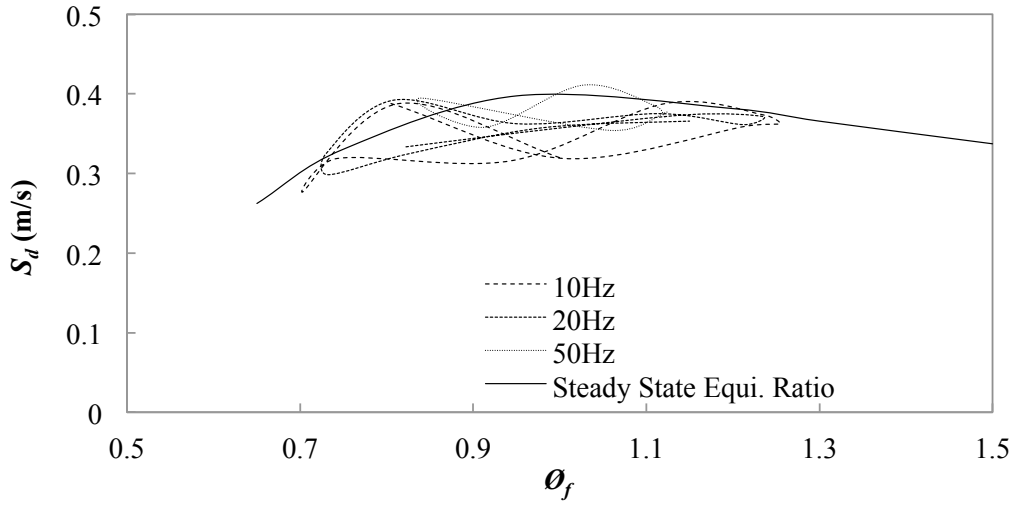

Figure 3-21 Dynamic response of the flame displacement speed in the lean rich crossover case ($\emptyset_m$ = 1.0 and $\emptyset_A$ = 0.3) at various oscillation frequencies compared with the steady state equivalence ratio along the central axis (r = 0).

3.3.3.4 Various oscillation amplitudes

Figure 3-22 shows the dynamic response of the flame location for various oscillation amplitudes in the lean rich crossover case at an oscillation frequency of 10 Hz. It can be seen that the flame movement amplitude increase as increases in the oscillation amplitude and it is agreed with experimental work in Fig. 3-23. Furthermore, shape of the flame location variation is similar, regardless of oscillation amplitude. It is also interesting to observe that the shape of the flame location variation almost the same when the oscillation amplitude of the equivalence ratio at the upstream edge of the preheat zone is the same regardless of the oscillation frequency as shown in Fig. 3-24. These results indicate that the oscillating flame location is determined by the flame location profile in the steady state condition and the equivalence ratio oscillation amplitude in upstream edge of the preheat zone.

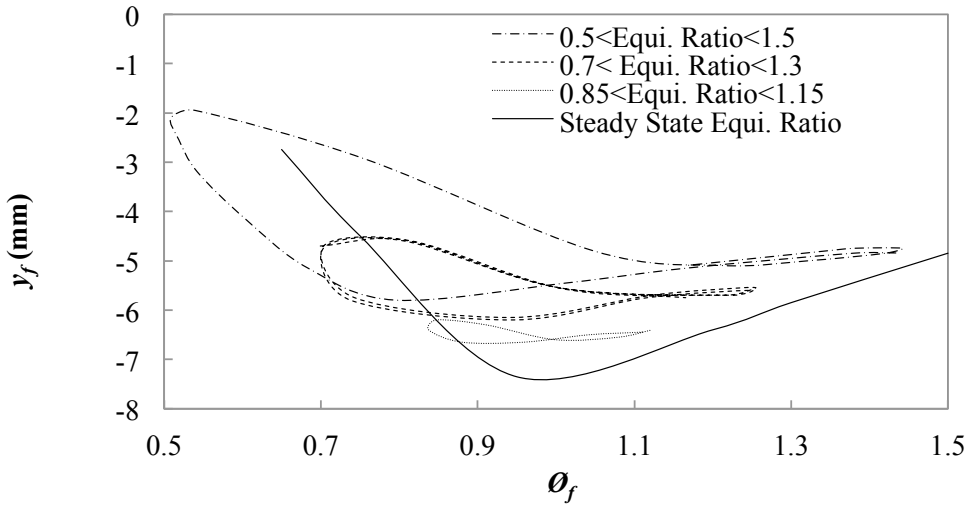

Figure 3-22 Dynamic response of the flame location in the lean rich crossover case at various oscillation amplitudes and f = 10 Hz compared with the steady state equivalence ratio along the central axis (r = 0).

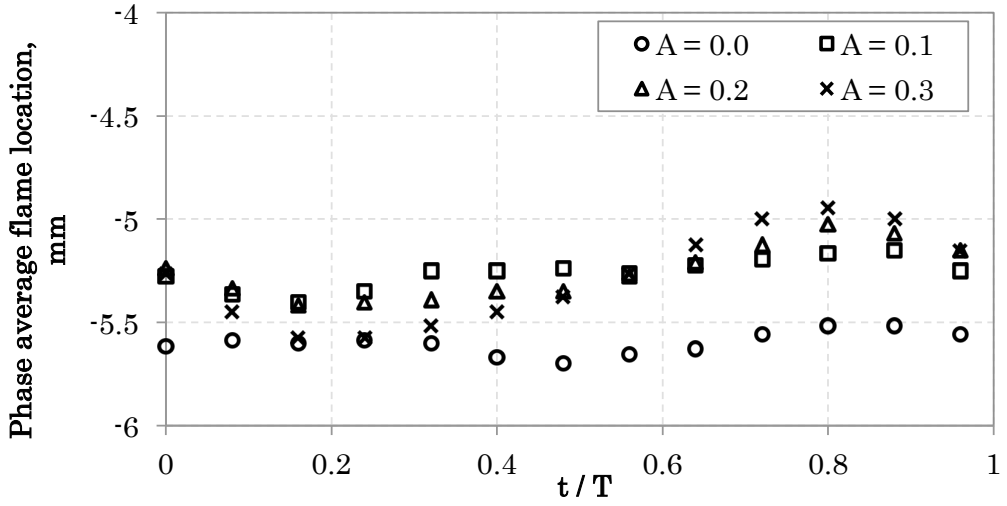

Figure 3-23 Experimental result of the cyclical variation flame position in lean case ($\emptyset_m$ = 0.7) for 10 Hz oscillation frequency at various equivalence ratio oscillation amplitudes.

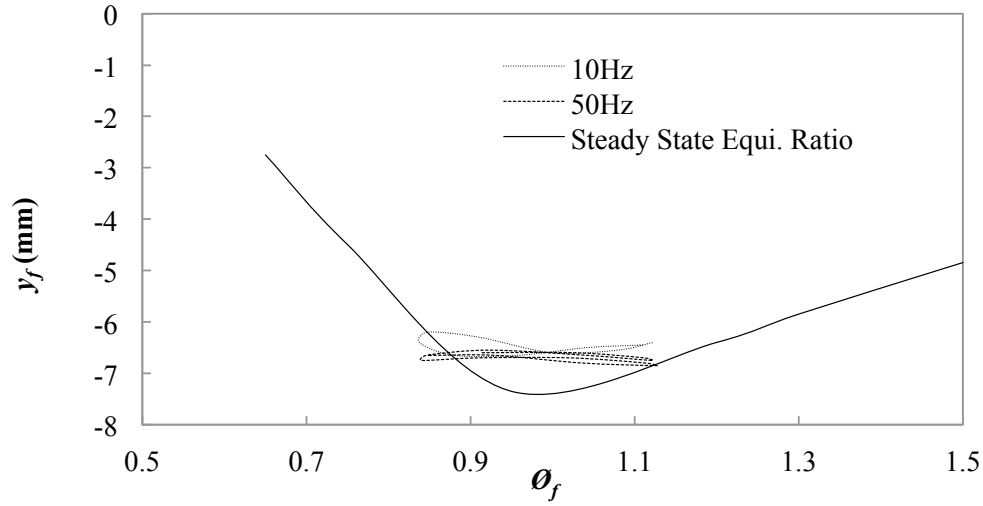

Figure 3-24 Dynamic response of the flame location in the lean rich crossover case ($Ø_m$ = 1.0 and $Ø_A$ = 0.15) at various oscillation frequencies compared with the steady state equivalence ratio along the central axis (r = 0).

3.4 Concluding remarks

The effect of the equivalence ratio oscillation on a premixed methane/air flame motion is studied computationally using an axi-symmetric stagnation flow field. The flame response to the oscillation frequencies of the equivalence ratio of 10, 20 and 50 Hz at three different oscillation cases (lean, rich and lean rich crossover cases) was investigated. The oscillation conditions are set at the exit of the burner.

The equivalence ratio oscillation amplitude attenuates between the exit of the burner and the upstream edge of the preheat zone. The attenuation is much significant for higher frequency of the oscillation. Following the attenuation of the equivalence ratio oscillation, the flame temperature oscillation is also attenuated.

Dynamic response of the flame location for lean, rich and lean rich crossover cases shows an interesting behavior. The flame location movements create the closed cycle around the flame location of correspond equivalence ratio in the steady state condition. The formation of the cycles can be explained by the back support effect.

The flame displacement speed variation is estimated. The results show that the time variation of the flame location plays a significant effect to the flame displacement speed.

The oscillating flame location is determined by the flame location profile in the steady

state condition and equivalence ratio oscillation amplitude at the upstream edge of the preheat zone.

Chapter 4

Concept of non-uniform scalar profile

4.1 Introduction

Hysteresis of the flame movement is seen in both the numerical and experimental work. This hysteresis is supposed to be due to effect of the temperature from the burned gas called back support effect. The back support effect is found to modify the flame dynamics in the stratified case (Marzouk *et al.* 2000, Pires *et al.* 2000). Moreover, the back support effect is a type of non-uniform scalar value profile in the downstream region of the flame zone. Researches in the stratified equivalence ratio perturbation case proposed that the non-uniform scalar value profile in the downstream of the flame zone affected the flame response, in the lean methane/air premixed flames, propagation speed of the flame movement from stoichiometric to lean flammability limit was enhanced by the heat and composition fluxes in the burned gas compared to steady state case at specific equivalence ratio (Pires *et al.* 2000). Additionally, Kang and Kyritsis (2007), (2009) found that the

cumulative heat from the burned gas enhances the flame propagation speed in lean case. On the other hand, Richardson *et al.* (2010) observes that the species fluxes play important role than the heat flux in an increase in flame propagation speed in lean case. Despite of the single dominated mechanism thermal or species diffusion, both mechanisms founds dominated in help the flame propagates beyond the lean or rich flammability limit compared to steady state case (Zhou and Hogchreb, 2013).

On the other hand, in the present study, non-uniform scalar value profile is seen in both upstream and downstream regions of the flame zone numerically. Thus, development of the flame movement hysteresis is suppose to be affected by the effect of non-uniform scalar value profile in both upstream and downstream regions of the flame zone. Therefore, in present chapter the concept of non-uniform scalar value profile in both upstream and downstream regions of the flame zone will be introduced. Moreover, the clarification of this concept is done by development of the simplified mathematical model based on approximation method.

4.2 Concept of the non-uniform scalar profile

The back support effect discussed by (Marzouk *et al*. 2000) is one of the thermal effects of the non-uniform scalar value profile in the downstream region of the flame zone. In the present study, the non-uniform scalar value profile in the upstream and downstream regions of the flame zone is seen in numerical work. Thus, similar to the back support effect can be considered in the upstream of the flame zone through the fuel molecular diffusion toward the reaction zone. Figure 4-1, shows the variation of the equivalence ratio at upstream of the flame preheat zone. Following the variation of the equivalence ratio, reactant of mass, Y_f and burned gas temperature, T_f varies at the upstream and the

downstream of the flame zone respectively (Fig. 4-2). Variations of the reactant of mass, Y_f and burned gas temperature, T_f are called as non-uniform scalar profile at the upstream and the downstream of the flame zone. Moreover, effect of the non-uniform scalar profile toward the flame dynamics can be illustrated using Fig. 4-3. Figure 4-3, shows the position of the flame is in lean case at respective equivalence ratio variations. As the flame is located at the top of the fuel concentration (near stoichiometric), (a) in Fig. 4-3, the reactant diffuses toward upstream direction due to decreasing fuel concentration profile toward the upstream direction and the heat diffuse toward the downstream direction due to the decreasing temperature profile toward the downstream direction. These losses of reactant and heat weaken the flame and flame propagation speed decreases. When the flame is located intermediate, the reactant diffuses toward the reaction zone from the upstream direction due to the increasing reactant profile toward the upstream direction, while the heat diffuses downstream direction as well as in the case (a). It means the intensification of the flame due to the diffusion of fuel toward the reaction zone is cancelled by the diffusion of heat from the reaction zone. When the flame is located at the bottom of the fuel concentration (near leaner region), both fuel and heat diffuse toward the reaction zone and the flame is intensified and the flame propagation speed is increased. Thus, the flame propagation speed shows deviation from the steady state case.

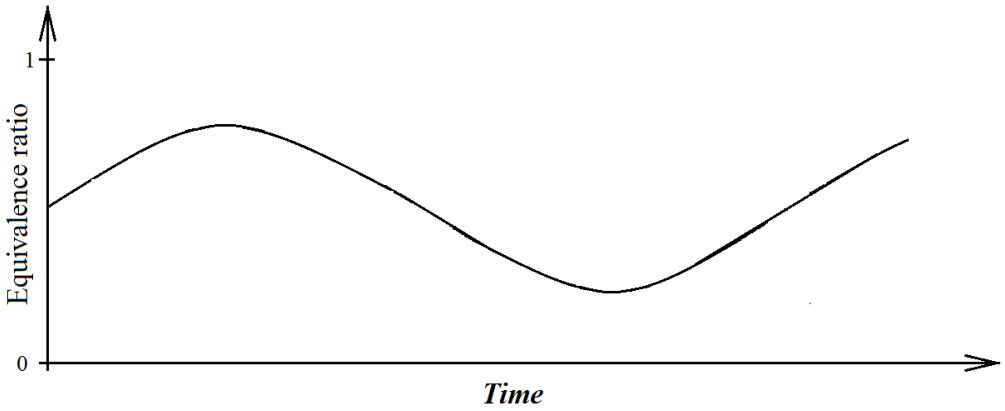

Figure 4-1 Variations of the equivalence ratio at the upstream of the flame zone.

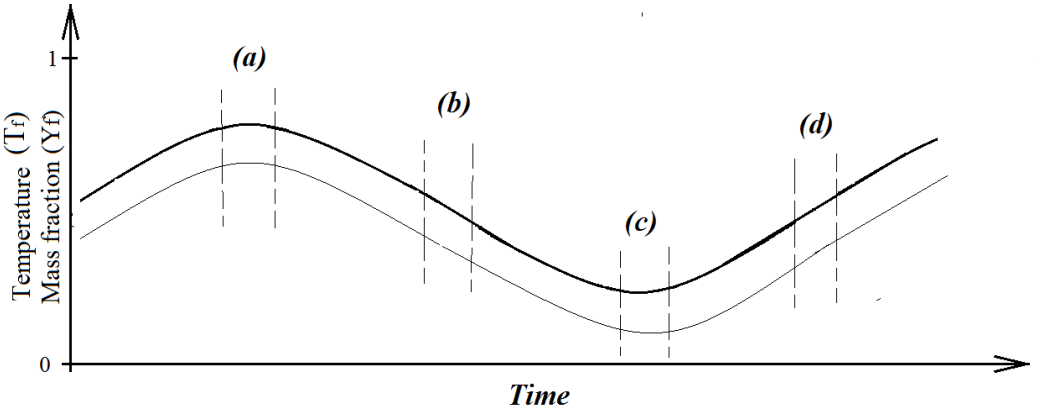

Figure 4-2 Variations of the reactant mass fraction, Y_f and burned gas temperature, T_f at upstream and downstream of the flame zone in lean case respectively.

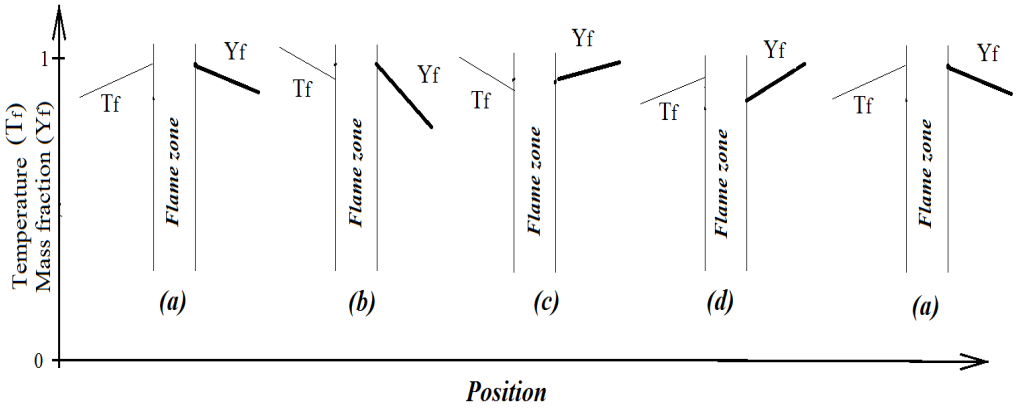

Figure 4-3, Illustration of the non-uniform scalar effect in the lean case.

Figure 4-4 shows the variations of the reactant mass fraction at the upstream and burned gas temperature at the downstream of the flame zone following the equivalence ratio variation (Fig. 4-1) in rich case respectively. Flame responded influences by the effect of the non-uniform scalar profiles are shown in Fig. 4-5. As the flame is located at the rich fuel, (a) in Fig. 4-5, the reactant diffuses toward upstream direction due to decreasing fuel concentration profile toward the upstream direction and the heat conducted into the flame zone due to the increasing temperature profile toward the downstream direction as shown in Fig. 4-5. These losses of reactant and support of heat stabilize the flame. When the flame propagates toward the stoichiometric condition (Fig. 4-4 (b)), the reactant diffuses out from the flame due to the decreasing reactant profile toward the upstream direction and the heat diffuses downstream direction as well (Fig. 4-5 (b)). As a result, the flame is weakened. On the other hand, as the flame is propagated toward rich condition (Fig. 4-4 (d)), both fuel and heat diffuse toward the reaction zone (Fig. 4-5 (d)) and the flame is intensified and the flame propagation speed increases. Thus, weaken and intensification of the flame result in deviation of the flame propagation speed from the steady state.

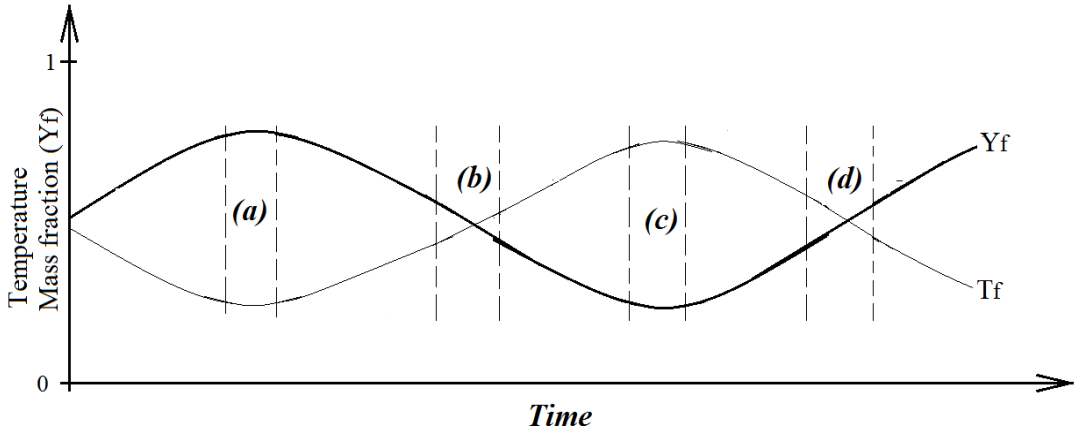

Figure 4-4 Variations of the reactant mass fraction, Y_f and burned gas temperature, T_f at upstream and downstream of the flame zone in rich case respectively.

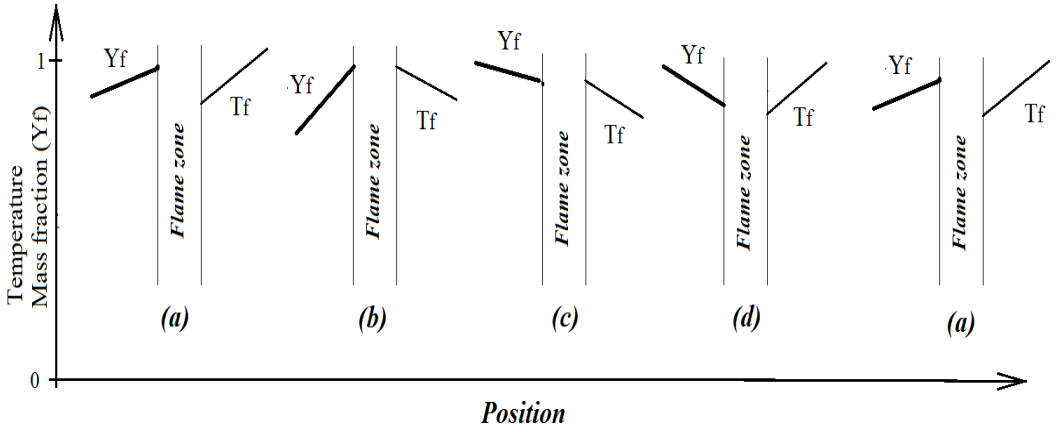

Figure 4-5 Illustration of the non-uniform scalar profile value in rich case.

4.3 Simplified mathematical model

An assumption was made as follows; 1) low equivalence ratio oscillation frequency is considered since the quasi-steady approximation is valid because the wavelength by the equivalence ratio oscillation is longer than the flame thickness, 2) flame is not affected by stretch and 3) c_p is constant. The flame response can be shown by the spatial coordinate as shown in Fig. 4-6. Using the quasi-steady approximation the integral analysis of Chung and Law (1988) is extended by addition of the non-uniform scalar value profile in the upstream and downstream sides' effect.

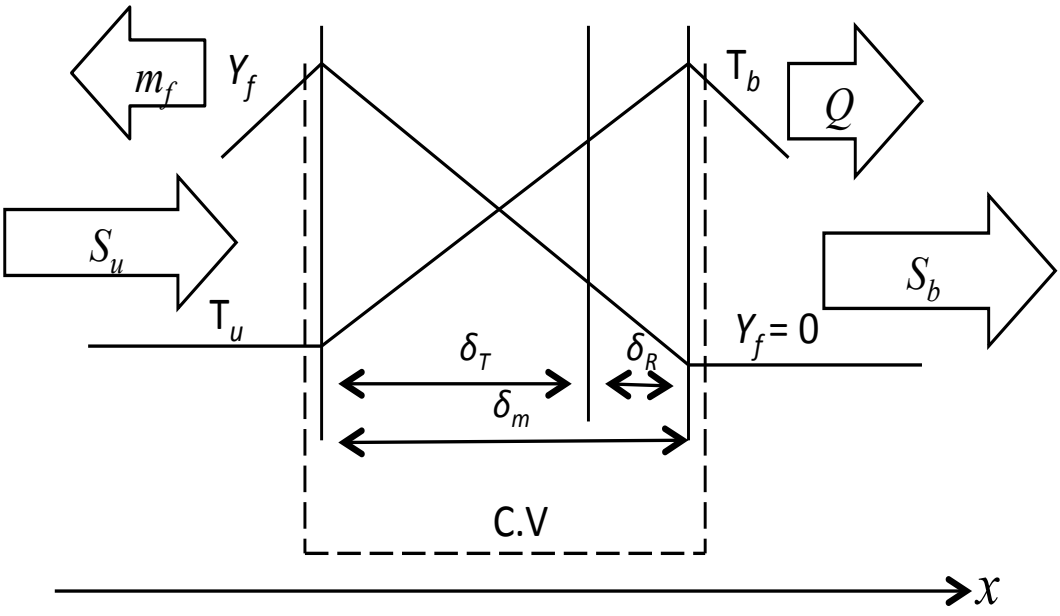

Figure 4-6 Schematic of the control volume with respective boundary.

Overall Mass conservation

$$\rho_b S_b = \rho_u S_u \qquad (4-1)$$

Overall Energy conservation

$$\rho_b S_b c_p T_b - \rho_u S_u c_p T_u = \left(\rho D \frac{dY_f}{\delta_m} - m_f\right) q - Q \qquad (4-2)$$

where $m_f = -\rho D \frac{dY_f}{dx}$, $\left[{\text{kg}}/{\text{m}^2\text{s}}\right]$ is a mass flux diffuse to the upstream and $Q = -\lambda \frac{dT_b}{dx}$, $\left[{\text{kJ}}/{\text{m}^2\text{s}}\right]$ is a heat diffuse to the downstream of the flame zone respectively.

Mass Balance at Flame

$$\rho D \frac{dY_f}{\delta_m} = Yk\ \delta_R \qquad (4-3)$$

Energy Balance at Flame

$$\lambda \left(\frac{T_b - T_u}{\delta_T}\right) = Yk\ \delta_R q - Q \qquad (4-4)$$

Convection-Diffusion Balance

$$\rho D \frac{dY_f}{\delta_m} = \rho_u S_u Y_f - m_f \qquad (4-5)$$

Substituting Eqs. (4-1), (4-5) into (4-2)

$$\rho_b S_b c_p T_b - \rho_u S_u c_p T_u = \left(\rho_u S_u Y_f - 2m_f\right) q - Q$$

$$\rho_u S_u c_p (T_b - T_u) = \left(\rho_u S_u Y_f - 2m_f\right) q - Q$$

$$(T_b - T_u) = \frac{1}{\rho_u S_u c_p} \left(\rho_u S_u Y_f q - 2m_f q - Q\right)$$

$$T_u = T_{ad} - \frac{Y_f}{c_p} q$$

$$T_b - \left(T_{ad} - \frac{Y_f q}{c_p}\right) = \frac{1}{\rho_u S_u c_p}\left(\rho_u S_u Y_f q - 2m_f q - Q\right)$$

$$T_b - \left(T_{ad} - \frac{Y_f q}{c_p}\right) = \frac{Y_f q}{c_p} - \left(\frac{2m_f q + Q}{\rho_u S_u c_p}\right)$$

$$T_b = \frac{Y_f q}{c_p} - \left(\frac{2m_f q + Q}{\rho_u S_u c_p}\right) + T_{ad} - \frac{Y_f q}{c_p}$$

$$T_b = T_{ad} - \left(\frac{2m_f q + Q}{\rho_u S_u c_p}\right) \qquad (4-6)$$

Dividing (4-6) with T_{ad},

$$\frac{T_b}{T_{ad}} = 1 - \left(\frac{2m_f q + Q}{\rho_u S_u c_p T_{ad}}\right) \qquad (4-7)$$

Non-dimensional relation representing as follow;

$$m_o = \frac{m_f q \left[{}^{\mathrm{kJ}}/_{\mathrm{m^2 s}}\right]}{\rho_u S_u c_p T_{ad} \left[{}^{\mathrm{kJ}}/_{\mathrm{m^2 s}}\right]}$$

$$Q_o = \frac{Q \left[{}^{\mathrm{kJ}}/_{\mathrm{m^2 s}}\right]}{\rho_u S_u c_p T_{ad} \left[{}^{\mathrm{kJ}}/_{\mathrm{m^2 s}}\right]}$$

Thus Eq. (4-7) can be re-write as

$$\frac{T_b}{T_{ad}} = 1 - (2m_o + Q_o) \qquad (4-8)$$

Qualitatively, Eq. (4-8) shows dependency of the flame temperature on the non-uniform scalar value profile in the upstream and downstream side of the flame zone. When the heat and the reactant mass loss are considered to diffuse out from the flame zone as shown in Fig. 4-6, the flame temperature will be lower than that of the adiabatic flame temperature. On the other hand, if the heat and the reactant mass are considered to diffuse to the flame zone (Fig. 4-7), the flame temperature will be higher than that of adiabatic flame temperature.

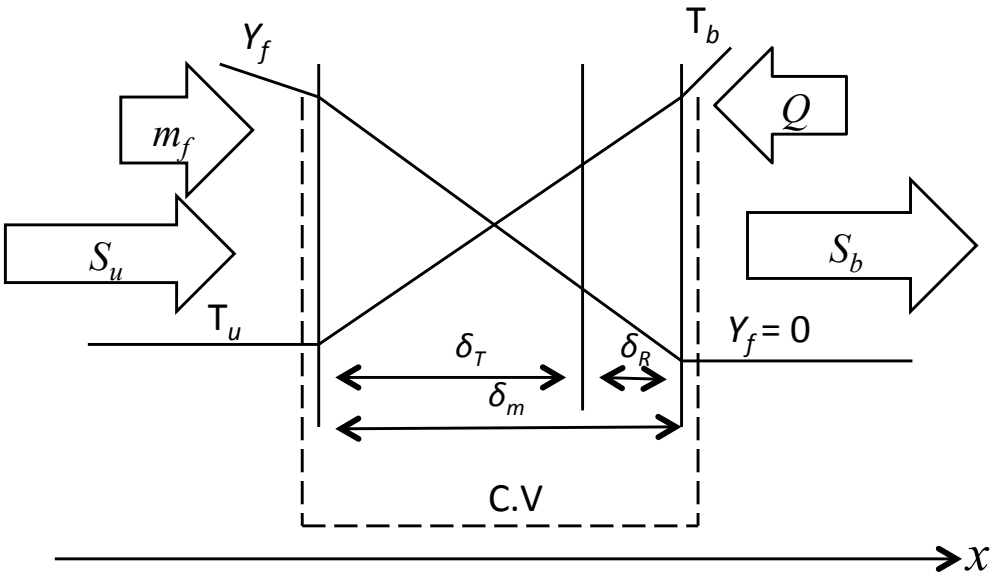

Figure 4-7 Schematic showing the control volume with reactant and heat diffuse to the flame.

If the heat is gain/loss and at the same time the reactant loss/gain from/to the flame zone as shown in Fig. 4-8, these gain and loss are cancelled out each other. As a result the flame temperature does not change from the adiabatic flame temperature.

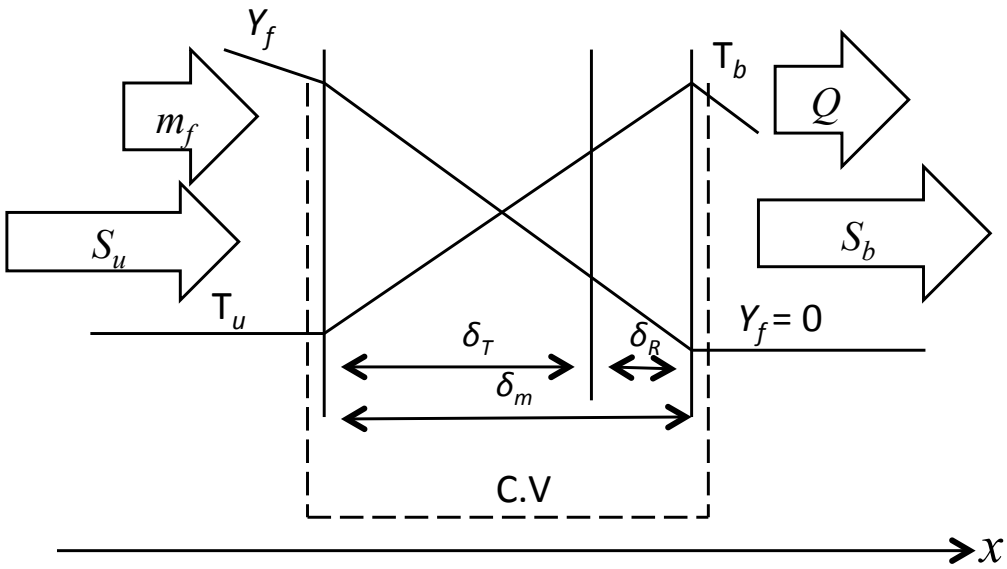

Figure 4-8 Schematic showing the control volume with reactant and heat are balanced.

Propagation speed relation given by Law (2006) is used to approximate the flame propagation speed influence by the non-uniform scalar profile model.

Law (2006) gives,

$$\left(\frac{S_u}{S_u^o}\right)^2 = \left(\frac{T_b}{T_{ad}}\right)^4 \exp\left[-T_a\left(\frac{1}{T_b}-\frac{1}{T_{ad}}\right)\right] \qquad (4-9)$$

where T_a is the activation energy.

By substituting Eq. (4-8) into Eq. (4-9) it gives,

$$\left(\frac{S_u}{S_u^o}\right)^2 = \left(1-(2m_o+Q_o)\right)^4 \exp\left[-T_a\left(\frac{1}{T_b}-\frac{1}{T_{ad}}\right)\right] \qquad (4-10)$$

Based on the Eq. (4-10), effect of the non-uniform scalar profile influenced the flame propagation speed can be deduced by approximating the amount of the m_o and Q_o at upstream and downstream of the flame zone.

4.4 Results and discussion

Variation of the fuel concentration and burned gas temperature seen in numerical work can be used to duplicate the flame response to non-uniform scalar profile at upstream and downstream of the flame zone. Assuming that variation of the mass of reactant $(\mathrm{mol/mol})$, Y_f at the upstream of the flame zone and burned gas temperature (K), T_b at the downstream are given as,

$$Y_f = A \sin \omega t \qquad (4-11)$$

$$T_b = B \sin \omega t \qquad (4-12)$$

where A and B are the amplitude of the oscillation and are define by the fuel properties, ω is the angular frequency and t is a time.

Taking,

$$S_u = \frac{dx}{dt}$$

then,

$$\frac{dY_f}{dx} = \frac{1}{s_u}\frac{dY_f}{dt} = \frac{A}{s_u}\omega \cos \omega t$$

$$\frac{dT}{dx} = \frac{1}{s_u}\frac{dT}{dt} = \frac{B}{s_u}\omega \cos \omega t$$

Substitute into,

$$m_f = -\rho D \frac{dY_f}{dx}$$

$$Q = -\lambda \frac{dT_b}{dx}$$

gives,

$$m_f = -\rho D \frac{A}{s_u} \omega \cos \omega t \qquad (4-13)$$

$$Q = -\lambda \frac{B}{s_u} \omega \cos \omega t \qquad (4-14)$$

Substituting Eq. (4-13) and Eq. (4-14) into Eq. (4-7),

$$\frac{T_b}{T_{ad}} = 1 - \left(\frac{2q(\rho D A \omega \cos \omega t) + \lambda B \omega \cos \omega t}{\rho_u {S_u}^2 c_p T_{ad}} \right)$$

$$\frac{T_b}{T_{ad}} = 1 - \left(\frac{2Aq\rho D\omega + \mathrm{B}\lambda\omega}{\rho_u {S_u}^2 c_p T_{ad}} \right) \cos \omega t \qquad (4-15)$$

In non-dimensional form,

$$m_o = \frac{A\rho D f q \left[{}^{\mathrm{kJ}}/_{\mathrm{m} \cdot \mathrm{s}^2} \right]}{\rho_u {S_u}^2 c_p T_{ad} \left[{}^{\mathrm{kJ}}/_{\mathrm{m} \cdot \mathrm{s}^2} \right]}$$

$$Q_o = \frac{\mathrm{B}\lambda f \left[{}^{\mathrm{kJ}}/_{\mathrm{m} \cdot \mathrm{s}^2} \right]}{\rho_u {S_u}^2 c_p T_{ad} \left[{}^{\mathrm{kJ}}/_{\mathrm{m} \cdot \mathrm{s}^2} \right]}$$

$$\frac{T_b}{T_{ad}} = 1 - 2(2\pi m_o + \pi Q_o) \cos \omega t \qquad (4-16)$$

Thus, the flame propagation speed influences by the non-uniform scalar profile is,

$$\left(\frac{S_u}{S_u^o} \right)^2 = (1 - 2\pi(2m_o + Q_o) \cos \omega t)^4 \exp \left[-T_a \left(\frac{1}{T_b} - \frac{1}{T_{ad}} \right) \right] \qquad (4-17)$$

Non-dimensional term of the $m_o$and Q_o consist effect of the oscillation frequency and oscillation amplitude. Thus, Eq. (4-17) shows that increases in the oscillation frequency and oscillation amplitude would increase the deviation of the S_u from the S_u^o. Figure 4-9 shows effect of the non-dimensional m_o and Q_o in Eq. (4-17). It is clearly seen that increases in m_o and Q_o is proportional to the increase in S_u/S_u^o.

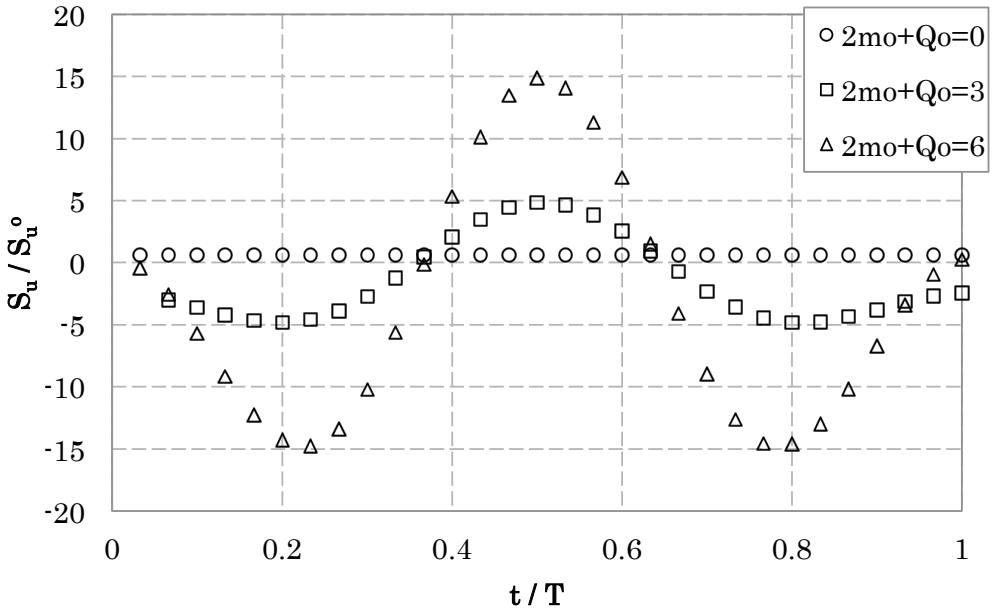

Figure 4-9 Variation of the S_u/S_u^o as a function of $2m_o + Q_o$.

Figure 4-10 shows the dynamics response of the flame propagation speed observed in numerical work. It is clearly seen the hysteresis exist in all cases and unsteady flame propagation speed deviates from the steady case as increase in oscillation frequency. Moreover, the flame propagation speed of unsteady case at leaner condition is higher than that steady case and opposite behavior occur near stoichiometric condition for both lean and rich cases.

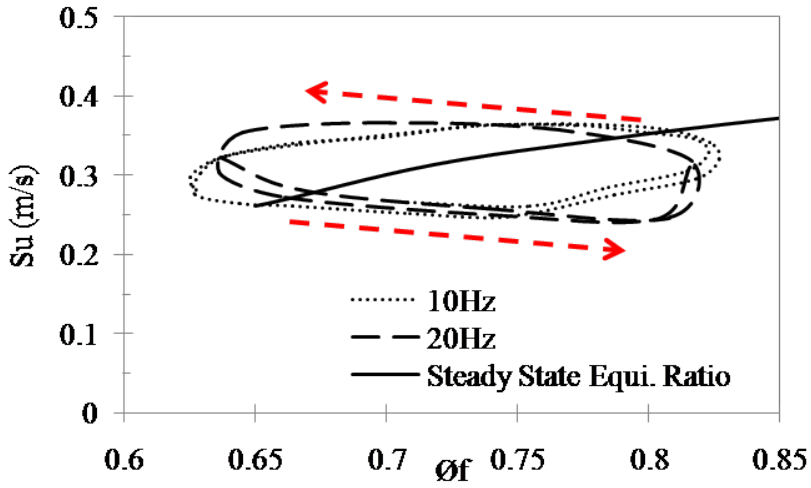

(a)

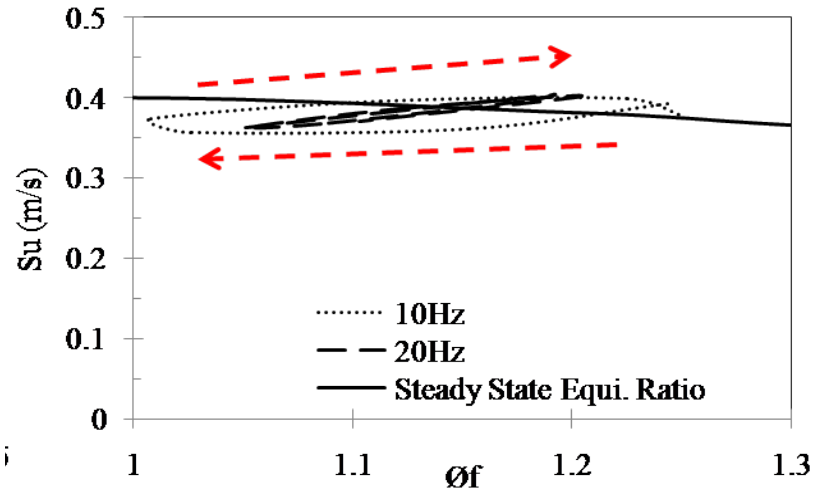

(b)

Figure 4-10 Dynamics response of flame propagation speed in numerical work for (a) lean condition case and (b) rich condition case.

Clarification of the dynamics response seen in Fig. 4-10, is approximate using Eq. (4-17).

The adiabatic flame temperature is calculated as following [Kang, 2009]:

$$T_{ad}(\emptyset) = -6256\emptyset^6 + 38210\emptyset^5 - 90760\emptyset^4 + 106080\emptyset^3 - 65234\emptyset^2 + 22123\emptyset - 1960\ (K) \quad (4-18)$$

Figures 4-11 and 4-12 show plot of the flame propagation speed variation in lean and rich condition based on Eq. (4-17) and it is qualitatively agree with the numerical result (Fig.4-10). Both numerical and simplified model shows that the flame propagation speed is higher when the equivalence ratio increasing than that is decreasing in rich case. Thus, the simplified model is clarified and the non-uniform scalar value profile in upstream and downstream of the flame significantly affected the flame dynamics.

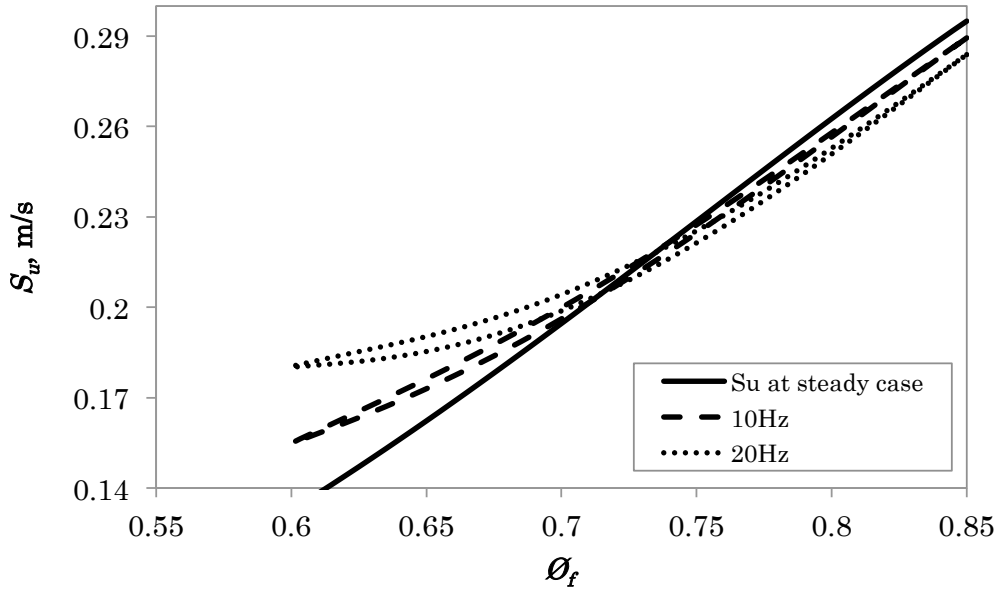

Figure 4-11 Dynamics response of flame propagation speed in analytical work for lean condition case.

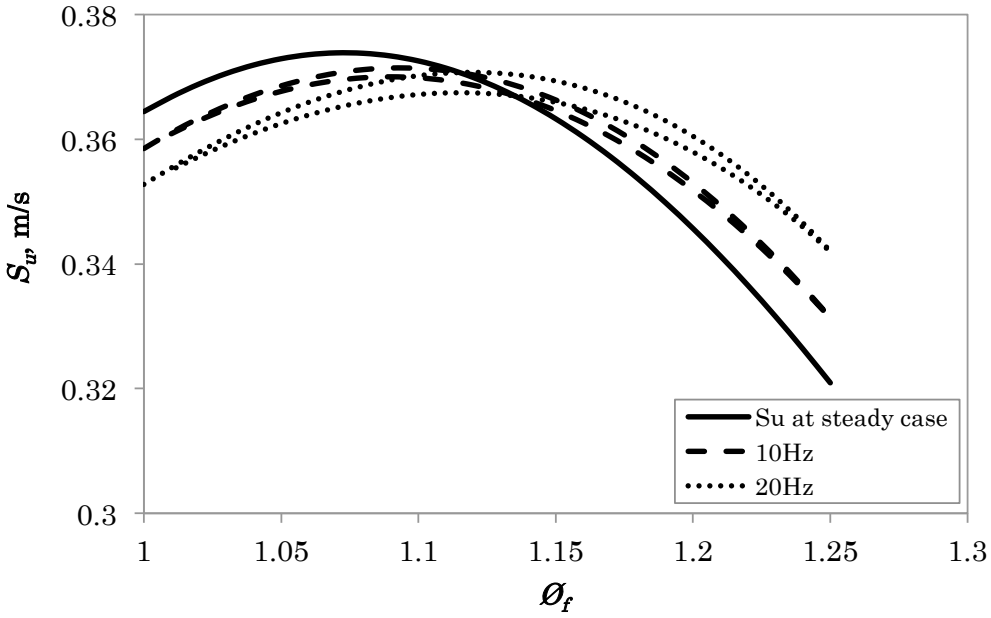

Figure 4-12 Dynamics response of flame propagation speed in analytical work for rich condition case.

4.5 Concluding remarks

Hysteresis motion of the flame movement is observed experimentally and numerically. Following the numerical results that have showed that the profiles of scalar variables in both upstream and downstream sides of the flame temporarily vary. Thus the concept of non-uniform scalar is introduced. This concept is verified by approximation method of an integral analysis. Following an integral analysis the simplified theoretical model that take into account the non-uniform scalar variations in both upstream and downstream directions of the flame zone was developed which confirmed the mechanism of the hysteresis motion.

Chapter 5

Dynamics of the conical laminar premixed flames – A numerical study

5.1 Introduction

Researchers have conducted fundamental studies to understand the mechanism of the dynamic flame response to equivalence ratio oscillations for stagnation flame configuration under lean condition (Lauvergne and Egolfopoulos, 2000, Sankaran and Im, 2002, Suenaga *et al.* 2003, Richardson *et al.* 2010), lean and rich conditions (Rahman *et al.* 2012) and crossover condition (Rahman *et al.* 2012). Conical-shaped and V-shaped flames have been used as well (Cho and Lieuwen, 2005, Birbaud *et al.* 2008, Ax *et al.* 2009, Shreekrishna *et al.* 2010, Riazi and Farshchi, 2011, Hemchandra, 2012).

Research on premixed flames influenced by the equivalence ratio oscillation has been more rigorously performed under a lean condition rather than under a rich condition (Lauvergne and Egolfopoulos, 2000, Sankaran and Im, 2002, Suenaga *et al.* 2003, Cho and Lieuwen, 2005, Birbaud *et al.* 2008, Ax *et al.* 2009, Richardson *et al.* 2010, Shreekrishna *et al.* 2010, Riazi and Farshchi, 2011, Hemchandra, 2012). Moreover, there are

disagreements between reduced order modeling and multidimensional flame studies (Karimi *et al.* 2009 and Shreekrishna *et al.* 2010, Hemchandra, 2012). A detailed study of the multidimensional flame to understand the flame response would be beneficial for both fundamental understanding and practical interest. Therefore, our goal is to investigate and elucidate the conical flame responses to the equivalence ratio oscillation at rich mean equivalence ratio oscillation.

5.2 Numerical details

Numerical analysis was performed for a two-dimensional axi-symmetric laminar conical flame, with a CH_4/air mixture. Mixture with an equivalence ratio oscillation was issued from a 12.0 mm tube burner into the atmosphere. The computational domain along with the boundary conditions and coordinate system are shown in Fig. 5-1. The CH_4/air mixture with T = 300 K is issued from the Inlet 1 into the atmospheric domain. At the Inlet 1, the velocity profile is set as shown in Fig. 5-2 following the experimental result. The equivalence ratio was oscillated by a sinusoidal variation of the methane mass fraction Y_{CH4}. The equivalence ratio variation is expressed by; $\emptyset(t) = \emptyset_M + \emptyset_A \sin \omega t$. Thus, the methane mass fraction is expressed by; $Y_{CH4}(t) = Y_{CH4M} + Y_{CH4A} \sin \omega t$. At Inlet 2, air flows into the domain by defining the boundary as a pressure inlet boundary condition. Air is assumed to be a mixture of 21 mol% oxygen and 79 mol% nitrogen. The flow moves out from the domain at the Outlet based on pressure outlet boundary conditions. The axis of symmetry corresponds to the centerline of the burner, hence the boundary conditions are $v_r = 0$ and $\frac{\partial}{\partial r} = 0$.

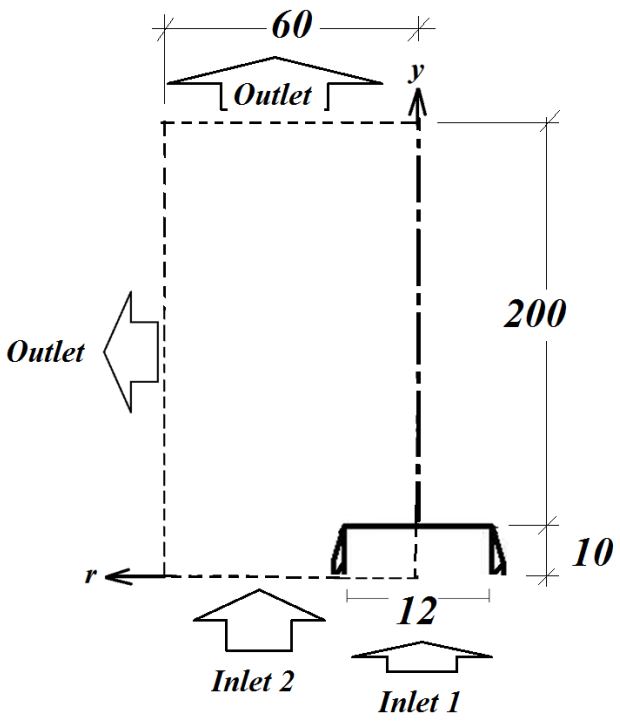

Figure 5-1 Computational domains with boundary conditions (unit mm).

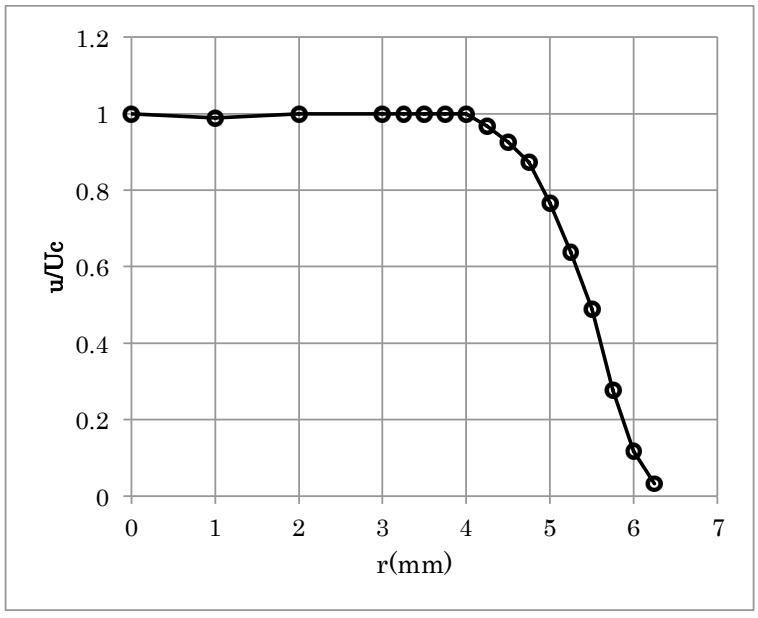

Figure 5-2 Velocity profile of the experimental work.

The generalized governing equations that is the conservation equation of mass, momentum (*y*-direction and *r*-direction), energy and chemical species respectively can be expressed as

$$\frac{\partial}{\partial t}(\rho\Phi) + \frac{\partial}{\partial y}(\rho v_y \Phi) + \frac{1}{r}\frac{\partial}{\partial r}(r\rho v_r \Phi) = \frac{\partial}{\partial y}\left(\Gamma\frac{\partial \Phi}{\partial y}\right) + \frac{1}{r}\frac{\partial}{\partial r}\left(r\Gamma\frac{\partial \Phi}{\partial r}\right) + S_\Phi \qquad (5-1)$$

where

$$\begin{matrix} \Phi \\ \begin{bmatrix} 1 \\ v_y \\ v_y \\ h \\ Y_i \end{bmatrix} \end{matrix} \quad \begin{matrix} \Gamma \\ \begin{bmatrix} 0 \\ \mu \\ \mu \\ k/cp \\ D_{im} \end{bmatrix} \end{matrix} \quad \begin{matrix} S_\Phi \\ \begin{bmatrix} 0 \\ g \\ 0 \\ 1 \\ 1 \end{bmatrix} \end{matrix}$$

The transport properties of a mixture such as the viscosity, thermal diffusivity and mass diffusivity are a function of temperature. Soret and Dufour effects and heat transfer by radiation are not considered in this study. The ideal gas assumption is applied.

The CH_4/air combustion reaction mechanism is very complex, consisting of hundreds of elementary reactions between dozens of intermediate gas species (Smith *et al.*). Since the objective of this work was to examine the dynamic response of the flame on the equivalence ratio oscillation, the reaction model was simplified. Since, Hemchandra (2012) uses a one-step overall reaction model for a lean mixture, the one-step overall reaction model is used in this study. Under a rich condition, the formation of CO usually occurs. Therefore, a two-step model, including CO-CO_2 conversion was examined. These reaction models follow those of Westbrook and Dryer (1981) as mentioned below:

One-step reaction mechanism,

$$CH_4 + 2O_2 \rightarrow CO_2 + 2H_2O \qquad (5-2)$$

The Arrhenius type reaction rate model as mentioned in Eq. (5-3) was used.

$$r_{f2} = \mathrm{A}_{f2} \times \exp\left(-\frac{2.027\times10^{8}\left(\frac{\mathrm{J}}{\mathrm{kmol}}\right)}{RT}\right) \times [CH_4]^{0.2}[O_2]^{1.3} \qquad (5-3)$$

Two-step reaction mechanism,

$$CH_4 + 3/2O_2 \rightarrow CO + 2H_2O \qquad (5-4)$$

$$CO + 1/2O_2 \leftrightarrow CO_2 \qquad (5-5)$$

The Arrhenius type reaction rate model as mentioned in Eqs. (4-6) - (4-8) was used.

$$r_{f4} = \mathrm{A}_{f4} \times \exp\left(-\frac{2.027\times10^{8}\left(\frac{\mathrm{J}}{\mathrm{kmol}}\right)}{RT}\right) \times [CH_4]^{-0.3}[O_2]^{1.3} \qquad (5-6)$$

$$r_{f5} = \mathrm{A}_{f5} \times \exp\left(-\frac{1.675\times10^{8}\left(\frac{\mathrm{J}}{\mathrm{kmol}}\right)}{RT}\right) \times [CO]^{1.0}[H_2O]^{0.5}[O_2]^{0.25} \qquad (5-7)$$

$$r_{b5} = \mathrm{A}_{b5} \times \exp\left(-\frac{1.675\times10^{8}\left(\frac{\mathrm{J}}{\mathrm{kmol}}\right)}{RT}\right) \times [CO_2]^{1.0} \qquad (5-8)$$

Following the suggestion by Westbrook and Dryer (1981), pre-exponential factors for the one-step and two-step reaction mechanism were adjusted and comparing the flame length of the numerical result, l_{fs} with that of the experimental results, l_{fex}. Generally, the calibration of the pre-exponential factor is performed at around $\emptyset$ = 1.0 where the flame speed is at the maximum value (Westbrook and Dryer, 1981). In this study, we calibrated the pre-exponential factor at $\emptyset$ = 1.1 and $\emptyset$ = 1.5 by comparing the flame length of the numerical result with the experimental one. This is because of the difficulty in reproducing

experimental flame properties at the equivalence ratio near the rich flammability limit compared to other equivalence ratios as shown in Ref. (Westbrook and Dryer, 1981). Tables 5-1 and 5-2, show the preliminary value of the pre-exponential factor for one-step and two-step reaction mechanism used in this study. As for the one-step reaction, varying A_{f2} compares the flame heights of predicted and experimental values. The value of $A_{f2} = 2.5 \times 10^{09}$ is used because the flame height of both $\emptyset = 1.1$ and $\emptyset = 1.5$ are fit with each other. For the two-step reaction, the value of A_{f4} is varied at first and then the value of pre-exponential factor of A_{f5} and A_{b5} are calibrated and finally found that $A_{f5} = 1.0 \times 10^{12}$ and $A_{b5} = 4.0 \times 10^{08}$ give the predicted flame height which fit with the experimental result.

Table 5-1 Pre-exponential factors for one-step reaction mechanism

A_{f2}	Results	
	$\emptyset = 1.1$	$\emptyset = 1.5$
Ref. (24) 6.7×10^{12}	$l_{fs} < l_{fex}$	$l_{fs} < l_{fex}$
5.0×10^{09}	$l_{fs} < l_{fex}$	$l_{fs} < l_{fex}$
2.5×10^{09}	***$l_{fs} = l_{fex}$***	***$l_{fs} \approx l_{fex}$***
1.0×10^{09}	$l_{fs} > l_{fex}$	$l_{fs} \approx l_{fex}$

Note: l_{fs} is a flame length in the numerical simulation; l_{fex} is a flame length in the experiment

Table 5-2 Pre-exponential factors for the two-step reaction mechanism

A_{f4}	A_{f5}	A_{b5}	Results	
			$\emptyset = 1.1$	$\emptyset = 1.5$
Ref. (24)2.3×10^{07}	$1.0 \times 10^{14.6}$	5.0×10^{08}	$l_{fs} > l_{fex}$	$l_{fs} > l_{fex}$
3.2×10^{09}	$1.0 \times 10^{14.6}$	5.0×10^{08}	$l_{fs} = l_{fex}$	$l_{fs} < l_{fex}$
3.2×10^{09}	**1.0×10^{12}**	**4.0×10^{08}**	***$l_{fs} = l_{fex}$***	***$l_{fs} \approx l_{fex}$***

Note: l_{fs} is a flame length in the numerical simulation; l_{fex} is a flame length in the experiment

Numerical calculation was performed by the finite volume method using Ansys FLUENT 12.1 (Ansys Fluent, 2009). All conservation equations were solved using a

segregated solver with an under relaxation method. A variable size grid with a minimum grid size of 1×10^{-5} m × 1×10^{-5} m was used. The minimum size of grid is determined to be around 1/100 of the flame thickness. The minimum grid sizes are set at the region where the flame is located. The maximum grid size is determined as 1/10 of the flame thickness. The grid size is varies from minimum to maximum at far from the flame to reduce the computation time.

The isothermal flow field was first calculated. Setting the temperature at the ignition zone shown in Fig. 5-1 at 2500 K then artificially ignited the mixture. When the reaction started and the flame was formed, the artificial ignition temperature was off and the flame freely moved to a stable position at which the incoming unburned velocity of the flame was equal to the laminar burning velocity. Subsequently, the equivalence ratio at the Inlet (1) was varied in a sinusoidal manner with the time step 1×10^{-5} s. The frequency of equivalence ratio variation is 10, 50 and 150 Hz. The simulations were performed on a Quad-Cores 3.33 GHz Intel Xeon processor with 12.0 GB RAM.

5.3 Results and discussion

Initially, the steady state case will be discussed to validate the reaction models. Later, the unsteady case is analyzed to discuss the dynamics of the conical flame with the equivalence ratio oscillation.

5.3.1 Steady state case

Flame length l_f, between the one-step reaction mechanism, two-step reaction mechanism and experimental data were compared to validate the reaction model. Experiments were performed in atmospheric pressure. An axis-symmetric, steady laminar premixed conical flame is generated with a straight pipe burner of 12.7 mm in diameter. A honeycomb was inserted in the burner to reduce the flow turbulence in order to use a shorter straight pipe. The total flow rate of the CH_4/air mixture is 10.0 l/min. Therefore, the Reynolds number of the present study is Re = 1107. The flow velocity profile and the turbulence intensity of the velocity fluctuation are measured at 1mm downstream of the burner exit using the hot wire anemometer. Air is issued from the burner instead of the CH_4/air mixture. The hot wire anemometer had a Tungsten sensing element of 5.0 μm in

diameter. Figure 5-3 shows the mean flow velocity profile at the exit of the burner normalized by the mean flow velocity at the centerline. The flat top shape of the flow velocity profile is formed in this burner. In Fig. 5-3, the turbulence intensity of the velocity fluctuation is plotted as well. The turbulence intensity was normalized as $\sqrt{\overline{u'^2}}/\overline{U}_{ref}$, where $\sqrt{\overline{u'^2}}$, is the root mean square of the fluctuations velocity and $\overline{U}_{ref}$, is defined as an average value of the mean velocity at the flat velocity profile in range of r = -3.0 mm to 3.0 mm. The low turbulence region at the middle of the burner can be clearly seen. The turbulence intensity is slightly increased near the burner wall mainly due to the steep decreases in the velocity toward the burner wall. This result confirmed the laminar flow is formed at the burner exit.

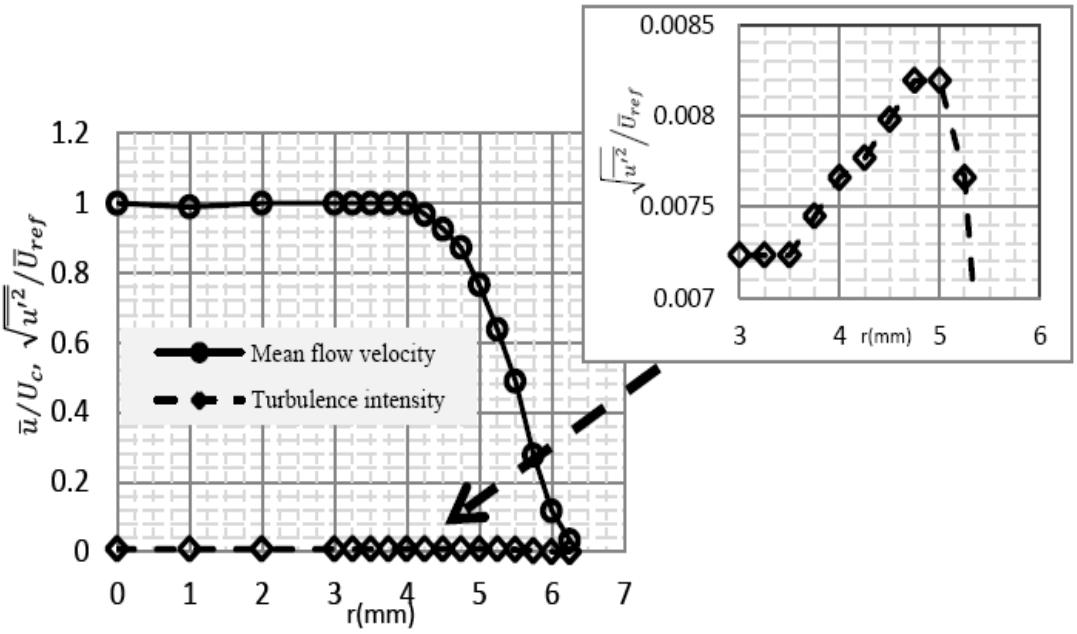

Figure 5-3 Normalized profile of the mean flow velocity and turbulence intensity of velocity fluctuation at 1 mm downstream from the exit of the burner.

Variations in l_f with the equivalence ratio are shown in Fig. 5-4. Here l_f is normalized as $l_f = (l_f - l_{f,min})/(l_{f,max} - l_{f,min})$. In Fig. 5-3, the experimental result shows that l_f increases monotonically with increasing equivalence ratio, $\emptyset$. For the one-step model, l_f is

higher compared to the experimental result at $\emptyset$ = 1.2 to $\emptyset$ = 1.45. In addition, beyond the $\emptyset$ = 1.45, the flame length becomes constant while the experimental result shows a steep increase with an increases in the equivalence ratio. This shows that the one-step model failed to predict the flame length especially near the rich flammability limit. On the other hand, the l_f of two-step model increases monotonically similar to the experimental result in all equivalence ratios although l_f is higher at $\emptyset$ = 1.2 and $\emptyset$ = 1.3. The difference of l_f between these two models and the experimental result is discussed by investigating the value of [CO] / [CO_2].

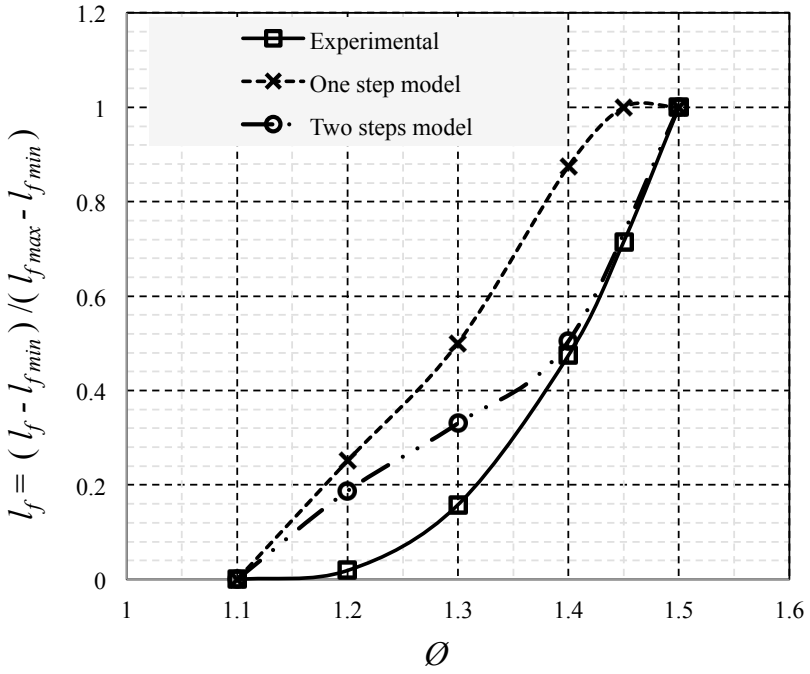

Figure 5-4 Comparison of the flame length between numerical and experimental result under steady state condition.

Figure 5-5 shows the variation in [CO] / [CO_2] of the one-step and two-step models. For the one-step model, the CO species is not considered in the reaction mechanism and leads to zero value of the [CO] / [CO_2] in all ranges of equivalence ratios, $\emptyset$ as shown in Fig. 5-5. On the other hand, the two-step model shows monotonically increments of the [CO] / [CO_2] with increasing equivalence ratio. Increases of the [CO] / [CO_2] with increasing the equivalence ratio are in agreement with Westbrook and Dryer (1981). The difference

between both models and the experimental result is therefore due to the substantial amounts of CO in the combustion products with CO_2 and H_2O for the two-step model. On the other hand, the deviation of the two-step model at $\emptyset$ = 1.2 and $\emptyset$ = 1.3 from the experimental result is questionable and probably because of the weak predictions of the [CO] / [CO_2]. Refinement of the [CO] / [CO_2] can be performed by manipulating the exponent in the Eq. (5-8) as discussed by Westbrook and Dryer (1981). Since it takes enormous computational time to simulate the unsteady flame motion, level set modeling of the G-equation and the one-step reaction model is used in the lean case (Hemchandra, 2012). In the present study, the two-step reaction model with CO formation is used because CO formation plays an important role in rich case.

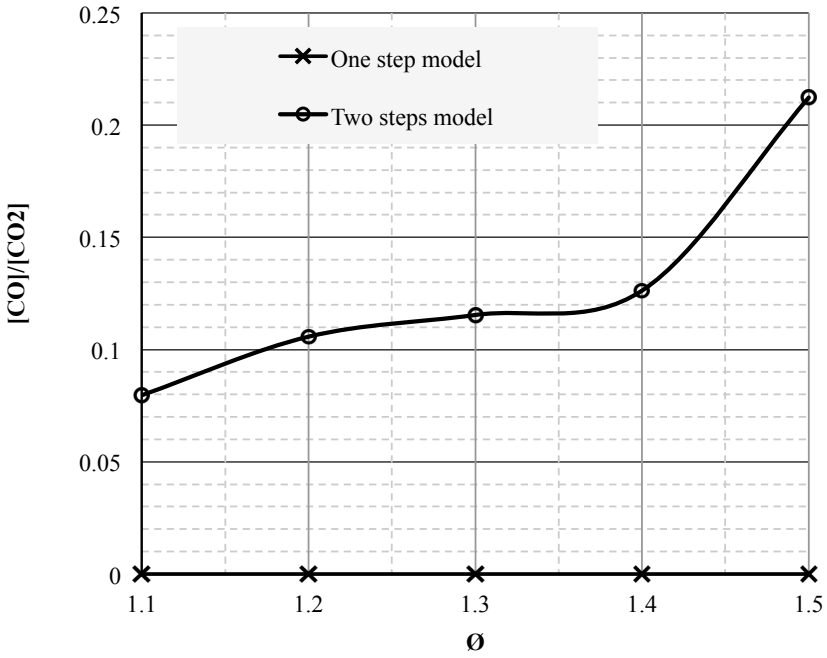

Figure 5-5 Burned gas equilibrium ratio from the one-step model and the two-step model under steady state condition.

Figure 5-6 shows qualitative comparison of the flame shape in the experiment and simulation with the two-step reaction model. The flame front is well resolved and the flame shape is predicted although the flame length at $\emptyset$ = 1.2 and $\emptyset$ = 1.3 of the experiment is slightly shorter than the simulation results.

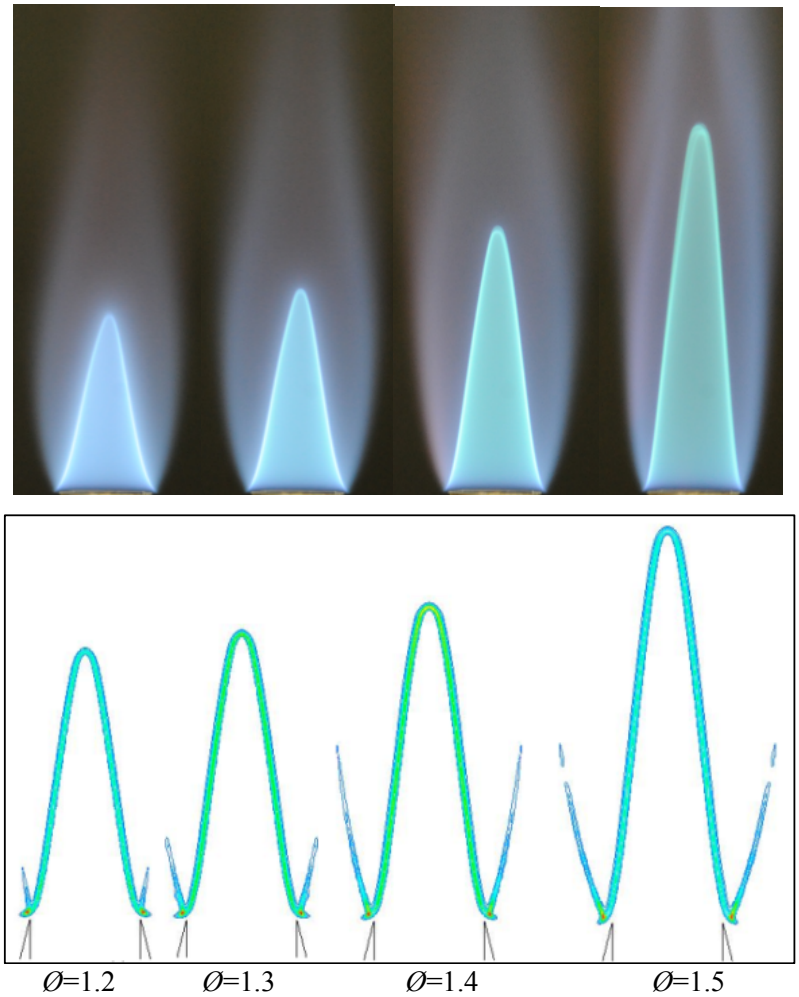

Figure 5-6 Comparisons of the flame shape in the experiment and simulation with various equivalence ratios at steady state.

5.3.2 Dynamics of the flames

The frequency of the equivalence ratio oscillation was chosen under three conditions: low frequency regime, medium frequency regime and high frequency regime. These regimes can be categorized by the wavelength of the equivalence ratio oscillation and the flame length, l_f. In the low frequency regime 10 Hz case, the equivalence ratio oscillation wavelength is estimated as $\lambda_{eq} = U_o/f$ =133 mm. This oscillation wavelength is larger than the flame length at mean equivalence ratio ($Ø_M$ = 1.3) l_f = 30 mm. At the middle frequency regime 50 Hz, the equivalence ratio oscillation wavelength $\lambda_{eq} = U_o/f$ =26.6

mm is comparable to l_f. $\lambda_{eq} = U_o/f = 8.87$ mm is defined as the high frequency regime, 150 Hz. The equivalence ratio oscillation wavelength is significantly less than the flame length at $\emptyset_M = 1.3$.

Figure 5-7 shows the variation of the conical flame tip at various oscillation frequencies. These cycles are obtained after a few transient cycles. This figure clearly shows that the flame tip moves sinusoidal at the low frequency regime following the sinusoidal variation in the equivalence ratio oscillation. The movement of the flame tip in the low frequency regime is similar to that of the observation in the experiment done by Ax *et al.* (2009). As the frequency regime is shifted to the medium regime, there is significant deviation of flame movement.

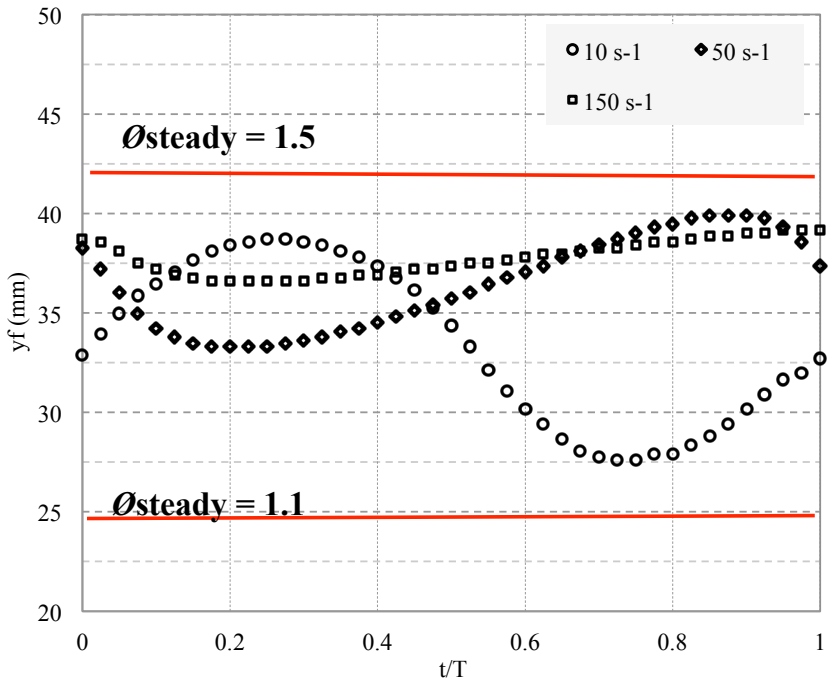

Figure 5-7 Dynamics of conical flame tip along the central axis (r = 0)at various oscillation frequencies.

Firstly, the attenuation of the flame tip movement is expected to be similar to the attenuation in the equivalence ratio oscillation amplitude as seen in Fig. 5-8. At high frequency regime attenuation of the flame tip movement is very significant compared to the low frequency regime. The mechanism of the attenuation is supposed to be that the

period of the equivalence ratio oscillation T = 1/150 s = 6.7 ms is significantly smaller than the convective transport time from the burner to the flame tip τ = 22.5 ms. Secondly, an interesting behavior of the dynamics of flame tip is seen. The flame tip gradually moves downstream and moves sharply upstream in one period of the oscillation cycle. This behavior shows is similar to the results obtained for the acoustically perturbed conical flame case (Kornilov, 2006). It is supposed that a similar parameter controlled the dynamics of the flame tip. To discuss the dynamics of the flame tip, the variation in the flame height oscillation as a function of frequency variation will be elaborated in the following section in detail.

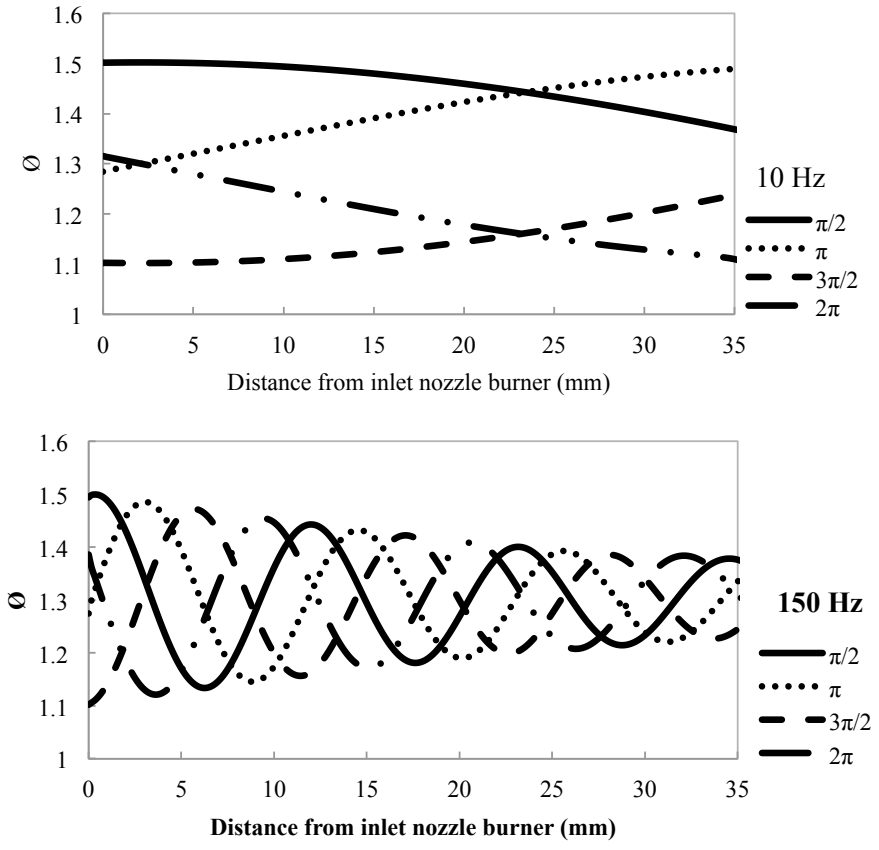

Figure 5-8 Attenuation of the equivalence ratio variation along the central axis (r = 0) as a function of the oscillation frequency at $Ø_m$ = 1.3 and $Ø_A$ = 0.2.

Figure 5-9 shows the behavior of the flame surface responding to the equivalence ratio

oscillation at the low frequency regime (10 Hz). Figure 5-9 shows the streamlines and the contour of CH_4 mass fraction variation. The CH_4 mass fraction varies gradually in flame length. The convective transport time of the equivalence ratio from the burner to the flame tip is expected to correspond to τ = 22.5 ms. Therefore, convective transport time is significantly smaller than the period of the equivalence ratio oscillation, T = 100 ms. In Fig. 5-8, at t/T = 0.00 fuel concentration varies gradually from near stoichiometric to rich conditions along the flame length. A higher burnt temperature is found in Fig. 5-9 at t/T = 0.00 because of the high flame temperature near the stoichiometric condition. As the time approaches to t/T = 0.25, the flame length increases. The flame length reached the maximum point at this time, but it is comparatively lower than the steady state case at $\emptyset_{steady}$ = 1.5 (Fig. 5-7). The flame length increases because the equivalence ratio is under a rich condition. A rich equivalence ratio reduces the flame temperature and produces a low burnt gas temperature (Fig. 5-9). A decrease in flame temperature reduces the burning speed. A low burning speed allows the flame surface to become convex toward the burnt gas and encounters increased fluid velocity. Therefore the flame surface tends to move further downstream. Moreover, the flame length in the unsteady case was not as high as in the steady state case due to the variation in the equivalence ratio along the flame length.

Later, at t/T = 0.50, the flame length reduces following the variations in the equivalence ratio toward the near stoichiometric condition. A decrease in flame length was expected since the equivalence ratio varies near the stoichiometric condition producing a high flame temperature and subsequently increases the burnt gas temperature (Fig. 5-9). A high flame temperature induces higher burning speed. At high burning speed the flame surface becomes concave toward the burnt gas and encounters decreased fluid velocity. As a result, the flame surface tends to move further upstream. At t/T = 0.75, the flame length was at minimum position for the unsteady case. This minimum position in the unsteady case is shifted downstream compared to the steady state case at $\emptyset_{steady}$ = 1.1. This behavior is similar to the case of maximum position shifted upstream from the steady state case. As a result, at the low frequency regime the flame surface is moving outward and inward as shown in Fig. 5-9. This finding fills the gap left by Birbaud *et al.* (2008) that only focus in the high frequency regime (375 Hz).

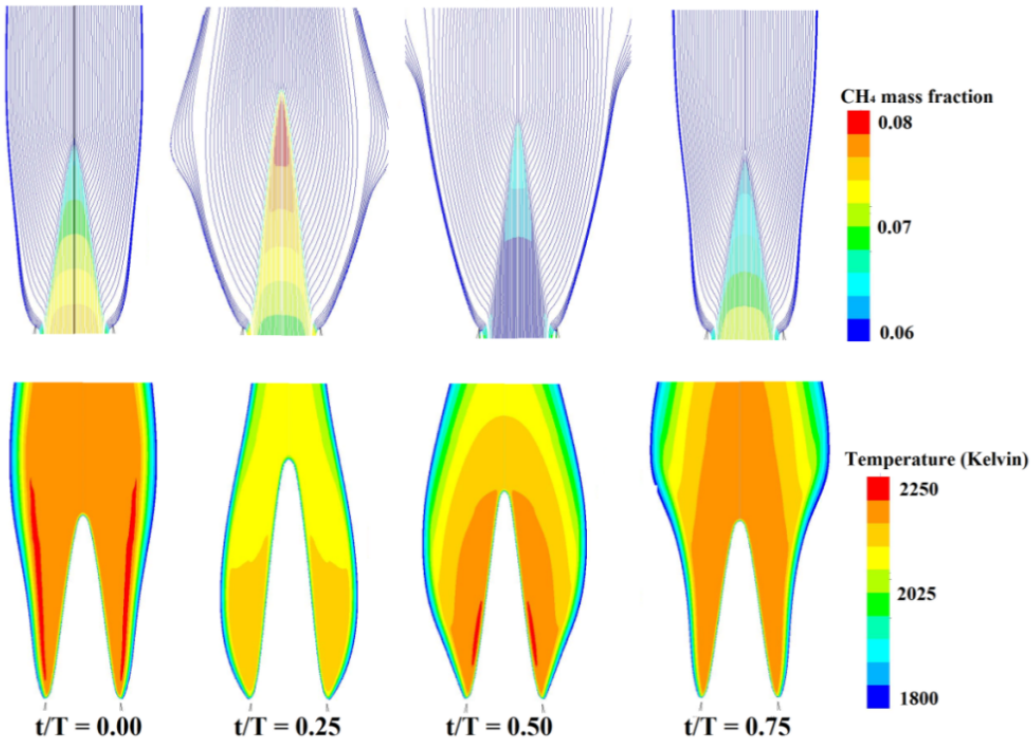

Figure 5-9 Streamlines and contours of CH_4 mass fraction and temperature contours for the 10 Hz oscillation frequency case.

An interesting phenomenon is observed at t/T = 0.75. At t/T = 0.75, the flame tip is at minimum (Fig. 5-7) although the equivalence ratio approaching the flame is higher than that at t/T = 0.50 (Fig. 5-9). This observation is ambiguous since the flame should reach the minimum flame length when the equivalence ratio nears the stoichiometric condition approaching the flame because the flame speeds at maximum value. To clarify this observation both the CH_4 mass fraction and flame temperature contours in Fig. 5-9 were examined. At t/T = 0.50, the equivalence ratio varies nears the stoichiometric conditions and produces a high burnt gas temperature. Later, at t/T = 0.75, increases in the equivalence ratio result in a low flame temperature. But, the high burnt gas temperature produced near the stoichiometric condition of the equivalence ratio previously covers all the flame surfaces. Therefore, heat is transferred from the burnt gas to the flame zone, which strengthens the flame and allows the flame surface to move upstream even though the high fuel concentration mixture reaches the flame zones. This mechanism is the back support effect in Ref. (Marzouk *et al*. 2000). Influences of the back support effect towards

flame dynamics have been discussed previously (Rahman *et al.* 2012, Rosdzimin *et al.* 2012). In the previous study (Rahman *et al.* 2012, Rosdzimin *et al.* 2012), responses of the premixed methane/air mixture flames under equivalence ratio oscillations were numerically investigated assuming axis-symmetric stagnation flow fields and the back support effect was found playing important role on the dynamics of the flame movement. An explanation of this back support mechanism is shown in Fig. 3-16. The back support mechanism occurs when the equivalence ratio becomes rich from the stoichiometric condition, which induces the flame temperature decrease. In turn, it induces a heat transfer from the burnt region to the flame zone and strengthens the flame. Therefore, the flame surface moves upstream. On the other hand, the flame temperature is low at the rich equivalence ratio, when the equivalence ratio nears the stoichiometric condition the flame temperature increases. Increasing the flame temperature induces heat transfer from the flame zone to the burnt region, whereupon the flame is weakened and the flame surface moves downstream.

Figure 5-10 shows the behavior of the flame surface response to the equivalence ratio oscillation at the medium frequency regime. In Fig. 5-10, the equivalence ratio varies between $\emptyset \approx 1.2$ to $\emptyset \approx 1.4$ in flame length. These variations are narrower than the initial equivalence ratio oscillation ($1.1 < \emptyset < 1.5$). This is expected because the period of equivalence ratio oscillation, $T = 20$ ms is almost equal to the convective transport time, $\tau = 22.5$ ms. Moreover, the maximum and minimum equivalence ratio in the flame length exist at all times. This observation is different from the 10 Hz case in that the equivalence ratio varies gradually in flame length. How the maximum and minimum equivalence ratio in the flame influence the flame surface is discussed in detail below:

The equivalence ratio variation at the flame tip region produces the variation in flame temperature. A higher/lower flame temperature induces a high/low burning speed and subsequently allows the flame surface to encounter decreased/increased fluid velocity. Therefore, the flame tip tends to moves further upstream/downstream and causes a variation in flame length.

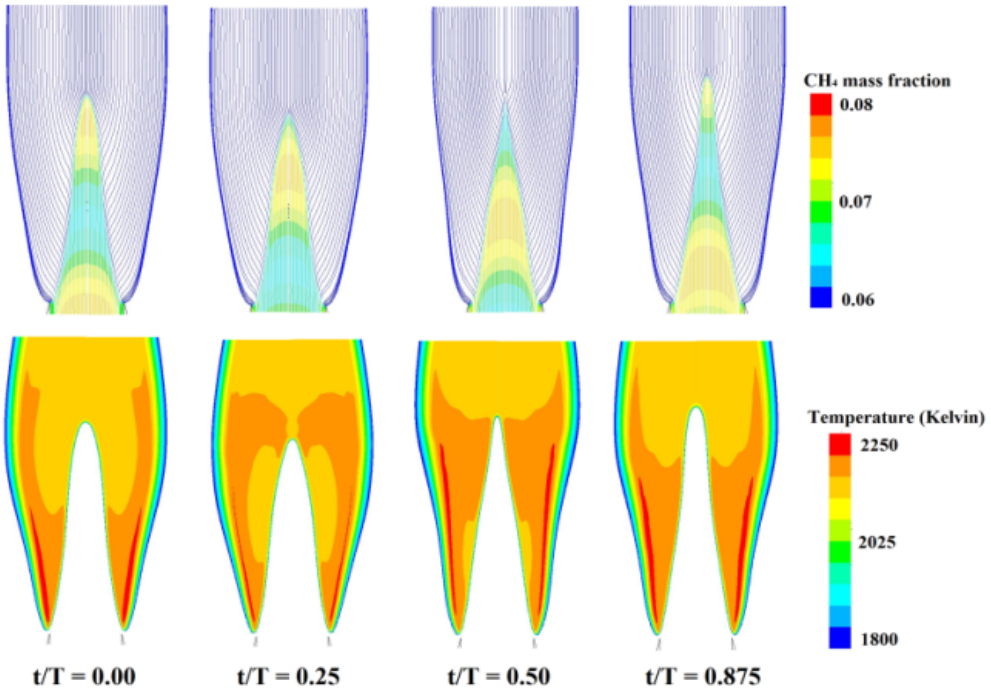

Figure 5-10 Streamlines and contours of CH_4 mass fraction and temperature contours for the 50 Hz oscillation frequency case.

A variation in the equivalence ratio along the flame influences the flame surface in different ways. As the maximum equivalence ratio mixture approaches near the flame tip, the minimum equivalence mixture ratio exists at the flame base. This variation occurs alternately in one period of the equivalence ratio oscillation cycle because the period of the equivalence ratio oscillation is almost equal to the convective transport time. Based on previous discussions, variation in the equivalence ratio allows the flame surface to become concave/convex toward the burnt gas and tends to move further upstream/downstream locally depending on the local equivalence ratio variation. Therefore, the large difference in the amplitude of the equivalence ratio variation between near the flame tip and near the flame base regions produces a concave and convex flame surface toward burnt gas in the flame length. As a result, wrinkling is seen along the flame surface. The flame wrinkling travels from the flame base to the flame tip following the convective transport of the equivalence ratio mixture variation as shown in Fig. 5-10. This observation is similar to the V flame case (Karimi *et al.* 2009). Then, an increase in the equivalence ratio oscillation

frequency induces the attenuation of the flame tip oscillation amplitude as shown in Fig. 5-7. In addition a weak wrinkling can be observed in Fig. 5-10 because one cycle of equivalence ratio oscillation emerges in a flame length. In this case, part of the flame surface is offset in the downstream and the other in the upstream direction simultaneously. Thus, the flame tip oscillation amplitude is attenuated. Therefore, at the medium frequency regime, the flame tip motion is attenuated (Fig. 5-7) for two reasons. One reason is the attenuation in the equivalence ratio amplitude and the second reason is the wrinkling of the flame surface.

Figure 5-11 shows the behavior of the conical flame at the high frequency regime. At the high frequency regime the period of the equivalence ratio oscillation is significantly smaller than the convective transport time from the burner to the flame tip as shown previously. The shorter period of the equivalence ratio oscillation produces more than two cycles of the equivalence ratio oscillation in a flame length. Therefore, the number of wrinkles increases and reduces the wavelength of the wrinkling. An increase in the number of wrinkles means that the number of the flame surface offset in the downstream and upstream directions simultaneously around the steady state flame surface locally increases. This phenomenon induces large attenuation of the flame tip oscillation amplitude in addition to the attenuation of the equivalence ratio oscillation amplitude.

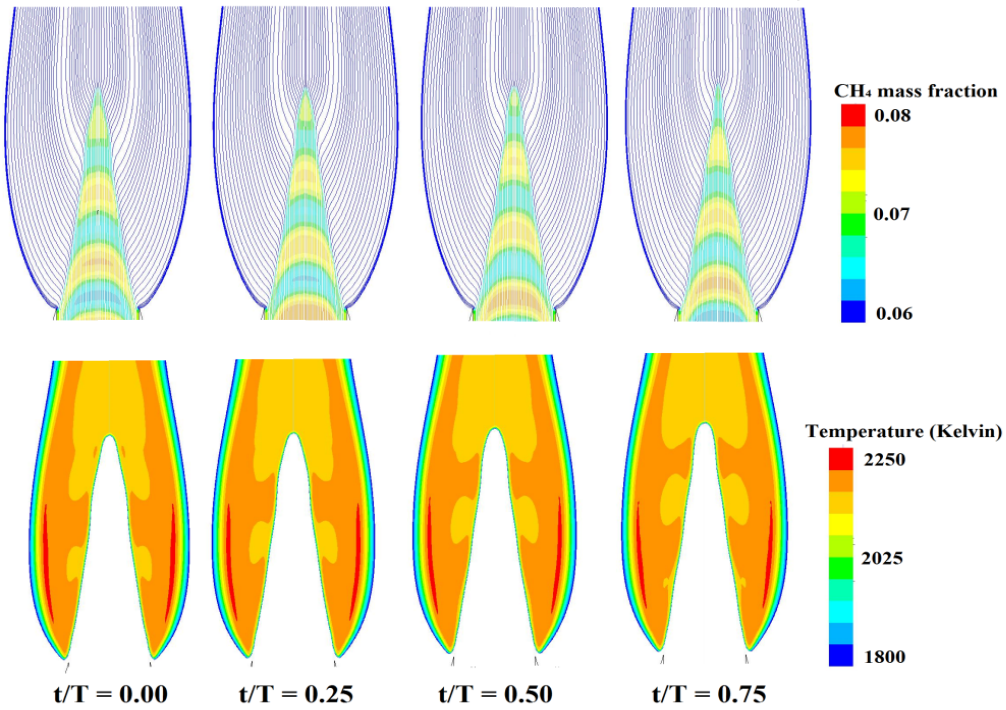

Figure 5-11 Streamlines and contours of CH_4 mass fraction and temperature contours for the 150 Hz oscillation frequency case.

The mechanisms of the unsteady flame tip behavior in Fig. 5-7 are qualitatively similar to the medium frequency regime case, even though the wavelength of the wrinkle is small. In the present study, an increase in the equivalence ratio oscillation frequency decreases the flame response. The flame tip dynamics in the 150 Hz case compare to those in the 50 Hz case. This observation agrees with the reduced order modeling approaches done by Cho and Lieuwen (2005) and Riazi and Farshchi (2011).

In the present study, the flame responses to the equivalence ratio variation were qualitatively similar to the acoustically perturbed (velocity variations) conical flames (Kornilov, 2006) when it is brought to the flame tip movement and wrinkles develop along the flame surface at a certain frequency. It is interesting to examine the parameter that controlled the flame responses for both cases. In this study we observed that the period of equivalence ratio oscillation, T and the convective transport time, τ controlled the flame response in terms of the flame tip movement and wrinkle development. We found that

when $T/\tau \geq 1.0$, the flame tip responds in a quasi-steady manner without wrinkles on the flame surface. On the other hand, when$T/\tau \leq 1.0$, the flame tip responds in an unsteady manner with wrinkles on the flame surface.

In the velocity variations case, we examined the results produced by Kornilov (2006) in Fig. 5-12. A conical flame is formed with a flat profile flow velocity with *Uo* =100 cm/s and *Ø* = 1.2 of methane/air mixture is used. The flame is 30 mm long. This means that the convective transport time is estimated as $\tau = l_f / Uo$ = 30 ms. The quasi-steady dynamic of the conical flame at 30 Hz perturbation frequency was observed (Kornilov, 2006), which corresponds to the period of perturbation oscillation, *T* = 33.33 ms. Moreover, they also measured the flame tip movement at 190 Hz, which corresponds to the period of perturbation oscillation, *T* = 5.26 ms and found that the flame tip moves up smoothly and drops sharply. In addition, increase in the perturbation frequency leads to the development of wrinkles as seen in Fig. 5-12.

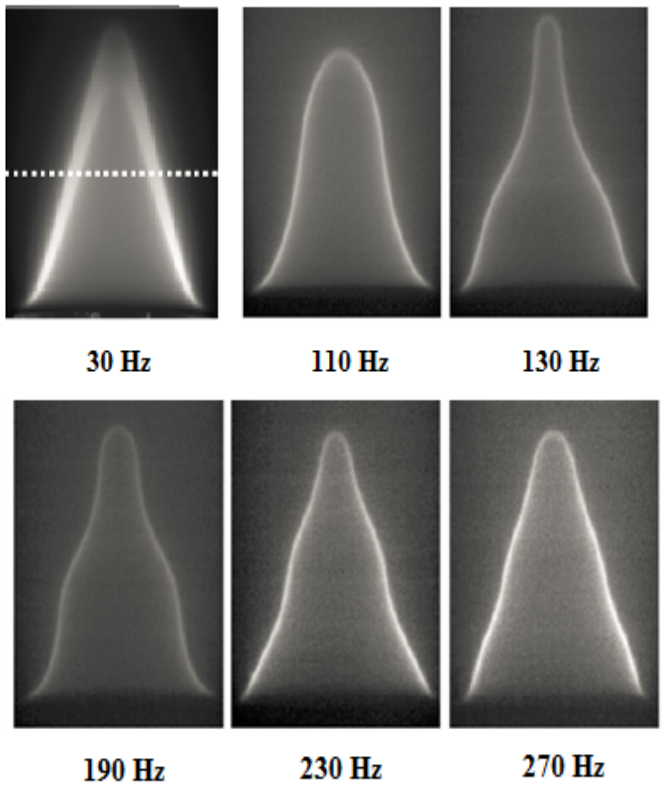

Figure 5-12 Velocity perturbation case (Kornilov, 2006).

In both cases T/τ is important for characterizing the flame dynamics. It indicates that the local balance between the burning velocity and approaching the flow velocity determines the flame shape variations. Therefore, we proposed T/τ is a controlling parameter of the conical flame response in a quasi-steady $(T/\tau \geq 1.0)$ or unsteady $(T/\tau \leq 1.0)$ manner for both cases of either the equivalence ratio or flow velocity variations.

On the other hand, in stagnation flame case the critical Strouhal number that divide the quasi-steady and unsteady case is $St = 1.0$. Strouhal number is defined as the ratio between the characteristics time of the flow and the characteristics time of the oscillation. In the present study, ratio between the conical flame height, L and characteristic length of the equivalence ratio oscillation, U_o/f is important since it show that if (L / (U_o/f)) < 1, the wrinkle is not exist and if (L / (U_o/f)) > 1, then the wrinkle exists. The existence of the wrinkle is important since it affected the flame tip motion in addition to the attenuation of the equivalence ratio oscillation amplitude as discuss previously. Moreover, it is interesting to see that if the ratio between the conical flame height, L over the characteristic length of the equivalence ratio oscillation, U_o/f is rearranged then it gives the ratio between the characteristics time of the flow, L/U_o and the characteristics time of the oscillation, $1/f$. Based on the definition of the Strouhal number for the conical flame, it produces similar critical value to the stagnation flame that divided between the quasi-steady (St < 1.0) and unsteady (St > 1.0) manner for both cases either the equivalence ratio or flow velocity variations.

5.4 Concluding remarks

The effect of the equivalence ratio oscillation on a conical premixed methane/air flame was studied computationally using an axis-symmetric flow field. The flame responses to the low, medium and high oscillation frequency regimes were investigated. The frequency regime was determined by comparing the equivalence ratio wavelength and the flame length at the mean equivalence ratio oscillation.

In this study we validated the reaction model used in numerical simulations with experimental results. We found that under the rich condition the two-step reaction mechanism with CO formation predicts well the variation in the flame shape of the steady

state condition with equivalence ratio variation while the one-step irreversible mechanism failed to predict the flame shape especially under the near rich flammability limit condition. Therefore, the two-step reaction mechanism was used in the present study.

In an unsteady case, the dynamic response of the flame tip for low (10 Hz), medium (50 Hz) and high (150 Hz) oscillation frequency regimes show interesting behavior. At the low frequency regime the flame tip varies with the equivalence ratio variation in a quasi-steady manner. At medium and high oscillation frequency regimes, wrinkling of the flame surface is observed. This is because the equivalence ratio oscillation cycle exists for more than one cycle in a flame length. Moreover, part of the flame surface is offset in the downstream and the others in the upstream direction simultaneously. Furthermore, an increase in the equivalence ratio oscillation frequency increases the number of wrinkles. As a result, the wrinkling attenuates the flame tip motion amplitude in addition to the attenuation of the equivalence ratio oscillation amplitude.

We found that the Strouhal number define as a ratio between the characteristic time of flow and the characteristic time of oscillation control the flame response in terms of the flame tip movement and wrinkle development in the case of the equivalence ratio or flow velocity perturbations. Therefore, we propose that St is a controlling parameter of conical flame response in a quasi-steady $St < 1.0$ or unsteady $St > 1.0$ manner.

Chapter 6

Conclusions and future works

6.1 Conclusions

Effect of the equivalence ratio oscillation on a premixed CH_4/air flame motion is studied experimentally and numerically. Stagnation flow field is considered in the experimental work. While stagnation and conical flow fields were used in numerical study. Range of the frequency focuses in this work is defined as a wavelength of the oscillation to be larger than that a nominal flame thickness. Oscillation frequencies of 2 to 20 Hz cases at lean equivalence ratio oscillation region were done in the experimental work. Flame response to the equivalence ratio oscillation frequencies of 10, 20, 50 Hz at three different oscillation cases (lean, rich and lean rich crossover cases) and 10, 50, 150 Hz at rich condition were considered in the numerical work for the stagnation and the conical laminar premixed flame respectively.

In an experimental work, lean region is focused because flame moves monotonically in equivalence ratio variations. It was observed that the flame moves periodically following the variation of the equivalence ratio oscillation produces by the novel oscillator. Movement of the flames is primarily due to the equivalence ratio oscillations, since the velocity perturbation is significantly suppressed in the present work. Moreover, the flame movement amplitude is significantly increases/decreases following an increase in the oscillation frequency at the oscillation frequency less/larger than 5 Hz. Increase in the flame movement amplitude at the oscillation frequency, $f < 5$ Hz is due to the characteristic of the piston type oscillator. On the other hand, at $f > 5$ Hz an oscillation frequency significantly influences the flame movement. Furthermore, the ratio between the characteristic time of the flow and the characteristic time of the oscillation called *Strouhal* number is an important parameter that categories the dynamics of the laminar premixed flame in quasi-steady ($St < 1.0, f < 6.5$ Hz) or unsteady ($St > 1.0, f > 6.5$ Hz) manner.

The experiment work shows that the flame dynamics is significantly affected by the oscillation frequency at $St > 1.0$. Therefore, to elucidate the mechanism of the flame response to the equivalence ratio oscillation at low oscillation frequency, a numerical work of the stagnation laminar premixed flames is focused at $St > 1.0$ ($f > 6.5$ Hz) (10 Hz, 20 Hz and 50 Hz) in lean, rich and lean rich crossover cases. The result shows that the flame moves periodically following the variation of the equivalence ratio oscillation at the upstream edge of the pre-heat zone. Moreover, the flame movement amplitude significantly decreased following an increase in the oscillation frequency. These observations agreed with the experimental results. Numerical result demonstrated that the flame location movements create the closed cycle around the flame location of correspond equivalence ratio in the steady state condition for all cases. Formation of the closed cycle

in lean, rich and lean rich crossover cases show an interesting behavior and the back support effect is assumed to influence the formation. Secondly, the flame displacement speed variation is estimated. The results show that the time variation of the flame location plays a significant effect to the flame displacement speed. In both the experimental and the numerical works of the stagnating flow, the equivalence ratio oscillation amplitude attenuates from the exit of the burner towards downstream region and it is much significant as an increase in the oscillation frequency.

Periodical variation of the flame movement is seen in the experiment and numerical work of the stagnation flame. Detailed analysis in the numerical work showed that the periodic variation of the flame movement is related to a hysteresis of the flame movements. Initially, it was supposed to be affected by a back support effect. Later, due to the non-uniform scalar value profile also exists in the upstream side; concept of the non-uniform scalar value profile is introduced. The concept is successfully predicted the periodic variation of the flame dynamics using simplified mathematical modeling and it is qualitatively agreed with the numerical results.

The analysis on a conical laminar CH_4/air premixed flame at the various *Strouhal* number have been done to discuss the generalization of the *Strouhal* number as a controlling parameter of the flame dynamics under the equivalence ratio oscillation. It is found that the *Strouhal* number defined as a ratio between the characteristic time of flow and the characteristic time of oscillation controls the flame response in terms of the flame tip movement and wrinkle development in the case of the equivalence ratio. Moreover, the present *Strouhal* number, works well in the flow velocity perturbation case (Kornilov, 2006) by showing the similar behavior. At the $St < 1.0$ (10 Hz) the flame tip varies quasi-steadily following the variation of the equivalence ratio. On the other hand, at $St >$

1.0, (50 and 150 Hz) the flame tip gradually moves downstream and moves sharply upstream in one period of the oscillation cycle and wrinkling of the flame surface is observed following the variation of the equivalence ratio.

Overall, a ratio between the characteristic time of the flow and the characteristic time of the oscillation called *Strouhal* number is an important parameter that generalizes the dynamics of the laminar premixed flame under equivalence ratio oscillation in quasi-steady (St < 1.0) or unsteady (St > 1.0) manner either the stagnation or conical flame configurations.

An observations of this work showed that the flame characteristics influenced by the equivalence ratio oscillation is significantly different from the steady case by varies the oscillation frequency and amplitude. Deviation of the flame movement from the steady case for the equivalence ratio oscillation case increases as an increase in oscillation frequency and amplitude. Moreover, Richards *et al.* (1999) observed that the combustion instability in the combustor is suppressed by modulating the equivalence ratio. The present work elucidated that; it is because that the flame movement produced by the equivalence ratio oscillation as seen in the present work suppressed the combustion instability. These observations suggest that the mechanisms that suppresses the combustion instability in real combustor by modulating an equivalence ratio with the frequency equal or less than that the combustion instability frequency.

6.2 Future works

Numerical study using multi-step and full-step reaction mechanism is important to investigate the dynamics of flame especially in the rich equivalence ratio region.

In the experimental work, first priority is to upgrade the experimental condition to use a

high-level oscillation frequency. Higher oscillation frequency is a great issue and this effort requires a lot of work in refining and conditioning the oscillator system.

Measurements of flow field variables such as velocity and temperature are needed for the completeness of the experimental tools in the present work. It is very important to use non-intrusive tools, essentially laser based techniques like PIV technique.

Measurement of mixing of lean and rich mixture in the combusting region is an important problem. It would be helpful to perform a quantitative analysis acetone PLIF.

References

Alan H. Epstein, Aircraft engines' needs from combustion science and engineering, *Combustion and Flame*, Vol. 159: (2012), pp.1791-1792.

Ansys Fluent 12.0, User's Guide, (2009).

Ax, H, Kutne, P., Meier, W., König, K., Maas, U., Class, A. and Aigner, M., Low Pressure Premixed CH_4/Air Flames with Forced Periodic Mixture Fraction Oscillations: Experimental Approach, *Applied Physics B: Lasers and Optics*, Vol. 94, No. 4 (2009), pp.705-714.

Bansal G. and Im H. G., Scaling Analysis on Dynamic Flammability Limits of Unsteady Premixed Methane/Air Flames, *45th AIAA Aerospace Sciences Meeting and Exhibit*, (2007), Nevada

Birbaud, A. L.**,** Ducruix, S.**,** Durox, D. and Candel, S.**,** The nonlinear response of inverted "V" flames to equivalence ratio non-uniformities, *Combustion and Flame*, Vol.154: (2008), pp.356-367.

Bray, K., Domingo, P. and Vervisch, L., Role of the progress variable in models for partially premixed turbulent combustion, *Combustion and Flame*, Vol. 141: (2005), pp.431-437.

Candel, S., Combustion dynamics and control: Progress and challenges, *Proceeding of the Combustion Institute,* Vol. 29: (2002), pp.1-28.

Cho, J. H., and Lieuwen*,* T., Laminar premixed flame response to equivalence ratio oscillations, *Combustion and Flame,* Vol. 140:(2005), pp.116-129.

Chung, S. H., and Law*,* C. K., An integral analysis of the structure and propagation of stretched premixed flames, *Combustion and Flame,* 72: (1988), pp.325-336.

Derbunovich, G.I., Zemskaya, A.S., Repik, E.U., Sosedko, Y.P., Optimal conditions of turbulence reduction with screen, *Fluid Dynamics*, Vol. 28 (1), (1993) pp.138-144

Egolfopoulos, F. N. and Campbell, C. S., Unsteady Counter flowing Strained Diffusion Flames: Diffusion Limited Frequency Response, *J. Fluid Mech*. Vol. 318: (1996), pp.1-29.

Hawkes, E. R. and Chen, J. H., Comparison of the direct numerical simulation of lean/methane air flame with strained laminar flame calculation, *Combustion and*

Flame, Vol. 144: (2006), pp.112-125.

Fleifil, M., Annaswamy, A. M., Ghoneim, Z. A. and Ghoniem, A. F., Response of a laminar premixed flame to flow oscillations: A kinematic model and thermo acoustic instability results, *Combustion and flame*, 106, (1996), pp.487-510.

Galizzi C. and Escudie D., Experimental Analysis of an Oblique Laminar Flame Front Propagation in a Stratified Flow, *Combustion and Flame*, Vol. 145: (2006), pp.621-634.

Garrido-López, D. and Sarkar, S., Effects of imperfect premixing coupled with hydrodynamic instability on flame propagation, *Proceedings of the Combustion Institute*, Vol. 30: (2005), pp.621-628.

Hemchandra, S., Premixed flame response to equivalence ratio fluctuations: Comparison between reduced order modeling and detailed computations, *Combustion and Flame*, Vol.159: (2012), pp.3530-3543.

Hemchandra, S., Recent advances in flame response prediction for combustion instability modeling, *Proceedings The Fifth European Conference on Computational Fluid Dynamics*, No.01885 (2010-6).

Hirota, M., Sekine, K., Hashimoto, K., Saiki, A., Takahashi, H. and Masuya, G., Measurement of fuel concentration profile at leading edge of lifted flame with acetone laser-induced fluorescene, *Journal of Thermal Science and Technology*, Vol. 4, No. 2, (2009), pp.238-247.

Im, H. G. and Chen, J. H., Effect of flow transient on the burning velocity of laminar hydrogen/air premixed flames, *Proceeding of the combustion Institute*, 28, (2000), pp.1833-1840.

Im, H. G., Bechtold, J. K. and Law, C. K., Response of counter flow premixed flames to oscillating strain rates, *Combustion and flame*, 105, (1996), pp.358-372.

Ishida K., Small and medium size gas turbines, *Buletin of GTSJ*, (2003).

Kang T. and Kyritsis D. C., A combined experimental/computational investigation of stratified combustion in methane-air mixtures, *Energy Conversion and Management,* Vol. 48: (2007), pp.2769-2774.

Kang T. and Kyritsis D. C., Departure from Quasi-Homogeneity during Laminar Propagation in Lean, Compositionally Stratified Methane Air Mixtures, *Proceeding of*

the Combustion Institute, Vol. 31: (2007), pp.1075-1083.

Kang T. and Kyritsis D. C., Phenomenology of Methane Flame Propagation into Compositionally Stratified, Gradually Richer Mixtures, *Proceeding of the Combustion Institute*, Vol.32: (2009), pp.979-985.

Kang, T. and Kyritsis, D. C., Theoretical investigation of flame propagation through compositionally stratified methane-air mixtures, *Combustion Theory and Modeling,* 13: 4 (2009), pp.705-719.

Karimi, N., Brear, M. J., Jin, S. H. and Monty, J. P., Linear and non-linear forced response of a conical, ducted, laminar premixed flame, *Combustion and Flame*, Vol.156: (2009), pp.2201-2212.

Krebs, W., Bethke, S., Lepers, J., Flohr, P., and Prade, B., Thermoacoustic Design Tools and Passive Control: Siemens Power Generation Approaches, *Progress in Astronautics and Aeronautics*, 210 (2005), pp.89-111.

Kornilov, V. N., Experimental research of acoustically perturbed Bunsen flames, Phd thesis, TU/e: Eindhoven, (2006), pp.89-103.

Kulkarni, V., Sahoo, N., and Chavan, S. D., Simulation of honeycomb-screen combinations for turbulence management in a subsonic wind tunnel, *Journal of Wind Engineering and Industrial Aerodynamics*, 99 (2011), pp.37-45.

Lauvergne, R. and Egolfopoulos, F. N., Unsteady response of C_3H_8/air laminar premixed flames submitted to mixture composition oscillations, *Proceedings of the Combustion Institute*, Vol. 28: (2000), pp.1841–1850.

Law, C. K.**,** Combustion Physics, (2006), Cambridge University Press, NY.

Law, C. K.**,** Dynamics of stretch flames, Symposium (International) on *Combustion*, Vol.22:1 (1989), pp.1381-1402.

Lieuwen, T., Neumeier, Y., and Zinn, B.T., The Role of unmixedness and Chemical Kinetics in Driving combustion Instabilities in Lean Premixed Combustors, *Combustion Science and technology*, 135, (1998), pp.193-211.

Lieuwen, T., Nonlinear kinematic response of premixed flames to harmonic velocity disturbances, *Proceeding of the combustion Institute*, 30, (2005), pp.1725-1732.

Loehrke, R. I and Nagib, H. M, Experiments on management of free-stream turbulence,

AGARD Report no. 598 (1972).

Marzouk, Y. M., Ghoniem, A. F. and Najm, H. N., Dynamic response of strained premixed flames to equivalence ratio gradients, *Proceedings of the Combustion Institute*, Vol. 28: (2000), pp.1859–1866.

Matsuyama, R., Kobayashi, M., Ogata, H., Horikawa, A., and Kinoshita, Y., Development of a Lean Staged Combustor for Small Aero-Engines, *ASME Turbo Expo 2012: Turbine Technical Conference and Exposition, Volume 2: Combustion, Fuels and Emissions, Parts A and B*, (2012) (No. GT2012-68272), pp. 211-218.

Mikhailova, N. P., Repik, E. U., Sosedko, Y. P., Optimal control of free-stream turbulence intensity by means of honeycomb, *Fluid Dynamics*, Vol. 29 (3), (1994) pp.163-174.

Mongia, H. C., Held, T. J., Hsiao, G. C., and Pandalai, R. P., Incorporation of Combustion Instability Issues into Design Process: GE Aeroderivative and Aero Engines Experience, *Progress in Astronautics and Aeronautics*, Vol. 210 (2005), pp.43-61.

Nakamura, Y., Yamada, Y., Hirota, M. and Saito, T., Strategy to diagnose ultra-lean ($\varphi <$ 0.6) premixed flames by acetone-OH simultaneous PLIF with one-laser and one-detector combination, Journal of Visualization, 14(1), (2011), pp.75-84.

Pires Da Cruz, A., Dean, A.M., and Grenda, J.M., A Numerical Study of the Laminar Flame Speed of Stratified Methane/Air Flames, P*roceedings of the Combustion Institute*,Vol. 28: (2000), pp.1925-1932.

Preetham, S. K. Thumuluru, H. Santosh and T. Lieuwen, Linear response of laminar premixed flames to flow oscillation: unsteady stretch effects, *Journal of Propulsion and Power*, Vol. 26, No. 3, (2010), pp.524-531.

Rahman, M. R. A., Yokomori, T., and Ueda, T., Numerical investigation of a flame response to the fuel concentration oscillation in stagnating laminar premixed methane/air flames, *Journal of Thermal Science and Technology*, Vol. 7, No. 1, (2012), pp.16-30.

Riazi, R., Farshchi, M., Laminar premixed V-shaped flame response to velocity and equivalence ratio perturbations: Investigation on kinematic response of flame, *ScientiaIranica, Transactions B: Mechanical Engineering,* Vol. 18:4(2011), pp.913-922.

Richards, G. A., Janus, M. and Robey, E. H., Control of Flame Oscillations with

Equivalence Ratio Modulation, *Journal of Propulsion and Power*, Vol. 15, No. 2 (1999), pp.232-240.

Richardson, E. S., Granet, V. E., Eyssartier, A. and Chen, J. H., Effects of equivalence ratio variation on lean, stratified methane–air laminar counter flow flames, *Combustion Theory and Modeling*, 14:6, (2010), pp.775-792.

Rosdzimin, A. R. M., Hagita, T., Yokomori, T., Ueda, T., The response of premixed flames to fuel concentration oscillation in lean rich crossover case, *Proceedings The Eighth KSME-JSME Thermal and Fluids Engineering Conference*, No.GST04-020 (2012-3), (on USB).

Sankaran, R. and Im, H. G., Dynamic flammability limits of methane/air premixed flames with mixture composition fluctuations, *Proceedings of the Combustion Institute*, Vol. 29: (2002), pp.77-84.

Schwarz H., Zimmer L., Durox D. and Candel S., Detailed Measurements of the Equivalence Ratio Modulation in Premixed Flames using Laser Rayleigh Scattering and Absorption Spectroscopy, *Exp. Fluids*, Vol. 49: (2010), pp.809-821.

Sewell, J. B. and Sobieski, P. A., Monitoring of Combustion Instabilities: Calpine's Experience, *Progress in Astronautics and Aeronautics*, Vol. 210 (2005), pp.147-162.

Shreekrishna, Hemchandra, S. and Lieuwin, T., Premixed flame response to equivalence ratio perturbations, *Combustion Theory and Modeling, 14: 5* (2010), pp.681-714.

Smith, G. P., Golden, D. M, Frenklach, M., Moriarty, N. W., Eiteneer, B., Goldenberg, M., Bowman, C. T., Hanson, R. K., Song, S., Gardiner, W. C., Jr., Lissianski, V. V. and Qin, Z., (online), available from<http://www.me.berkeley.edu/gri_mech/>

Suenaga, Y., Kitano, M. and Takahashi, Y., Propagation and extinction of a cylindrical premixed flame undergoing equivalence ratio fluctuation near the lean limit, *Journal of Thermal Science and Technology*, Vol. 5, No. 1, (2010), pp.124-134.

Suenaga, Y., Kitano, M., Yanaoka, H. and Fujita, N., Characteristics of the flame propagation through a mixture flow with periodic concentration fluctuation (effects of concentration fluctuation range on flame characteristic), *Transactions of the Japan Society of Mechanical Engineers, Series B*, Vol. 71: (2005), pp.1190-1196. (in Japanese).

Suenaga, Y., Kitano, M., Yanaoka, H., and Fujita, N., Characteristics of the flame

propagation through a mixture flow with periodic concentration fluctuation, *Transactions of the Japan Society of Mechanical Engineers*, Vol. 69: (2002), pp.2138-2143. (in Japanese).

Suenaga, Y., Kitano, M., Yanaoka, H., and Fujita, N., Response of a premixed flame to equivalence ratio fluctuation in stagnation flow, *Journal of the Combustion Society of Japan*, Vol. 45, No.134: (2003), pp.229-237. (in Japanese).

Sung, C. J. and Law, C. K., Structural sensitivity, response and extinction of diffusion and premixed flames in oscillating counter flow, *Combustion and flame*, 123, (2000), pp.375-388.

Takahashi Y, Suenaga Y, Kitano M, and Kudo M., Response of a Cylindrical Premixed Flame to Periodic Concentration Fluctuation, *JSME International Journal Series B*, Vol. 49, No. 4: (2006) pp.1307-1315.

Thurber, M. C., Acetone laser-induced fluorescence for temperature and multi-parameter imaging in gaseous flows, *Tropical report TSD-120*, (1999).

Westbrook, C. K., and Dryer, F. L., Simplified reaction mechanism for the oxidation of hydrocarbon fuels in flames. *Combustion Science and Technology*, Vol. 27: (1981) pp.31–43.

Yu, K. H. and Wilson, K. J., Scale-Up Experiments on Liquid-Fueled Active Combustion Control, *Journal of Propulsion and Power*, Vol. 18, No. 1 (2002), pp. 53-60.

Zhou, R. and Hochgreb, S., The behaviour of laminar stratified methane/air flames in counterflow, *Combustion and flame*, 160:6, (2013), pp.1070-1082.